SPECIAL REPORT 93-20

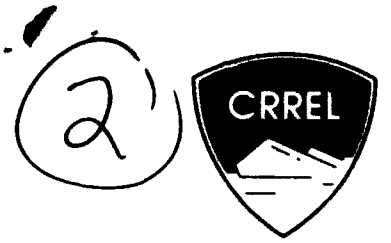

Electrical Properties of Ice

Victor F. Petrenko

August 1993

Abstract

This report examines the electrical properties of ice in the frequency range of 0–107 Hz, attempting to be suitable both as a simple and clear textbook for students and non-specialists and as a comprehensive review of recent developments and discoveries in the field. Corresponding to this double goal, the report consists of two parts. The first one is written in textbook style and contains most general theoretical and experimental results essential for understanding of unique electrical properties of ice. The theoretical interpretation of ice conductivity and ice dielectric permittivity is based on ice being a protonic semiconductor. Jaccard's elegant model is used to mathematically describe the electrical properties, and is expanded on cases of ice samples having finite size, boundaries and interfaces, and an inhomogeneous electric field. The statistics of charge carriers in pure and doped ice is discussed in detail, as are experimental techniques for measurements of conductivity and dielectric permittivity. The first part contains a comprehensive review of experimental results on ice conductivity, ice dielectric permittivity, mobility and electric charges of protonic charge carriers and activation energies of their generation and motion. The second part includes more complicated physical phenomena—proton injection, dielectric crossover, ice field effect transistor, thermostimulated currents, theory of ice/metal interface, field extraction of charge carriers and a recombination injection.

For conversion of SI metric units to U.S./British customary units of measurement consult ASTM Standard E380-89a, *Standard Practice for Use of the International System of Units,* published by the American Society for Testing and Materials, 1916 Race St., Philadelphia, Pa. 19103.

This report is printed on paper that contains a minimum of 50% recycled material.

Special Report 93-20

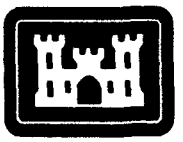

US Army Corps of Engineers
Cold Regions Research & Engineering Laboratory

Electrical Properties of Ice

Victor F. Petrenko

August 1993

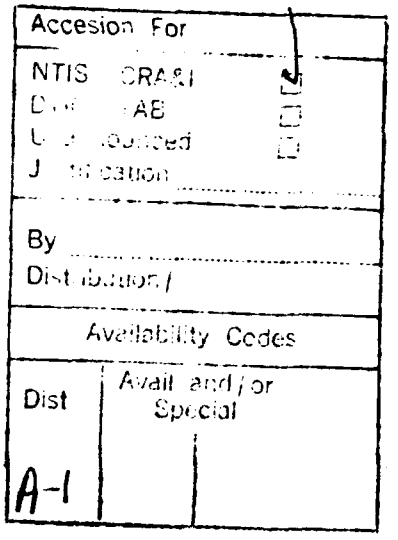

Prepared in cooperation with
THAYER SCHOOL OF ENGINEERING
DARTMOUTH COLLEGE

PREFACE

This report was prepared by Dr. Victor F. Petrenko, Professor of Engineering, Thayer School of Engineering, Dartmouth College, Hanover, New Hampshire. Funding was provided by the U.S. Army Research Office through contract DAAL 03-91-G-0164.

The author acknowledges Dr. Andrew Assur, Dr. George Ashton and Prof. Erland Schulson for their help, support and collaboration, without which this report would have had little chance to appear. He also expresses special thanks to Dr. John Glen, Prof. John Nagle, Dr. Ivan Ryzhkin and Dr. Robert Whitworth for numerous useful remarks and comments on the text. In many cases their suggestions improved the manuscripts in content and logic and identified errors the author had overlooked. The author appreciates the help of Linda Dorr, Linda Cuthbert and Oleg Nikolaev in drawing, typing and editing the manuscript.

FOREWORD

At the present time, thousands and thousands of people around the world deal with ice, snow and permafrost. They are scientists, educators, engineers, navigators, meteorologists and others. While a small fraction of these people contribute to the knowledge base in ice physics, all of them use knowledge from it frequently. Moreover, successful applied research is based upon fundamental science—one more reason for ice specialists to have a textbook on ice physics on their desks.

The first modern ice physics text was Fletcher's book on *The Chemical Physics of Ice* (1970). Fletcher's book is in typical textbook format: it is reasonably brief and easy to understand. He touched on a few of the most important topics, but not all of them.

The most comprehensive book on ice physics to date was published by Hobbs in 1974. Hobbs considered almost all of the basic aspects of ice as understood at that time. Moreover, he described and compared several (sometimes opposing) viewpoints. This fundamental and rather large (837 pages) book is commonly known as the "Ice Bible" by specialists in the field. In 1974 and 1975, two monographs on ice were produced by John Glen. These were briefly and clearly written and reviewed almost all ice-related subjects. This work was (and in some respects still is) a magnificent introduction to ice.

Finally, in 1981 Maeno wrote a simple, popular book for the express purpose of attracting people's attention to the subject.

During the past 20 years, a significant amount of new experimental and theoretical work has appeared, dramatically changing our views on ice physics. As a result, we are now able to formulate physical laws using more simple and direct methods. We have found some of the physical models used in the past to be completely wrong. The physics of ice is a much better developed subject than it was 20 years ago.

For the above reasons, we feel the time is ripe for a contemporary book on ice physics, incorporating the known and proven with almost 20 years worth of material not covered by previous works.

I have tried to prepare a "readable" book, and not one that requires the reader to be a uniquely educated person. It is my intent to present the material in such a way that any reader attracted by the title *Ice Physics* will be able to comprehend it. This is quite difficult for a book dedicated, not to a particular field of knowledge, but to a specific material. Indeed, for ice it means we have to consider a wide variety of subjects, including quantum chemistry, solid state physics, the theory of elasticity, ionic conductivity, synchrotron x-ray topography, crystal growth, the physics of surfaces and more.

The primary goal is to produce as simple a book as possible without sacrificing scientific accuracy. Experimental facts, physical ideas and theories will be strongly organized and bound together cohesively. The reader will be introduced to a wide variety of material on a step by step basis. Then the picture will be whole.

To accelerate materials publication, this book will appear first in the form of a series of joint CRREL–Dartmouth reports, later to be published in CRREL's Monograph series, on:

1. The structure of ordinary ice
   Part I: "Ideal" structure of ice. Ice crystal lattice
   Part II: Real structure of ice. Defects
2. Electrical properties of ice
   Part I: Conductivity and dielectric permittivity of ice
   Part II: Advanced topics and new physical phenomena
3. Optical properties
4. Electro–optical effects in ice

5. Thermal properties
6. Mechanical properties of ice. Elasticity and anelastic relaxation. Plastic properties. Fracture of ice
7. Electromechanical effects in ice
8. Surface of ice
9. Other forms of ice and their properties
10. Ice in space
11. Ice research laboratories

The reports will be prepared in a sequence convenient to the author. The present report is the first in the series.

CONTENTS

	Page
Preface	ii
Foreword	iii
Nomenclature	viii
Part I. Conductivity and Dielectric Permittivity of Ice	
Introduction	1
Nature of electric charge carriers of ice	6
Jaccard's model of electrical properties of ice of infinite size	8
Protonic charge carriers	8
Electrical properties—one type of charge carrier	11
Other charge carrier transfers and their effective charges	13
General consideration of Jaccard's model with four kinds of carriers	14
Analysis of Jaccard's results	16
Electrical properties of ice of finite size	19
Low-frequency, limit-screening lengths	21
Frequency dependence of dielectric permittivity	22
Concentration of charge carriers	23
Intrinsic charge carriers	23
Do superionic transitions and the superionic state of ice exist?	25
Protonic charge carriers introduced by doping	27
Experimental techniques for investigation of conductivity and dielectric permittivity of ice	31
Measuring circuits	32
Electrodes	34
Surface conductance and guard rings	35
Influence of inhomogeneity on the frequency dependence of ice conductivity	35
Review of experimental results on ice conductivity and dielectric permittivity	36
Part II. Advanced Topics and New Physical Phenomena	
Charge exchange at ice/metal interfaces	43
Relaxation times of electric polarization and electric fields in ice	45
Recombination injection of ions into ice	47
Recombination extraction of charge carriers from ice	50
Proton injection from Pd electrodes into ice	51
Field effect transistor made of ice	56
"Crossover" in the dielectric permittivity of ice	58
Thermally stimulated depolarization	60
Conclusion	64
Literature cited	65
Abstract	71

ILLUSTRATIONS

Figure

1. Potential energy of an ion in a crystal lattice W as a function of coordinate x with and without electric field E	3
2. Frequency dependence of conductivity of pure monocrystalline ice	4

Page

3. Direct current density I through the same ice sample as for Figure 2 as a function of time t 4
4. Temperature dependence of relative static dielectric permittivity of ice and water 5
5. Frequency dependence of pure ice dielectric permittivity at –10°C 6
6. Chain of water molecules in the ice I_h structure 8
7. Schematic representation of H_3O^+ ion and D-defect motion along a chain of hydrogen bonds in ice 9
8. Creation of two point defects when a proton is placed into a defect-free ice lattice 14
9. Ice sample connected into measuring circuit and its electrical equivalent circuits 16
10. Equivalent electrical circuit for high-frequency conductivity σ_∞ and for static or low-frequency conductivity σ_s 18
11. Cole–Cole diagram 19
12. Distribution of static electric field E inside the ice sample 21
13. Dependence of apparent static dielectric permittivity ε' on ice thickness L 22
14. Dependence of apparent static dielectric permittivity ε' on circular frequency ω 22
15. Logarithm of the ratio of ion concentration n to molecular concentration N as a function of reciprocal temperature T 26
16. Temperature of transition of ice into superionic state T_c as a function of E_1/E_2 26
17. Incorporation of impurities into the ice lattice 27
18. Schematic sketch of ac bridge circuit to measure ac impedance of ice sample 32
19. Schematic representation of "loop method" for ice ac impedance measurement 33
20. Cylindrical ice sample with two attached electrodes and the guard ring 34
21. Frequency dependences of pure ice dielectric permittivity ε and conductivity σ 36
22. Temperature dependence of bulk and surface conductance of pure ice specimen 41
23. Electronic energy levels in water and two metal electrodes 44
24. Current–voltage characteristic of ice specimen with two Pt electrodes 44
25. Characteristic time τ with which electric polarization of ice relaxes for different boundary conditions 46
26. Dependence of ac conductivity of pure water σ on time t, when a small dc bias was applied 47
27. Alternating current conductivity of water normalized on equilibrium conductivity σ_0 in the space between two electrodes 48
28. Variations in low-frequency conductivity of pure ice measured at 30 Hz when 10-V dc bias was turned on and off 49
29. Current–voltage characteristic of a thin ice specimen with ohmic electrodes .. 50
30. Dependences of normalized high-frequency conductivity σ_∞ and direct current I on voltage for thin single crystal ice 50
31. Dependence of σ_∞ on sample thickness L 51
32. Injection of protons into ice from Pd electrode saturated by hydrogen 52
33. Theoretical current–voltage characteristic for proton injection into ice 53
34. Dispersion curves for pure monocrystalline ice specimen with two H-loaded Pd electrodes 54

Page

35. Direct current I, capacitance C and conductance G at 100 Hz, as functions of bias voltage V for specimen with two H-loaded Pd electrodes 55
36. Dielectric/conductor interface with applied static electric field $E\perp$ 56
37. Field effect ice transistor 57
38. Time diagrams of ice surface conductivity λ_s and dc bias applied to the transistor shown in Figure 37 57
39. Temperature dependences of H_3O^+ ion conductivity σ_+ and Bjerrum defects' conductivity σ_{DL} calculated from experimental results, using best-fit method 59
40. $\Delta\varepsilon = \varepsilon_s - \varepsilon_\infty$ as a function of temperature for ice doped with HF concentrations 59
41. Static relative permittivity ε_s and dielectric relaxation time τ at –10°C as a function of the concentration n_{HF} in the solution from which the polycrystalline ice was formed 60
42. Schemes of polarization and depolarization in the TSD technique 61
43. TSD currents of ice specimens 63

TABLES

Table

1. Data on high-frequency and static conductivities of ice 38
2. Mobilities of charge carriers in ice 40
3. Ratio of effective electric charge of H_3O^+ ion and of D-defect to proton charge 41

NOMENCLATURE

$< >$	sign of averaging
a	interatomic space
C	capacitance, electric capacitance
D	diffusion coefficient
$\vec{D}$	electric displacement vector
e	proton charge
$\vec{E}$, E	electric field strength
E_a	activation energy
E_{aB}	energy of creation of a pair of Bjerrum defects
E_{ai}	energy of creation of an ion pair
E_{as}	activation energy of static conductivity σ_s
$E_{a\infty}$	activation energy of high-frequency conductivity σ_∞
E_{H_2}	electron level on hydrogen system
E_{O_2}	electron level on oxygen system
E_f	electron Fermi-level
e_i	defects' electric charge (i = 1, 2, 3, 4)
E_{mi}	activation energies of protonic defects' motion (i = 1, 2, 3, 4)
E_τ	activation energy of Debye relaxation time
F	free energy
F_d	free energy of defects
f, ν	frequencies
I	electric current
i	$= \sqrt{-1}$
j_i	flux density of defects (i = 1, 2, 3, 4)
$\vec{J}$, J	electric current density
k_B	Boltzmann constant
L	sample thickness
m_e	electron mass
N	number of water molecules
n	concentration (in m^{-3})
n_D	D-defects concentration
n_{H_2O}	concentration of water molecules in ice
n_i	concentration of defects (i = 1, 2, 3, 4)
n_L	L-defects concentration
$\vec{p_i}$	elementary dielectric dipole
$\vec{P}$	polarization vector
q, e_i	electric charge of carriers
R	electric resistance
r_i	coordinate of i^{th} particle or dipole
r_{oo}	oxygen–oxygen distance in ice lattice (2.76 Å)
S	entropy
s	sample surface area
S_c	configurational entropy
S_v	vibrational entropy

T	temperature
t	time
U	internal energy
U_m	activation energy of ionic motion
$\vec{v}_d$	drift velocity
$\vec{v}_i$	velocity of i^{th} particle
V	voltage
W	number of configurations of a system
x,y,z	coordinates
$\delta(x)$	delta function
ε	relative dielectric permittivity
ε_o	dielectric permittivity of a vacuum
ε_s	static dielectric permittivity ($\omega << \omega_D$)
ε_∞	high-frequency ($\omega>>\omega_D$) dielectric permittivity
ξ	dimensionless factor in Jaccard theory
$1/\kappa$	screening length
λ_D	diffusion length
μ	mobility
ν_h	frequency of proton hops along a hygrogen bond
ρ	electric charge density
σ	conductivity
σ_B	Bjerrum defect conductivity $\sigma_B = \sigma_3 + \sigma_4$
σ_i	partial conductivity of "i" charge carrier
σ_{ij}	tensor of conductivity
σ_{ion}	ionic conductivity $\sigma_{ion} = \sigma_1 + \sigma_2$
σ_s	static or low-frequency conductivity ($\omega << \omega_D$)
σ_{sf}	surface charge density
σ_∞	high-frequency conductivity ($\omega>>\omega_D$)
τ	relaxation time
τ_D	$= \omega_D^{-1}$ Debye relaxation time
τ_L	lifetime of charge carriers
τ_m	Maxwell relaxation time
τ_p	impulse relaxation time
ϕ	$\equiv 3.85\, k_B T\, r_{oo}$
φ	electric potential
χ	electric susceptibility
$\vec{\Omega}$	configurational vector
ω	circular frequency
ω_D	Debye frequency

Electrical Properties of Ice

VICTOR F. PETRENKO

PART I. CONDUCTIVITY AND DIELECTRIC PERMITTIVITY OF ICE

INTRODUCTION

A wide variety of the physical properties of materials is generally considered to be their "electrical properties." Among them are dc and ac conductivities, dielectric permittivity, piezoelectricity, electrostriction, photoelectric phenomena, etc. This report is devoted only to conductivity and electrical polarization of ice in frequency ranges from 0 to 10^7 Hz. The rest of the phenomena associated with electric fields and electric currents will be considered in future reports in this series.

We will begin with some elementary definitions and then compare the electrical properties of ice with those of other materials.

According to the definition of conductivity σ

$$\vec{J} = \sigma \vec{E} \tag{1}$$

where $\vec{J}$ is electric current density and $\vec{E}$ is electric field strength.

Equation 1 expresses the well known Ohm's law for isotropic materials. In the case of an anisotropic conductor, we have to use the more complicated equation

$$J_i = \sigma_{ij} E_j \tag{2}$$

where σ_{ij} is a second-rank tensor of conductivity and J_i and E_j are components of vectors $\vec{J}$ and $\vec{E}$ (Ney 1985). Here in eq 2 and also below we use Einstein's summation convention: when a letter suffix occurs twice in the same term, summation with respect to that suffix is to be automatically understood. As we will see later, ice I_h demonstrates almost perfect isotropic conductivity despite its hexagonal symmetry. That is why we will use eq 1 more often than eq 2.

When one kind of electric charge carrier with electric charge q and a concentration of n is present

$$\vec{J} = qn \langle \vec{v}_d \rangle \tag{3}$$

where $\langle \vec{v}_d \rangle$ is a mean drift velocity of the charge carriers in the electric field.

If the electric field is not too strong, so that there is no increase in temperature of the conductor lattice or the charge carriers, the mean drift velocity $\langle \vec{v}_d \rangle$ turns out to be a linear function of the electric field strength $\vec{E}$

$$\langle \vec{v}_d \rangle = \mu \vec{E} \tag{4}$$

where the constant of proportionality μ is called mobility. In both electron and ionic conductors, μ turns out to be constant in a wide range of field strengths, but for different reasons. In electron conductors (metals and semiconductors), the conduction electrons are moving in a chaotic motion with very high velocities ($\approx 10^6$ m/s in metals and $\approx 10^5$ m/s in semiconductors at room temperature). An application of a "weak" electric field barely changes the mean absolute value of the velocity, since the mean drift additions to the velocity are very small. This is why the average time of relaxation of the electron impulse τ_p does not change, whether it is defined by either collisions with the defects of the crystal lattice or by scattering on the phonons. The mean drift velocity, acquired by electrons in this process between the collisions in the direction of the electric field, is

$$\langle \vec{v}_d \rangle = \frac{e \cdot \vec{E}}{m_e} \cdot \tau_p \propto \vec{E} \tag{5}$$

that is

$$\mu = \frac{e\,\tau_p}{m_e} = \text{const} \tag{6}$$

as long as τ_p and m_e are independent of $\vec{E}$. Comparing the formulas 1, 3 and 4 gives an obvious result

$$\sigma = |q| \mu n \,. \tag{7}$$

If the charge is transferred by several carriers, moving independently of each other, then their contributions have to be added together

$$\vec{J} = \sum_{i=1}^{K} \vec{J}_i = \vec{E} \left(\sum_{i=1}^{K} \sigma_i \right) = \left(\sum_{i=1}^{K} |q_i| \, \mu_i \, n_i \right) \vec{E} \tag{8}$$

where $i = 1, 2, \ldots K$, K being the number of carrier types, and the resultant conductivity σ

$$\sigma = \sum_{i=1}^{K} \sigma_i \tag{9}$$

comes out to be equal to the sum of the partial conductivities of all the carriers of the charge σ_i.

In the ionic conductors, mobile ions jump between the closest stable positions in the lattice. A simple case of one-dimensional motion of an ion is shown in Figure 1. To move one interatomic distance in the direction of the field, the positive ion would need activation energy $U_m - qEa/2$, and to move against the field, $U_m + qEa/2$.

The frequency of ion jumps in the direction of the field is expressed by

$$f_1 = \nu \exp\left\{ - \frac{U_m - qaE/2}{k_B T} \right\} \tag{10}$$

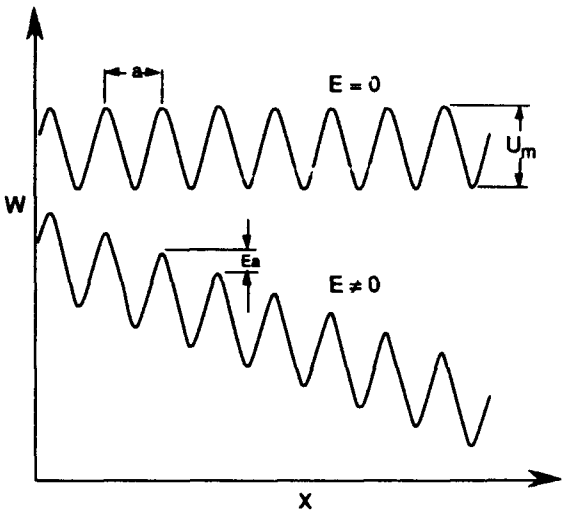

Figure 1. Potential energy of an ion in a crystal lattice W *as a function of coordinate* x *with* (E ≠ 0) *and without* (E = 0) *electric field* E; a *is an interatomic distance.*

and against the field

$$f_2 = \nu \exp\left\{-\frac{U_m + qaE/2}{k_B T}\right\} \tag{11}$$

where ν is the frequency of ion oscillations in a potential well (in equilibrium). Since every jump moves the ion over the distance *a*, it is apparent that the mean drift velocity of the ion in the direction of the field becomes

$$\langle v_d \rangle = a\,(f_1 - f_2) = 2\nu\, a\, \exp^{-U_m/k_B T} sh\left(\frac{qEa}{2k_B T}\right) \tag{12}$$

since usually

$$q\,E\,a << 2\,k_B T. \tag{13}$$

We can substitute the argument of *sh* instead of *sh* in eq 12

$$\langle v_d \rangle = \left[\left(\frac{\nu q a^2}{k_B T}\right) \exp^{-U_m/k_B T}\right] E. \tag{14}$$

So, the ion mobility is

$$\mu = \left(\frac{\nu q a^2}{k_B T}\right) \exp^{-U_m/k_B T} \tag{15a}$$

and is independent of *E*. U_m usually stands for the movement activation energy.
Also notice that

$$\nu \exp^{-U_m/k_B T} = \nu_h. \tag{15b}$$

This represents the probability of jumps or the mean real number of jumps per second. For chaotic thermal motion of this kind, the Einstein relation, connecting mobility μ and the diffusion coefficient *D* is also true

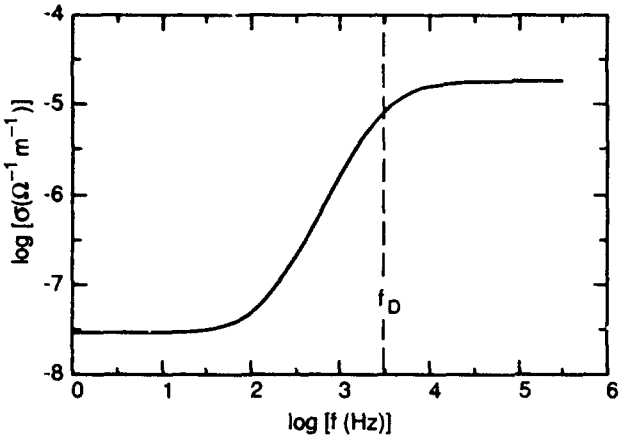

Figure 2. Frequency dependence of conductivity of pure monocrystalline ice; σ is measured in Ω^{-1} m^{-1}, f in Hz; T = –10 °C.

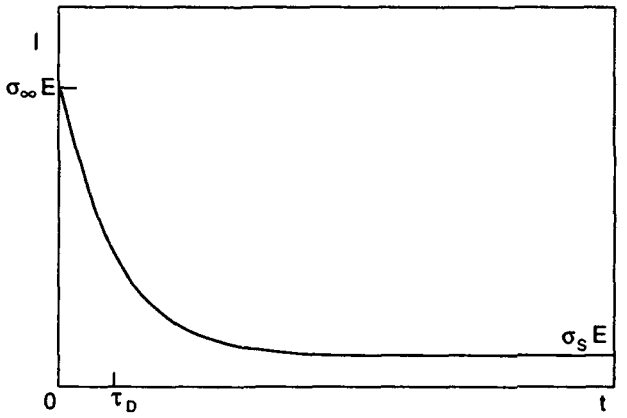

Figure 3. Direct current density I through the same ice sample as for Figure 2 as a function of time t; E = 0 for t < 0, E = const for t ≥ 0; I = E(σs + σ∞ exp(–t/ τD)). The definition of τD will be given below.

$$D = \frac{k_B T}{|q|} \cdot \mu . \tag{16}$$

In ordinary electronic and ionic conductors, σ is independent of frequency up to very high frequencies (while $\omega << \frac{1}{\tau}$, where τ is either the time of relaxation or the period of ion vibration).

However, ice behaves in a much different way. A characteristic frequency dependence of electric conductivity of pure monocrystalline ice at –10°C is shown in Figure 2. The most noticeable thing is that there are two major values of electric conductivity: low-frequency σ_s and high-frequency σ_∞, which differ by three orders of magnitude. Dependent on temperature, the characteristic frequency of transition $\omega_D = 2\pi f_D$, which is called the Debye frequency and changes from 10^5 Hz (0°C) to zero at the low temperature. (At 77 K this frequency is already immeasurable in pure ice.) One of the outcomes of the frequency dependence in Figure 2 is the unusual time dependence of the electric current through ice, if a steady electric field is applied to it. This dependence, created under the same conditions as in Figure 2, is shown in Figure 3.

It is interesting that the temperature dependence of electric conductivities of pure ice (σ_s and σ_∞) can be closely approximated by exponential dependencies such as

$$\sigma \propto \exp\left\{-\frac{E_a}{2k_B T}\right\} \tag{17}$$

where the conductivity activation energies E_a are equal to about 1 eV for σ_s and 1.16 eV for σ_∞ (see the *Review of Experimental Results on Ice Conductivity and Dielectric Permittivity* section).

Such relationships of electrical conductivities are typical for electron semiconductors. Even the absolute values of E_a are very close to the value for silicon (1.14 eV at $T = 300$ K [Long 1968]).

Also, the absolute value of σ_∞ of pure ice at $T = 0°C$ is typical for many pure electron semiconductors. One of our first goals will be explaining these observations.

The second major electric characteristic of ice, its polarizability, is also unusual. The state of the dielectric medium in the external electric field E is described by a vector of polarization $\vec{P}$

$$\vec{P} = \sum \vec{p}_i \tag{18}$$

where the summation is done over all elementary electric dipoles $\vec{p}_i$ present in a unit volume. In other words, $\vec{P}$ is the dipole momentum per unit volume. The following equation is also true

$$\vec{P} = \sum q_i \vec{r}_i \tag{19}$$

where q_i and $\vec{r}_i$ are respectively the charges and coordinates of elementary charges present in a unit volume. In many cases eq 18 is more useful than eq 19.

In nonferroelectric crystals

$$\vec{P} = \varepsilon_0 \chi \vec{E} \tag{20}$$

where χ is the electric susceptibility of a material and ε_0 is the dielectric permittivity of vacuum. χ is the major value determining the ability of a dielectric medium to polarize. More frequently found in practical use is the relative dielectric permittivity ε

$$\varepsilon = 1 + \chi; \vec{D} = \varepsilon_0 \varepsilon \vec{E} \tag{21}$$

where $\vec{D}$ is a vector of electric displacement.

Polarization of water is determined by two factors. The first is the large, constant, elementary dipole of a water molecule. A part of these dipoles is oriented along the external field $\vec{E}$, causing the creation of a sizable polarization. The larger the initial elementary dipole $\vec{p}_i$ and the higher its concentration in the medium, the larger the value of ε that can be achieved.

Secondly, the value of $\vec{p}_i$ is increased somewhat because of rearrangement of the charges inside the H_2O molecule. However, for water and ice this is the less significant mechanism for creating ε of the order of 3 only. Figure 4 shows the experimental temperature dependence of

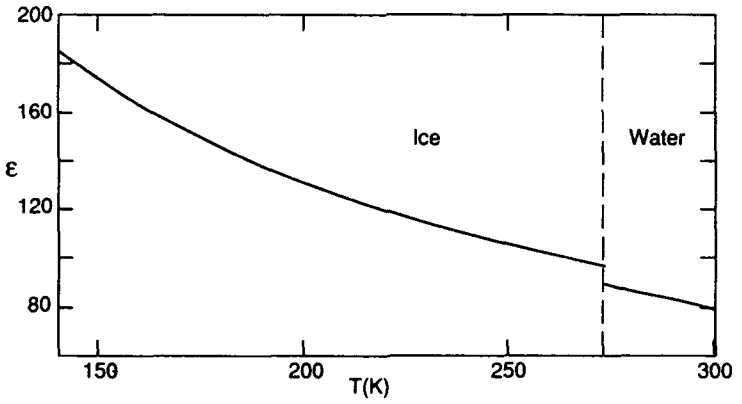

Figure 4. Temperature dependence of relative static dielectric permittivity of ice (Johari and Whalley 1981) and water (Malmberg and Maryott 1956). Extrapolation equations found in these papers were used to draw the plot. In ice, below ≈ 200 K, a peculiarity called "crossover" may occur.

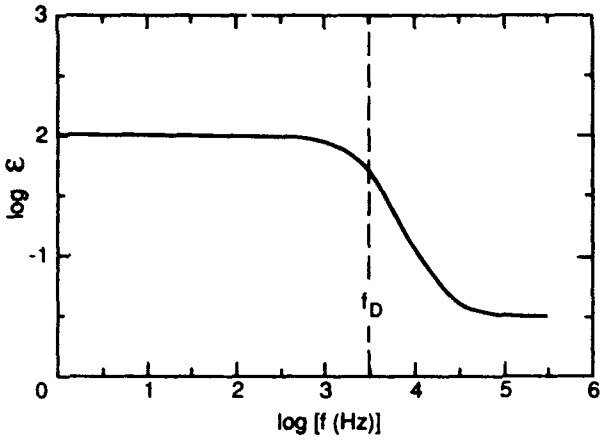

Figure 5. Frequency dependence of pure ice dielectric permittivity at –10°C.

the static dielectric permittivity ε for ice and water around 0°C. The most noticeable fact is that for ice $\varepsilon \approx 10^2$, even larger than for water at this temperature. This is, of course, evidence that even in the "rigid" crystal structure of ice, the H_2O molecules (and their $\vec{p_i}$) have the ability to turn, like the molecules in a liquid or a gas. The second important fact is that, despite the lower density of ice (i.e., a smaller concentration of water molecules or elementary dipoles), it has a larger ε value than water. Apparently, this cannot be understood without considering intermolecular interactions. In the dispersion curve ε (Fig. 5) for pure ice, obtained under the same conditions as diagrammed in Figure 2, we again notice two values: ε_s, static or low-frequency permittivity and high-frequency permittivity ε_∞. The transition from ε_s to ε_∞ occurs again at the same frequency f_D. $\varepsilon_\infty \cong 3.2$ is conditioned by electronic and ionic polarization of water molecules, i.e., small displacements of charges within such a "rigid" body as water molecules. Large static permittivity ε_s can be explained only in terms of the water molecule's considerable reorientation in space.

This short introductory review of the electric properties of ice yields a general idea about what kind of properties the physical model of ice conductivity should describe. After an introduction of this model, we will get acquainted in detail with vast experimental results and conduct an analysis and comparison.

NATURE OF ELECTRIC CHARGE CARRIERS IN ICE

To get acquainted with modern theoretical descriptions of the electrical properties of ice, we will discuss a question concerning the nature of charge carriers in ice.

Any physical model describing the electrical properties of ice must, first of all, be based upon knowledge of charge carrier type. One could assume a priori that charge carriers are either conduction electrons (holes) or ions (as in water). As suggested by Chesnakov et al. (1987), because of the fractional electric charge of ions in ice (see the *Other Charge Carrier Transfers and Their Effective Charges* section), the latter can accept or return electrons, changing the sign, while staying charged. So, these peculiar radicals (ions ± electrons) may also be put in the category of possible charge carriers.

The dispute about the nature of charge carriers in ice (electrons vs protons) has a rather long history. Back in 1957 Decroly et al. (1957) carried out an experiment that was for a long time considered to be decisive in proving the proton nature of ice conductivity. The idea of the experiment was simple and elegant. If in ice (as in water) the appearance of charge carriers is caused by thermoactivated reaction in the bulk

$$2H_2O \rightleftarrows H_3O^+ + OH^- \quad (22)$$

then, when an electric current is passing, one would expect hydrogen to be produced at the cathode

$$4H_3O^+ + 4e \rightarrow 2H_2\uparrow + 4H_2O \quad (23)$$

and oxygen to be yielded at the anode

$$4OH^- - 4e \rightarrow O_2\uparrow + 2H_2O\,. \quad (24)$$

According to eq 23 and 24, in the case of ionic conductivity, the passage of every four electrons must be followed by the yielding of two hydrogen molecules and one oxygen molecule. That is, Faraday's law of electrolysis must be fulfilled. If the amount of generated gas comes out to be less, then one should seek other charge carriers. Such an experiment using direct current requires special electrodes to be designed. The problem is that a stable electron exchange between ice and metal electrodes is usually impossible. Direct current through an ice sample with metallic electrodes ceases after a short time (the reasons for this will be discussed in detail in the *Charge Exchange at Ice/Metal Interfaces* section). That is why Decroly et al. used layers of frozen HF between ice and metal. Such layers can easily exchange charges with both ice and metal electrodes. The experiments were carried out at –10°C and it was shown that exactly the same amount of hydrogen was generated, as follows from eq 23.

On this basis, they concluded that conduction in ice was protonic. This result satisfied the overwhelming majority of scientists and was not re-examined until 1990 (though it should have been done in the 1960s). By that time (1960s) the large surface conductivity had come to be widely known at temperatures above –25°C. This conductivity is conditioned by the presence on ice surfaces of a so-called quasi-liquid layer. This layer decreases in thickness when the temperature decreases (starting from ~1000 Å at 0°C), and its contribution to conductivity becomes negligible at $T \leq -25$ to –30°C. Besides, if we take into account the extremely great mobility of fluorine ions in ice reported by Haltenorth and Klinger (1969), we have to agree that the ice specimens were strongly doped and most of the impurities were being contained at grain boundaries and surfaces, thus increasing surface conductivity rather than bulk conductivity.

So, the conclusion of protonic conductivity can be made only with respect to ice surfaces from the experiments of Decroly et al. Unfortunately, even this inference couldn't be drawn from their experiments. If the ice specimen were changed to a piece of metal, the same amount of hydrogen would be yielded from the HF layer, which is a protonic conductor. The experiment of Decroly et al. *proved* nothing, although indirect evidence of the protonic conductivity of ice existed. First, the dc conductivity of heavy ice is about 100 times less than that of ordinary ice (Engelhardt 1973). Second, it has been established that proton injection from Pd electrodes into the bulk of ice increases its conductivity (Bullemer et al. 1969, Petrenko et al. 1983). Certainly, these results do not mean that conductivity is entirely determined by proton motion.

Eventually, all doubts were dispersed after Decroly's experiments were repeated using new, specially designed electrodes that provided a free charge exchange between ice and metal, even at very low temperatures (Petrenko and Chesnakov 1990a). We will describe in detail the principle of action of such electrodes with deposited monomolecular charged layers in the *Charge Exchange at Ice/Metal Interfaces* section.

In these experiments, hydrogen and oxygen generation in the electrolysis of pure ice was measured. The dc conductivity of pure ice was entirely determined by proton motion within the temperatures range of 0 to –42°C (experimental error ± 3%).

JACCARD'S MODEL OF ELECTRICAL PROPERTIES OF ICE OF INFINITE SIZE

At present, several theories describing the electrical properties of ice are well known. We will start getting acquainted with them by looking at Jaccard's (1959, 1964) model, which enjoys a special place among others, for several reasons. It was the first successful model of ice properties (both dielectrical and conductivity) and is extraordinarily elegant and clear. It is this model that is disseminated among ice physicists at the present time.

Protonic charge carriers

Jaccard proceeded from the assumption that charge carriers in ice are protons. If we take a look inside an ice lattice (Fig. 6), we will discover that, for protons to be transferred at sizable distances (such motion is necessary for dc flow), they must go through a succession of jumps, both along hydrogen bonds and from bond to bond. It is obvious that there is no such opportunity for protons in a defect-free ice structure. Indeed, any hopping along the bond from one molecule to another will create H_3O^+ and OH^- ions, and any jump from one bond to another will give rise to a pair of Bjerrum defects: L- and D-defects. Both H_3O^+ and OH^- ions and Bjerrum defects will be discussed in another report (see *Foreword*).

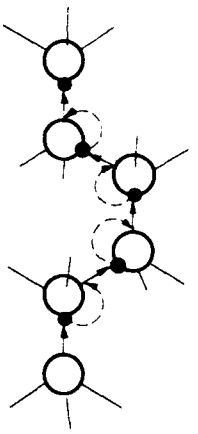

Figure 6. Chain of water molecules in the ice I_h structure. Successive hops of the proton along the hydrogen bonds and between them are forming charge transfer under the action of the electric field.

Since the creation of each pair of such defects requires energy of approximately 1 eV, the process of proton transfer via the creation of defects by the field turns out to be possible only in extremely strong electric fields.

$$E \gtrsim \frac{1\ \text{eV}}{e \cdot a} \sim 3 \times 10^{10}\ \text{V/m} \tag{25}$$

Actually, in a real situation, the application of an electric field does not give rise to new protonic charge carriers, but sets in motion the already existing ions and Bjerrum defects. The structure of hydrogen bonds, along which the protons move, represents itself as a three-dimensional grid. The transfer along this grid of any of the above four charge carriers reorients water molecules in such a fashion that the second defect of the same type cannot pass along the same path in the same direction.

To understand better what happens to water molecules' orientation under ionic and Bjerrum defect transfer, let us consider the track of an arbitrary charge carrier, a positive ion—H_3O^+ for instance. When we are speaking about ionic or Bjerrum defect transfer, it is important to keep in mind that it is just a convention—as a matter of fact, oxygen atoms do not hop from one molecular site to the next one. Only protons move; plus there is a small redistribution of electronic density at neighboring molecules, since a proton is a powerful center of attraction for external valence electrons. Thus, when speaking about H_3O^+ motion we have in mind that a characteristic distribution of three protons near the oxygen atom shifts in space. This is a convenient convention.

So, let us make an ion (H_3O^+) track into a straight line for simplicity and follow the reorientation of water molecules as the ion moves from left to right, as shown in Figure 7. Comparison

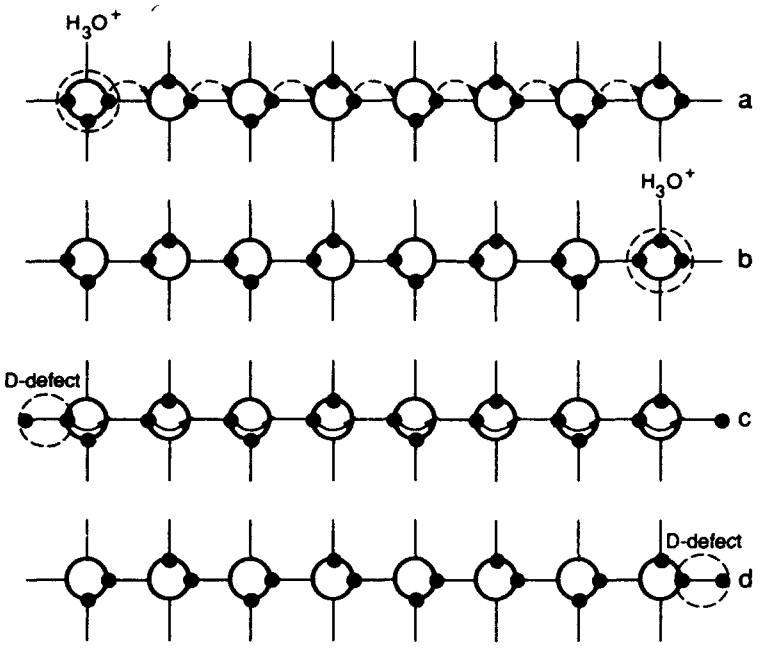

Figure 7. Schematic representation of H_3O^+ ion (a, b) and D-defect (c, d) motion along a chain of hydrogen bonds in ice. a) Initial arrangement of H_3O^+ ion and water molecules in the chain before the ion moves from the left to the right. The arrows indicate successive proton hops (along the bonds) by means of which the ion moves. b) The chain after the ion has passed. Obviously, no one H_3O^+ ion can go along the same chain in the same direction. c) D-defect motion from left to right along the same chain. The arrows indicate successive hops of protons from one bond to the next. d) The chain after the D-defect has passed. Comparison with Figure 7a shows that the motion of D-defect restored positions of the protons along the chain. It is ready (or "open") now for the passage of another H_3O^+ ion.

of Figures 7a and 7b leads us to two simple conclusions. First, the ion's ability to jump right or left is determined by the orientation of the molecules on the left and right of the ion. Let us designate the concentration of water molecules that enables an ion to jump to the right n_{right} and to the left n_{left}. Secondly, ionic motion to the right switches all molecules on the way from n_{right} to n_{left}. Of course, the reverse holds for motion to the left. These simple observations, as it turns out, are sufficient to derive equations that describe ion fluxes in ice.

Let us consider the direction of ion motion from left to right as positive, and ice to be composed of tracks such as those shown in Figure 7, which of course is schematic. It is obvious that total ionic flux to the right j_1 will be proportional to 1) the frequency of protons' attempts to jump along bond ν_h, 2) ionic concentration n_1, 3) the difference between water molecule concentration (n_{right}–n_{left}) and 4) the length of jump, i.e., the distance between two water molecules r_{oo} (O–O distance).

$$j_1 \propto n_1 \left(n_{right} - n_{left}\right) \nu_h \, r_{oo} \,. \tag{26}$$

In fact, instead of n_{right} and n_{left}, we should use their ratio to the total concentration of water molecules, n_{H2O}, which is equal to the probability of finding a molecule in either the n_{right} or in the n_{left} group.

$$j_1 \propto n_1 \left(n_{\text{right}} - n_{\text{left}}\right) v_h \, r_{oo} / n_{H_2O} \,. \tag{27}$$

Since, at first, before the current passage

$$n_{\text{right}} \equiv n_{\text{left}} \tag{28}$$

and the difference between these concentrations is just equal to the difference in the number of jumps that have already occurred to the left and to the right in a unit volume

$$n_{\text{right}} - n_{\text{left}} = \sum \begin{pmatrix} \text{jumps} \\ \text{to the left} \\ \text{since beginning} \\ \text{of motion} \end{pmatrix} - \sum \begin{pmatrix} \text{jumps} \\ \text{to the right} \\ \text{since beginning} \\ \text{of motion} \end{pmatrix} \tag{29}$$

then it is obvious that

$$n_{\text{right}} - n_{\text{left}} \propto -\frac{1}{r_{oo}} \int_0^t j_1(t)\,dt \tag{30}$$

where integration is held over t.

In the initial moment of time $t = 0$, the water molecules had no distinguishing orientation. For the sake of notation simplicity, let us designate the integral in eq 30 as Ω

$$\Omega(t) = \int_0^t j_1(t)\,dt \,. \tag{31}$$

Then, substituting eq 31 and 30 into 27

$$j_1(t) \propto - n_1 v_1 \, \Omega(t) \,.$$

Using v_h from eq 15a and 15b, derived for such ion jumps ($a = r_{oo}$), we obtain

$$j_1(t) \propto -\frac{n_1 \mu_1}{e_1 n_{H_2O}} k_B T \, \frac{\Omega(t)}{r_{oo}^2} \tag{32}$$

where e_1 denotes the effective charge carried by the ions. Since $n_{H_2O} \propto \frac{1}{r_{oo}^3}$ we get the ultimate result

$$j_1(t) = \phi \Omega \left(\frac{n_1 \mu_1}{e_1}\right) \tag{33}$$

where factor $\phi = \xi \, k_B T \, r_{oo}$. A dimensionless term, ξ cannot be found from such a simple schematic consideration.

This simple analysis reflects most of the significant physical aspects of ion transfer in ice, but does not take into account the complex, three-dimensional structural topology of the ice crystal lattice. The strict analysis is extremely difficult and time-consuming and has not yet been carried out. Jaccard was the first to give a theoretical consideration yielding ξ in 1959 and again in 1964. The results obtained by Jaccard (1964) gave

$$\xi = 16/\sqrt{3} \approx 9.238 \tag{34}$$

regardless of defect types.

In the previous paper, Jaccard (1959) found that for ion transfer

$$\xi = 32/(3\sqrt{3}) \approx 6.16 \tag{35}$$

and for Bjerrum defects transfer

$$\xi = 3\sqrt{3} \approx 5.2\,. \tag{36}$$

Currently, we prefer to use the results obtained by Hubman (1979a, b) from the analysis of a large number of experimental data

$$\xi = 3.85 \pm 5\%\,. \tag{37}$$

Careful theoretical treatment conducted by Nagle (1974) showed that the predicted theoretical anisotropy of the dielectric properties of ice should be of the order of 10^{-4}, if any. As we will see later, it is the constant ϕ that yields the magnitude of the dielectric permittivity, so we will consider it to be isotropic, i.e., scalar, and extend our particular result (eq 33) to three dimensions.

$$\vec{j_1}(t) = -\phi\,\vec{\Omega}\left(\frac{n_1 \mu_1}{e_1}\right) \tag{38}$$

where

$$\phi \approx 3.85\, k_B T\, r_{oo} \tag{39}$$

and $\vec{\Omega}$, which we will call a configurational vector from now on

$$\vec{\Omega}(t) = \int_0^t \vec{j_1}(t)\,dt\,. \tag{40}$$

Thus, we have discovered that ion fluxes (eq 38) in ice depend upon a "prehistory" of ion motion (eq 40). Let us see what else it leads to.

Electrical properties—one type of charge carrier

What kind of conductivity and dielectric-permittivity properties should ice with one type of charge carrier (H_3O^+) ions exhibit?

Let us start with ice behavior in a constant electric field. Let an electric field $E = E_o$ be applied to ice in the initial moment of time $t = 0$ and the ice be unpolarized at $t = 0$. Let us find current density J as a function of time—the total current is a sum of currents caused by the electric field and special flux from eq 38

$$\begin{cases} J = e_1 j_1 \\ j_1 = (e_1 E - \phi\Omega)\dfrac{\sigma_1}{e_1^2}; \qquad \sigma_1 = e_1 \mu_1 n_1\,. \\ \Omega = \displaystyle\int_0^t j_1(t)\,dt; \quad E = E_o \end{cases} \tag{41}$$

The solution of this simple system of equations yields an exponentially decaying current

$$J(t) = J_o \exp\{-t/t_D\} \tag{42}$$

$$1/\tau_D = \frac{\phi \sigma_1}{e_1^2} \tag{43}$$

$$J_o = \sigma_1 E_o . \tag{44}$$

Thus, a stable current does not exist in this system. Relaxation time τ_D is called Debye relaxation time. As ions shift subject to E, an opposite flux arises, caused by an increasing number of water molecules oriented in such a fashion that ion motion against the field is stimulated.

In a state of equilibrium ($t = \infty$), these two fluxes cancel each other completely. In a particular sense, the value $\vec{\Omega}$, a configurational vector, is similar to a force field acting upon ions. The dielectric properties of ice are determined by rising polarization P

$$\vec{P} = \sum e_i \vec{r}_i; \quad \frac{d\vec{P}}{dt} = \dot{\vec{P}} = \sum e_i \vec{v}_i = \vec{J} \tag{45}$$

where the summation is over all mobile charges. Using eq 42 and initial condition $\vec{P}(0) = 0$, we see that

$$\vec{P}(t) = \int_0^t \vec{J}(t)\,dt = \vec{J}_o \tau_D \left[1 - e^{-t/\tau_D}\right]. \tag{46}$$

The stationary magnitude of polarization ($t = \infty$)

$$\vec{P} = \vec{J}_o \tau_D = \frac{e_1^2}{\phi} \vec{E} = \varepsilon_o \chi \vec{E} . \tag{47}$$

In an external electric field there also arises polarization that is not associated with ion displacements, but is caused by a redistribution of charges inside the molecule

$$\vec{P}_e = \varepsilon_o \chi_e \vec{E} . \tag{48}$$

The usual time taken to produce such polarization is comparable to a period of internal molecular vibrations. Hence this polarization is very "fast." The total polarization P_t

$$\vec{P}_t = \vec{P}_e + \vec{P} = \varepsilon_o (\chi_e + \chi) \vec{E} = \varepsilon_o \chi_t \vec{E} . \tag{49}$$

The entire relative dielectric permittivity of ice is then

$$\varepsilon_s = 1 + \chi_t = 1 + \chi + \chi_e = \varepsilon_\infty + \chi \tag{50}$$

where we denote the "fast" part of ε_s as ε_∞. This part of the permittivity has no connection to the motion of defects and it determines the dielectric properties of ice at "high" frequencies when $\omega >> 1/\tau_D$. From eq 50 and 47

$$(\varepsilon_s - \varepsilon_\infty) = e_1^2/\varepsilon_o \phi . \tag{51}$$

One can easily check that $\varepsilon_s - \varepsilon_\infty$ is about 10^2.

Other charge carrier transfers and their effective charges

Let us look now at what happens when other protonic charge carriers move. First, we should introduce a particular formalism. Let 1, 2, 3, 4 represent H_3O^+ and OH^- ions, and D- and L-defects respectively. Thus e_3, for instance, denotes the electric charge of a D-defect and n_2 stands for OH^- ion concentration. Figure 7 shows what happens in a water molecule chain (discussed above) if an H_3O^+ ion or D-defect moves along it. As can be seen from this sketch, the effect of a D-defect is quite opposite to that of an H_3O^+ ion. Using the same consideration as in Figure 7, we can see that the motion of an L-defect causes the same reorientation of hydrogen bonds in a chain as in the case of H_3O^+, while an OH^- ion causes the opposite reorientation, all defects moving in the same direction. Therefore, in the case when all four charge carriers are present, we should take into account all four fluxes affecting the formation of the configuration vector $\vec{\Omega}$. Keep in mind the sign change mentioned above.

$$\vec{\Omega}(t) = \int_0^t (\vec{j_1} - \vec{j_2} - \vec{j_3} + \vec{j_4})dt \ . \tag{52}$$

If we introduce $\eta_i = (1, -1, -1, 1)$, $i = 1, 2, 3, 4$, then

$$\vec{\Omega} = \int_0^t \left(\sum_{i=1}^{4} \eta_i \vec{j}_i \right) dt \ . \tag{53}$$

Accordingly, the direction of defect fluxes caused by molecular reorientation is different for different defects. Having conducted the same consideration as in the case of H_3O^+ ions, we will find

$$\vec{j}_i = \left(e_i \vec{E} - \eta_i \phi \vec{\Omega} \right). \tag{54}$$

Equations 53 and 54 express in mathematical terms the fact that a flux of particular defects in ice is determined not only by the magnitude and the direction of the applied electrical field, but by the history of motion of all charge carriers as well!

Let us touch on the question of the value of a charge carried by defects. Since H_3O^+ and OH^- ions and L- and D-defects are created and annihilated in couples, it is obvious that

$$e_1 = -e_2 \text{ and } e_3 = -e_4 \ . \tag{55}$$

If we place an extra "foreign" proton into an otherwise normal ice lattice, we will inevitably obtain two carriers at once: an H_3O^+ ion and a D-defect, as shown in Figure 8. Hence the sum of those charges equals a proton charge e

$$e_1 + e_3 = e \ . \tag{56}$$

To find out how an elementary proton charge is shared between an ion and a D-defect, we must consider two circumstances: 1) a fraction of the intermolecular distance that a proton travels, in case of ions and Bjerrum defect transfer, and 2) displacement of electron density, when a charge carrier is moving along the chain.

The most strict theoretical analysis of this problem was conducted by Scheiner and Nagle (1983), who found that

$$e_3 = (0.36 \pm 03)e \ . \tag{57a}$$

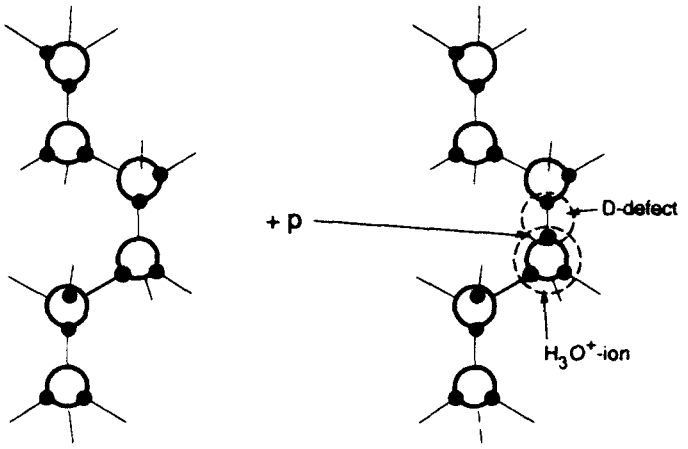

Figure 8. Creation of two point defects (H_3O^+ ion and D-defect) when a proton is placed into a defect-free ice lattice.

The other way to find e_1 and e_3 is experiment. As we have seen (eq 51), the charge of the predominant defect is incorporated into the formula for ε_s. Using this fact and analysis of experimental data of measurements of ε_s for specially doped ice (in such fashion, that either ions or Bjerrum defects predominated), Hubman (1979a, b) has found

$$e_3 = (0.38 \pm 0.01)e \tag{57b}$$

which is also remarkably close to the calculations of Scheiner and Nagle. Other experimental results for e_3 and e_1, obtained during recent years, are found later in Table 3. These results are close to those represented in eq 57a and 57b.

General consideration of Jaccard's model with four kinds of carriers

Let us now try to find a mathematical description of σ and ε as functions of frequency for ice containing all four kinds of charge carriers, with charges e_i, mobilities μ_i and concentration n_i (i = 1, 2, 3, 4). We will designate through σ_i their partial conductivities.

$$\sigma_i = |e_i| \mu_i n_i . \tag{58}$$

The main condition restricting the universality of this consideration will be a requirement of uniformity of ice, i.e., the ice has no boundaries (is infinite) and the distribution of charge carriers is uniform

$$\text{grad } n_i = 0 . \tag{59}$$

Equation 59 defines the absence of diffusion fluxes of particles and the independence of all functions from coordinates. We will also consider that ice is electrically neutral, i.e., there are no space charges.

Suppose an oscillating electric field is applied to ice

$$\tilde{E} = E \exp(i\omega t) \tag{60}$$

where ω = the cyclic frequency $\omega = 2\pi f$
t = time
i = $\sqrt{-1}$
"~" = complex value, as usual.

The total density of electric current J is the sum of the drift current J_{dr} and the displacement current J_{dis}

$$\tilde{J} = \tilde{J}_{dr} + \tilde{J}_{dis} \tag{61}$$

$$\tilde{J}_{dis} = e_0 e_\infty \frac{d\tilde{E}}{dt} . \tag{62}$$

The drift current results from fluxes of all particles

$$\tilde{J}_{dr} = \sum_{i=1}^{4} e_i \tilde{j}_i \tag{63}$$

$$\tilde{j}_i = \left(e_i \tilde{E} - \eta_i \phi \tilde{\Omega}\right) \frac{\sigma_i}{e_i^2}; \quad i = 1, 2, 3, 4 \tag{64}$$

$$\vec{\Omega} = \int_0^t \sum_{i=1}^{4} \left(\eta_i \tilde{j}_i\right)\left(\eta_i \tilde{j}_i\right) dt . \tag{65}$$

This system of equations (eq 61–65) fully defines our problem for eight unknown functions $\tilde{J}_{dis}$, $\tilde{J}_{dr}$, $\tilde{J}$, $\tilde{\Omega}$, $\tilde{j}_1$, $\tilde{j}_2$, $\tilde{j}_3$, $\tilde{j}_4$. We will look for solutions for some function $\tilde{f}(\omega, t)$ as usual in the form

$$\tilde{f}(\omega, t) = \tilde{f}(\omega) \exp\{i\omega t\} \tag{66}$$

where $\tilde{f}(\omega)$ is an amplitude of oscillations of variable $\tilde{f}$. Since the system made up of eq 61–65 is linear, after substitution of eq 66 and canceling coefficients $\exp\{i\omega t\}$, we obtain a rather simple system of algebraic equations. The procedure of finding solutions is routine and we present it here in ultimate form

$$\tilde{\sigma}(\omega) = \frac{\tilde{J}}{\tilde{E}} = \sigma_s - \frac{i\omega\tau_D\left(\sigma_\infty - \sigma_s\right)}{1 - i\omega\tau_D} \tag{67}$$

$$\tilde{\varepsilon}(\omega) = \frac{\tilde{J}}{\varepsilon_0 \dfrac{\partial \tilde{E}}{\partial t}} = \varepsilon_\infty + \frac{\varepsilon_s - \varepsilon_\infty}{1 - i\omega\tau_D} . \tag{68}$$

We have introduced new terms

$$\sigma_\infty = \sum_{i=1}^{4} \sigma_i \tag{69}$$

$$e^2/\sigma_s = \frac{e_1^2}{\sigma_1 + \sigma_2} + \frac{e_3^2}{\sigma_3 + \sigma_4} \tag{70}$$

$$\tau_D^{-1} = \omega_D = \phi\left[\frac{\sigma_1+\sigma_2}{e_1^2} + \frac{\sigma_3+\sigma_4}{e_3^2}\right] \tag{71}$$

$$\varepsilon_s = \varepsilon\infty + \frac{1}{\varepsilon_0\phi}\left(\frac{\sigma_1+\sigma_2}{e_1} - \frac{\sigma_3+\sigma_4}{e_3}\right)^2 \Big/ \left(\frac{\sigma_1+\sigma_2}{e_1^2} + \frac{\sigma_3+\sigma_4}{e_3^2}\right)^2. \tag{72}$$

From eq 67 and 68 one easily obtains real parts of σ and ε

$$\sigma'(\omega) = Re\,[\sigma(\omega)] = \sigma_s + \frac{(\sigma_\infty - \sigma_s)(\omega\tau_D)^2}{1+(\omega\tau_D)^2} \tag{73}$$

$$\varepsilon'(\omega) = Re\left[\tilde{\varepsilon}(\omega)\right] = \varepsilon_\infty + \frac{\varepsilon_s - \varepsilon_\infty}{1+(\omega\tau_D)^2}. \tag{74}$$

We are most interested, of course, in analysis of eq 73 and 74, describing the real parts of σ and ε. Now we will proceed to this analysis.

Analysis of Jaccard's results

Despite the complicated form of eq 73 and 74 at first glance, they have very simple asymptotics, namely

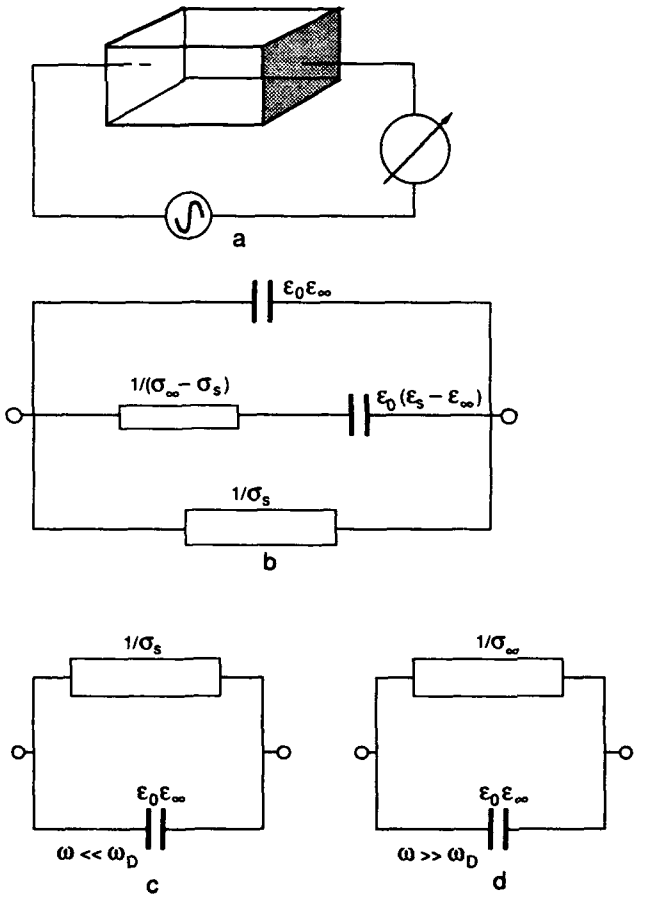

Figure 9. Ice sample connected into measuring circuit (a) and its electrical equivalent circuits (b–d).

$$\lim_{\omega \to 0} \sigma'(\omega) = \sigma_s; \quad \lim_{\omega \to \infty} \sigma'(\omega) = \sigma_\infty; \tag{75}$$

$$\lim_{\omega \to 0} \varepsilon'(\omega) = \varepsilon_s; \quad \lim_{\omega \to \infty} \varepsilon,(\omega) = \varepsilon_\infty; \tag{76}$$

Plots of the functions $\sigma'(\omega)$ and $\varepsilon'(\omega)$ are depicted in Figures 2 and 5; solid lines are drawn for the values of parameters: $\tau_D = 5.06 \times 10^{-5}$ s, $\sigma_\infty = 1.9 \times 10^{-5}\ \Omega^{-1}\ m^{-1}$, $\sigma_s = 3 \times 10^{-8}\ \Omega^{-1}\ m^{-1}$, $\varepsilon_\infty = 3.16$, $\varepsilon_s = 100.8$.

The transition from low-frequency (s) to high-frequency (∞) values occurs in the vicinity of the Debye frequency $f_D = \omega_D/2\pi = 1/2\,\pi\,\tau_D \cong 3.14$ kHz (Fig. 2 and 5).

For clarity we can devise an equivalent circuit having the same frequency response as a cube of ice with sides of 1 m (Fig. 9).

If we take a look at eq 69, we see that high-frequency conductivity σ_∞ is determined by the greatest partial conductivity among σ_i. Usually, it is σ_4 in pure ice for $T \gtrsim -50°$C, i.e., conductivity of L-defects. The fact that σ_∞ incorporates all σ_i in an additive fashion implies that at high frequencies ($\omega >> \omega_D$) charge carriers move independently of each other. One can imagine this situation as a parallel connection, as shown in Figure 10a. At frequencies much smaller than ω_D and for direct currents, reverse values of conductivities rather than conductivities are summed up (eq 70) for ions $\sigma_1 + \sigma_2$ and Bjerrum defects $\sigma_3 + \sigma_4$. This is common to series circuits, as shown in Figure 10b. Such conductivity σ_s is controlled by the smaller of two conductivities: ionic $\sigma_{ion} = \sigma_1 + \sigma_2$ or Bjerrum defects $\sigma_B = \sigma_3 + \sigma_4$. In pure ice at relatively high temperatures ($T \lesssim -50°$C), it is ionic conductivity. The character of σ_s is attributable to the fact that in the case of dc conductivity, carriers' fluxes must be stationary. Since E is constant, then Ω also must be constant, as can be seen from eq 64. This is possible only under conditions of

$$j_1 - j_2 - j_3 + j_4 = 0 \tag{77}$$

from which (noting that $J_{ion} = e_1\,[j_1 - j_2]$ and $J_B = e_3\,[j_3 - j_4]$) we obtain

$$\frac{J_{ion}}{e_1} = \frac{J_B}{e_3} \tag{78}$$

i.e., ionic and Bjerrum defect currents are approximately the same. Under this condition (eq 78) all hydrogen bonds restore the initial position from time to time. As we have seen, if an ionic current "locks" chains of hydrogen bonds, then a Bjerrum defect current "unlocks" them, and vice versa. Using an equivalent electrical circuit in ice, shown in Figure 9b, we can easily obtain a time dependence of current through the ice specimen when a rectangular voltage pulse is applied ($E = 0$ when $t < 0$; E = constant when $t \geq 0$), portrayed in Figure 3. Of course, we could obtain the same dependence from the system of made up eq 61–65 at given initial conditions. In the *Relaxation Times of Electric Polarization and Electric Fields in Ice* section, we also will consider effect of boundary conditions on the electric relaxation in ice.

Let us analyze now how we can account for a large, static dielectric permittivity of ice ε_s. In Jaccard's model, dipole moments of water molecules do not appear! This is an advantage since the concept of molecular dipole moments in ice has proven to be a complicated issue (Nagle 1979).

The polarization $\vec{P}$ is defined in terms of the spatial displacements of charge carriers, as can be seen from eq 45. Large electrical polarization arises during a time interval of about τ_D after an electric field has been applied and is determined by displacements of the majority charge

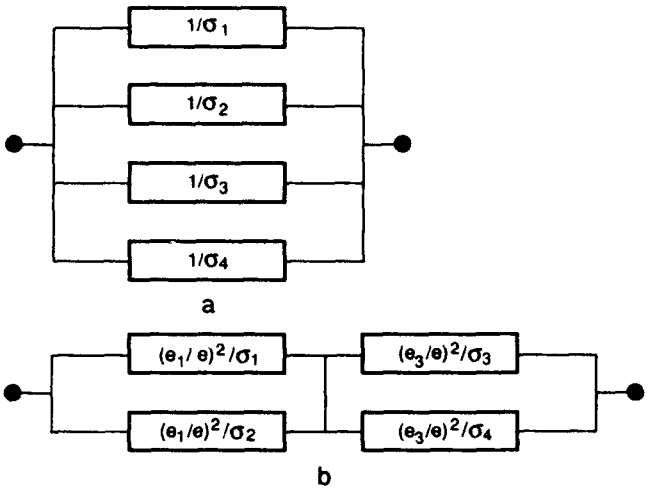

Figure 10. Equivalent electrical circuit for high-frequency conductivity σ_∞ (a) and for static or low-frequency conductivity σ_s (b).

carriers (usually Bjerrum defects) under the action of the electric field. This displacement grows until a force resulting from $\vec{\Omega}$ balances the electric field force. The balance is achieved within a characteristic time interval τ_D, which, as can be seen from eq 71, is also defined in terms of conductivity of majority charge carriers. It is interesting to compare τ_D with the well-known Maxwell relaxation τ_M, which is the case when the only restoring force is the electric field originating from electrical charges building up

$$\tau_M = \varepsilon_0 \varepsilon_\infty / \sigma_\infty \,. \tag{79}$$

At $T \equiv -10°C$, τ_M comes out to be about 30 times smaller than τ_D! In other words, $\vec{\Omega}$ is not such an efficient restoring force. It is useful to estimate an average displacement of majority charge carriers $\langle x \rangle$, building up the polarization of ice

$$P = \varepsilon_0 \chi E = e_4 \langle x \rangle n_4 \tag{80}$$

$$\langle x \rangle = \frac{\varepsilon_0 (\varepsilon_s - 1)}{e n_4} \,. \tag{81}$$

For typical values of $E \sim 10^2$ V m^{-1} and $n_4 \sim 10^{21}$ m^{-3} (–10°C), we obtain

$$\langle x \rangle \sim 10^{-9} \text{ m} = 10 \text{ Å} \tag{82}$$

i.e., $\langle x \rangle$ is quite microscopic. Notice also that $\langle x \rangle << n_4^{-1/3} \approx 10^{-7}$ m is the average distance between L-defects. Hence, we see that the defects move independently.

In the conclusion of this section, we will derive formulas for so-called Cole–Cole diagrams (Cole and Cole 1941), which are frequently used for experimental data analysis. From eq 68

$$\tilde{\varepsilon}(\omega) = \varepsilon'(\omega) + i\varepsilon''(\omega) \tag{83}$$

where $\varepsilon'(\omega)$ is given by eq 74 and

$$\varepsilon''(\omega) = \frac{\varepsilon_s - \varepsilon_\infty}{1 + \omega^2 \tau_D^2} \omega \cdot \tau_D \,. \tag{84}$$

It is easy to verify that ε' and ε'' are connected by the relationship

$$\left[\varepsilon' - \left(\frac{\varepsilon_s - \varepsilon_\infty}{2}\right)\right]^2 + (\varepsilon'')^2 = \left(\frac{\varepsilon_s - \varepsilon_\infty}{2}\right)^2 \tag{85}$$

which can be represented graphically as a semicircle, portrayed in Figure 11.

If experimental data closely fit the Cole–Cole diagram, it is strong evidence in favor of an existing relaxation process with only one relaxation time.

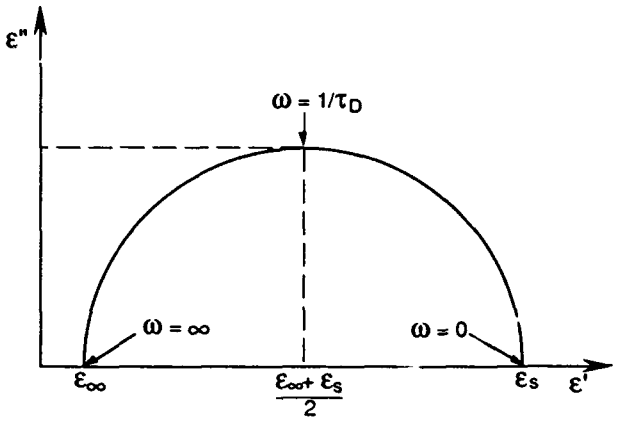

Figure 11. Cole–Cole diagram.

ELECTRICAL PROPERTIES OF ICE OF FINITE SIZE

In previous paragraphs, we have conducted a theoretical treatment of the electrical properties of ice that has no boundaries and is absolutely uniform. In practice, this is an unattainable ideal, and attempts to compare such a "uniform" theory with experimental results can raise doubts about the credibility of this theory, although this theory plays no role in that.

For electrical measurements to be carried out, ice specimens must be put into particular electrical circuits. This cannot be done without creating some kinds of interfaces, such as ice/dielectric, ice/metal, ice/semiconductor, ice/protonic conductor or even ice/plasma. The presence of these interfaces causes considerable change in the simple dispersions $\sigma(\omega)$ and $\varepsilon(\omega)$, depicted in Figures 2 and 5. However, as we will see later, extra dispersions appearing in these experiments allow us to determine the concentrations and mobilities of numerous charge carriers in ice. In practice, it turns out to be extremely difficult to accomplish an efficient electric charge exchange between metallic electrodes (which are electronic conductors) and ice, which, as mentioned above, is a protonic conductor. Ways to achieve such an exchange will be discussed later.

It is much easier to suppress such an exchange completely, by placing a thin dielectric film between ice and electrode. The thinner the film, the smaller its contribution to measurements. A thin oxidized layer of Al_2O_3, i.e., sapphire, at the surface of an Al electrode, or SiO_2 at the surface of a silicon electrode, can successfully play the role of such a thin film. These electrodes are called perfectly blocking, and the electrical properties of ice with such electrodes were theoretically, exhaustively considered by Petrenko and Ryzhkin (1984a).

Experimentally, $\varepsilon'(\omega)$ is determined from the capacitance $C(\omega)$ of the capacitor in which the ice specimen to be investigated acts as a dielectric

$$\varepsilon'(\omega) = \frac{LC(\omega)}{\varepsilon_0 S} \tag{86}$$

where we consider a rectangular ice specimen of length L, directed along the x coordinate and cross section s. Two perfectly blocking electrodes have the same area s and are located at $x = 0$ and $x = L$. The problem of finding $\varepsilon'(\omega)$ is then reduced to finding $C(\omega)$ for a plane capacitor. Let us suppose that an ice specimen has ideal blocking electrodes that are connected to an ac circuit so that a surface density of electric charge on the blocking electrodes varies with time according to the harmonic law $\propto \exp\{-i\omega t\}$. We can describe this charge as a function of time t and coordinate x as

$$\rho_o(x,t) = \left[\delta(x) - \delta(x-L)\right] \sigma_{sc} \exp\{-i\omega t\} \tag{87}$$

where $\delta(x)$ is a delta function and σ_{sc} is an amplitude of the surface charge on the electrodes.

From the capacitance determination

$$C(\omega) = Re\left[s\sigma_{sc}/\Delta\varphi(\omega)\right] \tag{88}$$

where $\Delta\varphi(\omega)$ is the amplitude of the potential difference.

$$\Delta\varphi(t) = \Delta\varphi(\omega)\exp\{-i\omega t\}. \tag{89}$$

Now, to find $\Delta\varphi(\omega)$ we have to write a closed system of equations for all the quantities connected with the electric field in ice. There are ten such quantities: $E(x,t)$ and $\Omega(x,t)$ are, respectively, the projections of the electric field strength and the configuration vector onto the x-axis; $n_i(x,t)$ are the concentrations of the defects ($i = 1, 2, 3, 4$), and $j_i(x,t)$ are the projections of the densities of the defect fluxes onto the x-axis. This problem is different from the one considered above in two ways. First, by the presence of a space charge, we have to add the Poisson equation

$$\varepsilon_o \varepsilon_\infty \frac{\partial E}{\partial x} = \sum_{i=1}^{4} e_i \Delta n_i + \rho_o(x,t) \tag{90}$$

where $\Delta n_i = (n_i - n_{io})$, n_{io} being the original concentrations of the defects when $E = 0$.

The second difference from the homogeneous problem is the appearance of diffusion terms in the equations for the defect fluxes

$$j_i = \left(e_i E - \eta_i \phi\Omega\right)\frac{\sigma_i}{e_i^2} - D_i \frac{\partial(\Delta n_i)}{\partial x}; \quad (i = 1, 2, 3, 4). \tag{91}$$

Adding four continuity equations

$$\frac{\partial \Delta n_i}{\partial t} + \frac{\partial j_i}{\partial x} = 0, \quad i = 1, .. 4 \tag{92}$$

and an equation for the configuration vector, we obtain

$$\frac{\partial \Omega}{\partial t} = \sum_{i=1}^{4} \eta_i j_i. \tag{93}$$

Thus, we get the closed system of ten equations (eq 90–93). This system can be solved in a linear approximation when $|e_i\Delta\varphi| << k_B T$, when we can substitute σ_i in the two equations (eq 91) by making σ_{io} = constant. In this case, by employing the Fourier transform in x, we shall switch over to a system of algebraic equations that are easily solvable. We are not going to frighten the

reader with this procedure—we will only show the results obtained in that way. The case of $|e_i\Delta\varphi| >> k_BT$ will be analyzed below in the *Field Effect Transistor Made of Ice* section.

Low-frequency limit-screening lengths

With $\omega\to 0$ an electric field inside the ice specimen is distributed in accordance with the presence of two screening lengths, $1/\kappa_1$ and $1/\kappa_2$

$$E(x) = \frac{\sigma_{sc}}{2\varepsilon_0}\left[\frac{1}{\varepsilon_\infty}\left(\exp^{-\kappa_1 x} + \exp^{-\kappa_1(L-x)}\right) + \frac{1}{\varepsilon_s}\left(\exp^{-\kappa_2 x} + \exp^{-\kappa_2(L-x)}\right)\right] \tag{94}$$

In the case when Bjerrum defects are majority charge carriers

$$\kappa_1 \equiv \left[\frac{e_3^2\,(n_{30}+n_{40})}{\varepsilon_0\varepsilon_\infty k_B T}\right]^{1/2}; \quad \kappa_2 \equiv \left[\frac{e^2\phi\,(n_{10}+n_{20})}{e_3^2\,k_B\,T\varepsilon_\infty}\right]^{1/2}; \quad \varepsilon_s \equiv \frac{e_3^2}{\varepsilon_0\phi} \tag{95}$$

Figure 12 shows the electric field E inside the ice specimen. At the screening length κ_1^{-1}, which is determined by the concentration of majority carriers $(n_{30}+n_{40})$ and coincides with the well-known expression for the Debye screening length κ_1^{-1}, the field drops down from the original value $\sigma_{sc}/\varepsilon_0\varepsilon_\infty$ to $\sigma_{sc}/\varepsilon_0\varepsilon_S$. As we have seen, $\varepsilon_S \approx 10^2$, i. e., κ_1^{-1} is a characteristic length at which ε_S attains a steady-state value. At large x the field drops down to zero because of screening by minority charge carriers, i.e., ions with a larger characteristic screening length κ_2^{-1} determined by ion concentrations $(n_{10}+n_{20})$.

Figure 13 shows an "apparent" static $(\omega\to 0)$ dielectric permittivity of ice ε' as a function of a specimen length L. First of all, notice that the only value of the permittivity for ice of thickness $L << \kappa_1^{-1}$ is ε_∞ so that the Debye dispersion (Fig. 5) disappears. Notice also that, using experimental dependence $\varepsilon'(0, L)$, we can determine κ_1 and κ_2, i.e., $(n_{10}+n_{20})$ and $(n_{30}+n_{40})$.

Ignoring the dependence of ε on sample thickness L can result in significant errors when ε is measured at low temperatures for which κ^{-1} and L are comparable. Since within surface layers

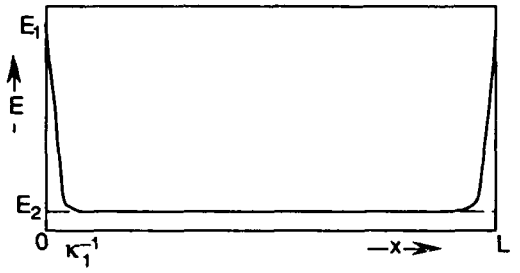

a. Only Bjerrum defects are taken into account.

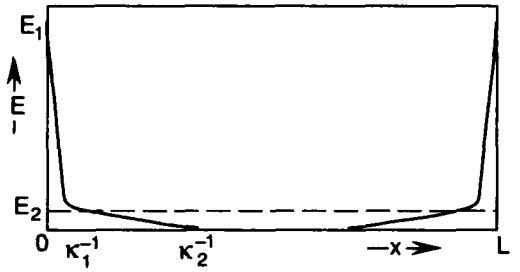

b. Bjerrum defects and ions are considered.

Figure 12. Distribution of static electric field E *inside the ice sample;* $E_1 = \sigma_{sc}/\varepsilon_0\varepsilon_\infty$ $E_2 = \sigma_{sc}/\varepsilon_0\varepsilon_s$ *(after Petrenko and Ryzhkin 1984a).*

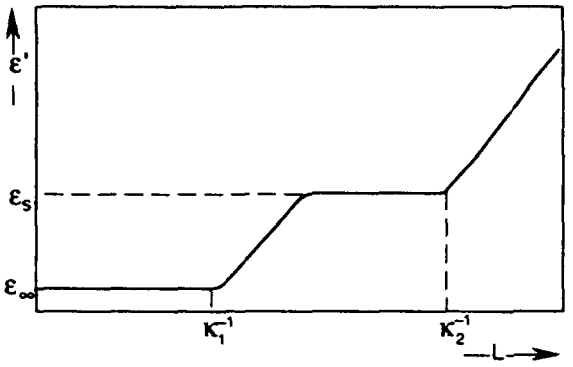

Figure 13. Dependence of apparent static dielectric permittivity ε′ on ice thickness L. L-defects and H_3O^+ ions attend (after Petrenko and Ryzhkin 1984a).

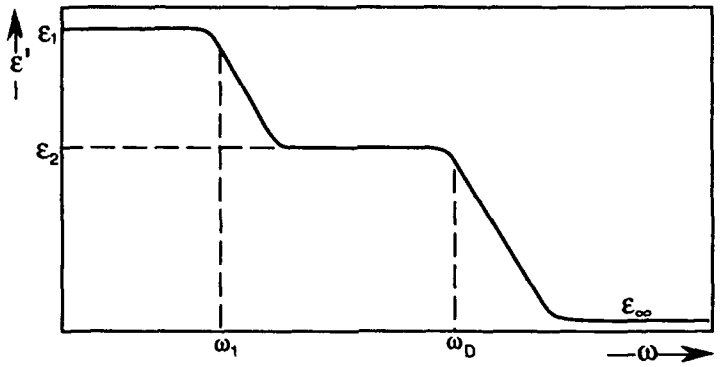

Figure 14. Dependence of apparent static dielectric permittivity ε′ on circular frequency ω. L-defects and H_3O^+ ions attend (after Petrenko and Ryzhkin 1984a).

of thickness κ_1^{-1} the permittivity is $\varepsilon_s/\varepsilon_\infty$ times smaller than in the bulk, it is necessary to take the dependence of ε from L into account for $L \leq \varepsilon_s/\varepsilon_\infty \kappa^{-1} \approx (0.5\text{–}1.0)$ mm at $T = 150$ K. However, that was a typical sample thickness used by many researchers to determine the critical temperature T_c in the Curie-Veiss law

$$\varepsilon_s \propto \frac{1}{T - T_c}. \tag{96}$$

Ignoring $\varepsilon_s(L)$ dependence could also be responsible for wide scattering of the experimental value of T_c (see the *Review of Experimental Results on Ice Conductivity and Dielectric Permittivity* section).

Frequency dependence of dielectric permittivity

As was shown theoretically by Petrenko and Ryzhkin (1984a), on ice/dielectric boundaries new dispersion "steps" appeared on the ε′(ω) plot. While the main Debye dispersion occurs at $\omega_D = 1/\tau_D$, where τ_D is a characteristic time of relaxation of majority charge carriers, three other characteristic frequencies correspond to relaxation times τ_i for three other types of charge carriers. In the paper referred to, an explicit solution was found for two types of charge carriers (for instance, L-defects and H_3O^+ ions). The frequency dependence for this case is shown in Figure 14, with some changes. The characteristic parameters indicated on Figure 14 are

$$\omega_1 = D_4 \kappa_2^2, \quad \omega_D = \phi\left(\sigma_1/e_1^2 + \sigma_4/e_4^2\right) \tag{97}$$

$$\varepsilon_2 = \varepsilon_\infty \left[\frac{\varepsilon_\infty}{\varepsilon_s} + \frac{1-\exp^{-\kappa_1 L}}{\kappa_1 L} \right]^{-1} \tag{98}$$

$$\varepsilon_1 = \varepsilon_\infty \left[\frac{1-\exp^{-\kappa_1 L}}{\kappa_1 L} + \frac{\varepsilon_\infty}{\varepsilon_s} \frac{1-\exp^{-\kappa_2 L}}{\kappa_2 L} \right]^{-1} . \tag{99}$$

Notice that the four equations above contain only four unknown quantities, namely, D_1, D_4, n_1 and n_4, since κ_1, κ_2, σ_1 and σ_4 are the functions of these variables. Therefore, we are able to determine all of them from an experimental curve $\varepsilon(\omega)$. Owing to the Einstein relation between D_i and μ_i ($\mu_i = |e_i| D_i / k_B T$), we find μ_i as well. This method was used by Zaretskii et al. (1987a) and Zaretskii (1991) to determine the mobilities of L-defects and of H_3O^+ ions.

CONCENTRATION OF CHARGE CARRIERS

So far, we have discussed conductivity provided by protonic defect motion in ice (ions and Bjerrum defects), unrelated to how such charge carriers can appear in ice. In fact, three sources of protonic charge carriers in ice are known. Two of those exist in a state of thermal equilibrium. They are, first, thermal generation of carriers, and second, atoms and molecules of impurities. The third source is various types of external excitation, such as strong electric fields, ultraviolet radiation or high-energy particle beams. We will begin our discussion of charge carrier concentration with a consideration of pure ice in a state of thermal equilibrium.

Intrinsic charge carriers

Mobile defects of a protonic subsystem in ice can be created by thermal fluctuations in a crystal lattice. As in the majority of solid materials (excluding some solid gases with extremely weak van der Waals bonds), the typical energy required for an intrinsic point defect pair to be created is about 1 eV. As we will see later, the activation energy in ice is about 1 eV for H_3O^+ and OH^- ions and about 0.68 eV is required for the creation of L- and D-defects. These values largely exceed the average energy of thermal vibration, $k_B T \approx 0.023$ eV (–10°C), and by primary inspection, the appearance of a large number of these defects is unjustified. However, it is common knowledge that the state of thermal equilibrium at constant temperature and volume is attained at a minimum of free energy F rather than at a minimum of internal energy U.

$$F = U - T \cdot S . \tag{100}$$

The appearance of defects increases internal energy U, of course, but owing to an increase in entropy S, the equilibrium is attained at some finite value of point defects concentration.

We can illustrate this point with a simple model example. Let us consider a crystal lattice consisting of N identical points (atoms, molecules or elementary cells). A point defect with activation energy E_o could appear at any of the points with equal probability. Then, the part of free energy ascribable to the appearance of defects will equal

$$F_d = E_o n - T S_c \tag{101}$$

where S_c in turn is the configurational entropy of defects in the lattice

$$S_c = k_B \ln W \tag{102}$$

and W is the number of arrangements of n identical defects over these N identical sites

$$W = \frac{N!}{n!(N-n)!}. \tag{103}$$

At equilibrium

$$\frac{\partial F_d}{\partial n} = 0. \tag{104}$$

Substituting eq 101–103 into 104 and using the Stirling formula

$$\ln(N!) \cong N \ln N - N \quad (N >> 1)$$

we obtain

$$\frac{n}{N-n} = \exp\left\{-\frac{E_o}{k_B T}\right\}. \tag{105}$$

Assuming $E_o >> k_B T$, $N >> n$, we get

$$n \cong N \exp\left\{-\frac{E_o}{k_B T}\right\}. \tag{106}$$

To be more precise, the appearance of a point defect not only changes the configurational entropy, but also affects the vibrational entropy because of a slight change in the elastic lattice vibration spectrum. This vibrational entropy change $-S_V$ would lead to an additional factor of $\exp\{S_V/k_B\}$ in eq 106, but as S_V is so small the factor is very close to unity and so will be omitted below.

Since the number of possible protonic configurations in ice is rather large, the calculation of S_c in ice is more complicated than in the above example. For ice with ionic defects, such a calculation was conducted by Ryzhkin (1985). Considering ice with ions, he first noticed that each water molecule could be in one of fourteen states: six orientations of neutral water molecules that correspond to the possible placement of two close protons at four hydrogen bonds (4!/2!2! = 6); four orientations of OH^- ions and four orientations of the H_3O^+ ion. Let the number of molecules in these states equal N_i (i = 1, 2,...14); then the full number of arrangements of N molecules over these states equals

$$N! / \prod_{i=1}^{14} N_i! . \tag{107}$$

Among that number there are "right" configurations with one proton on each bond and "wrong" ones with two protons or without any protons. The probability of finding a right bond equals 1/2. Therefore, for the number of right configurations, we obtain

$$W = (1/2)^{2N} N! / \prod_{i=1}^{14} N_i! \tag{108}$$

where $2N$ is the number of bonds. In an isotropic case we have

$$N_1 = N_2 ... = N_6 = (N - 2n_i)/6; \quad N_7 = N_8 ... = N_{14} = n_i/4 \tag{109}$$

where n_i is the number of H_3O^+ or OH^- ions (the concentrations are equal in undoped ice when a space charge is absent).

The entropy of the ice with ions equals

$$\frac{S_c}{k_B} = \ln W = -2n_i \ln\left(\frac{n_i}{N}\right) - (N - 2n_i) \ln\left[\frac{2(N - 2n_i)}{3N}\right]. \tag{110}$$

This coincides with Pauling's (1935) result $W = N^{3/2}$ when $n_i \to 0$, i.e., in defect-free ice. Minimizing F with the entropy given by eq 110, we obtain for the equilibrium concentration of ions

$$\frac{n_i}{N - 2n_i} = \frac{2}{3} \exp\left\{-\frac{E_{ai}}{2k_B T}\right\} \tag{111}$$

and since $E_{ai} >> 2k_B T$

$$n_i \cong \frac{2}{3} N \exp\left\{-\frac{E_{ai}}{2k_B T}\right\}. \tag{112}$$

As we can see, the specific structure of ice manifested itself only in appearance in eq 106 of a factor of 2/3 before the exponent. The factor 1/2 is in the exponent because ions exist in pairs.

A general case of the presence of ions and Bjerrum defects was considered also by Ryzhkin (1985, unpublished). Let us denote D-defect concentration as n_D, and the concentration of L-defects as n_L. If D- and L-defects are formed by thermal fluctuations, i.e., in pairs, then obviously

$$n_D = n_L . \tag{113}$$

Using a similar way as we have seen above, Ryzhkin found that in the presence of both types of defects

$$S/(k_B N) = -2x \ln(x) - (1-2x) \ln(2(1-2x)/3) - 4y \ln(2y) - 2(1-2y) \ln(1-2y) \tag{114}$$

where

$$x = n_i/N \text{ and } y = n_D/N . \tag{115}$$

Minimizing a free energy of ice with the entropy from eq 114, we obtain for Bjerrum defect concentration

$$n_D = n_L = N \exp(-E_{aB}/2k_B T). \tag{116}$$

Do superionic transitions and the superionic state of ice exist?

While deriving formulas, accounting for H_3O^+ and OH^- ion concentration (eq 111 and 112) and Bjerrum defect concentration (eq 115 and 116), we considered activation energies E_{ai} and E_{aB} to be constants. In 1985, Ryzhkin noticed that this is not always the case. In particular, in the case of large defect concentrations, the activation energy is no longer independent of defect concentration that results in a phase transition under certain conditions. The main idea underlying Ryzhkin's theory is that the energy of formation of the defect pair, ions H_3O^+ and OH^-, for instance, can be split into two parts.

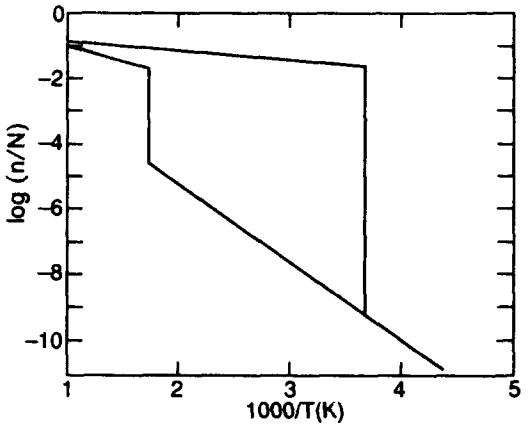

Figure 15. Logarithm of the ratio of ion concentration n *to molecular concentration* N *as a function of reciprocal temperature* T. *The steep rises correspond to transition into the superionic state of ice. The upper curve is for* $E_1/E_2 = 0.26$, *the lower curve for* $E_1/E_2 = 0.58$ *(after Ryzhkin 1985).*

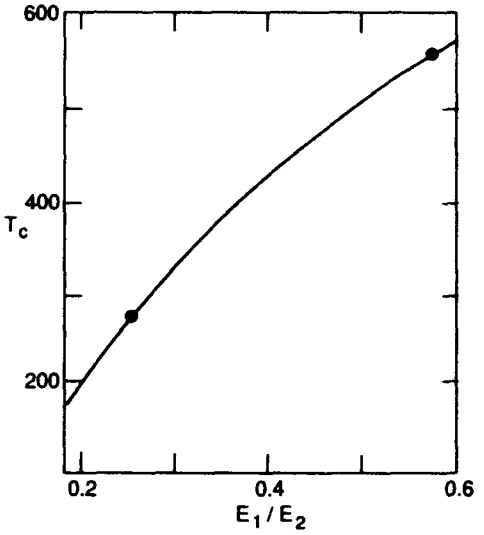

Figure 16. Temperature of transition of ice into superionic state T_c *as a function of* E_1/E_2 *(after Ryzhkin 1985).*

$$E_a = E_1 + E_2(n) \tag{117}$$

where E_1 is the energy of forming an ion pair at distance r_{oo}, i.e., at two neighboring water molecules. In other words, E_1 is the energy required for the proton to be moved along the hydrogen bond from one neutral water molecule to another neutral one. $E_2(n)$ is the energy equal to the work of separation of formed ion pairs. This part of the activation energy can be dampened drastically because of the screening effect. (Ions are screened electrostatically by other mobile charge carriers.) In fact, this must result in a kind of "chain reaction": increasing ion concentration (by means of gradually increasing temperature) will lower $E_2(n)$ and hence the entire E_a, which in turn causes an increase in n and a decrease in E_a. This relationship of E_a and n becomes essential only when the concentration reaches some critical value, which is followed by an E_a jump and an increase of n by orders of magnitude (see Fig. 15). Unfortunately, it is extremely difficult to calculate the value of E_2 precisely, because of the uncertain value of dielectric permittivity ε_∞ at distances about interatomic distance. That is why Ryzhkin assumed that $1 \leq \varepsilon_\infty \leq 3.2$, i.e., it lies between values of ε for vacuum and average macroscopic value. The result of this uncertainty of ε is that the theory can predict only qualitative dependence of critical temperature as a function of ratio E_1/E_2, as shown in Figure 16. Since the transition indicated above does not occur at $T = 273$ K, this implies that $E_1/E_2 \geq 0.26$ and $\varepsilon \geq 2.53$.

The sharp change in concentration, indicated in Figure 15, can be interpreted as a transition into the superionic state, since ion concentration reaches $\equiv 0.1 - 1$, i.e., it becomes comparable with molecular concentration. Of course, in this case the ice structure itself can experience qualitative changes, resulting in a disordering of the oxygen system (quasi-liquid state).

Naturally, all considerations presented by Ryzhkin for ions also hold for Bjerrum defects. Under usual conditions the superionic transformation predicted by Ryzhkin does not occur up to ice melting temperature. However, this effect could be significant on the ice surface or in the vicinity of the dislocation core, where charge carrier concentration can exceed the bulk concen-

tration by several orders of magnitude, because of the presence of strong electric fields and elastic strain fields (Ossipyan and Petrenko 1988, Ryzhkin 1992).

Protonic charge carriers introduced by doping

Although liquid water is a very good solvent for many substances, its solid phase—ice—dissolves to almost nothing. Most of the impurities dissolved in water either get repelled from ice back into the water or precipitate as a second phase inside the ice bulk, in the form of segregations and clusters during the process of ice growth. There are some exceptions, such as a few acids (HF, HCl), ammonia (NH_3), some alkalies (KOH, NaOH) and their derivatives like NH_4F or KCl. These substances, first, can be included properly into the ice crystal lattice and, second, they drastically change the protonic carrier concentration in the ice.

To understand how these impurities affect the electrical properties of ice, let us consider probable patterns of their incorporation into the ice lattice (see Fig. 17). Note that although there now exist a number of experimental techniques for investigating real atomic structure, which allow us to obtain atomic resolution (transmission electron microscopy of high resolution, scanning tunneling microscopy, atomic force microscopy), the real structure of such defects in ice has not been studied yet. Patterns such as those represented in Figure 17 turn out to be just hypotheses (assumptions) based upon ionic radii analysis, as well as analysis of energies and lengths of atomic bonds, etc. The ionic radius of F^-, for example, is rather close to that of O^{-2}, and it is natural to assume that fluorine substitutes for oxygen successfully in an ice lattice. As can be seen from Figure 17a, since the HF molecule can provide only one proton for the four nearest hydrogen bonds, one bond appears to be lacking any protons at all, i.e., substitution of

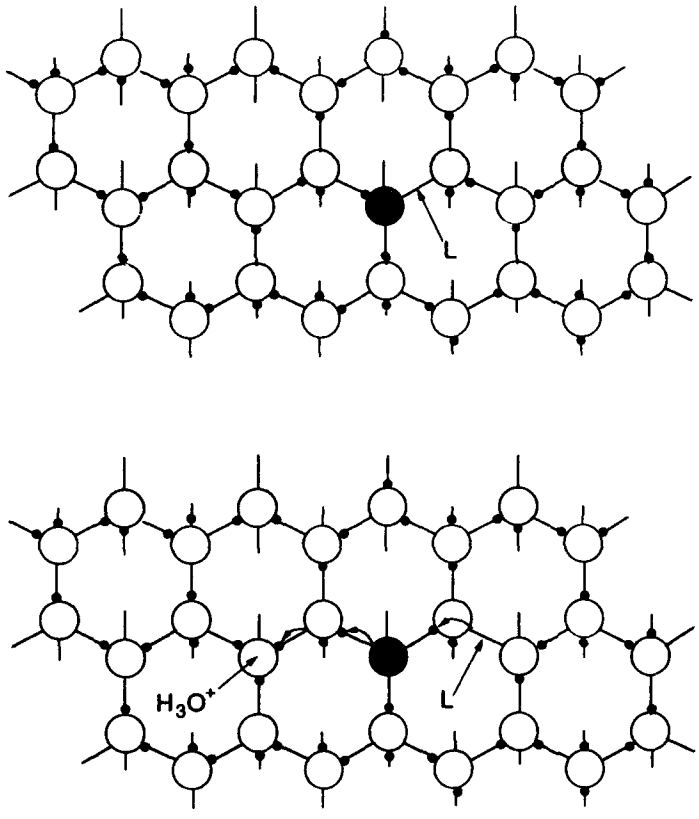

a. HF. Top: Ice lattice with incorporated HF molecule. Bottom: The same after H_3O^+ ion and L-defect were released by means of sequential hops of protons (along the hydrogen bonds to release H_3O^+ ion and between the bonds to release L-defect).

Figure 17. Incorporation of impurities into the ice lattice.

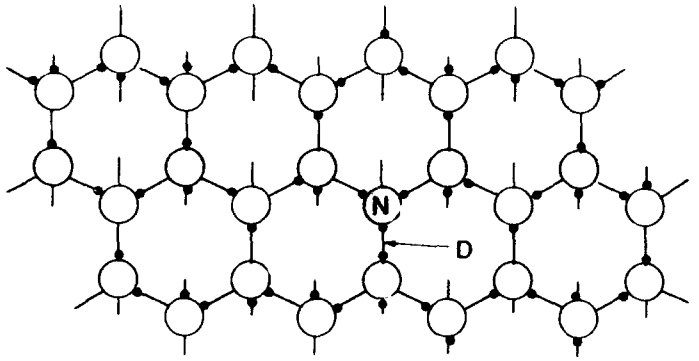

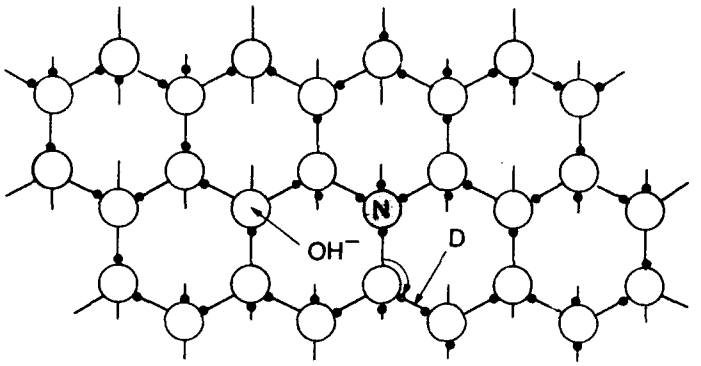

b. NH_3. Top: NH_3 molecule incorporated into ice structure. Bottom: The same after release of OH^- ion and D-defect from the NH_3 molecule.

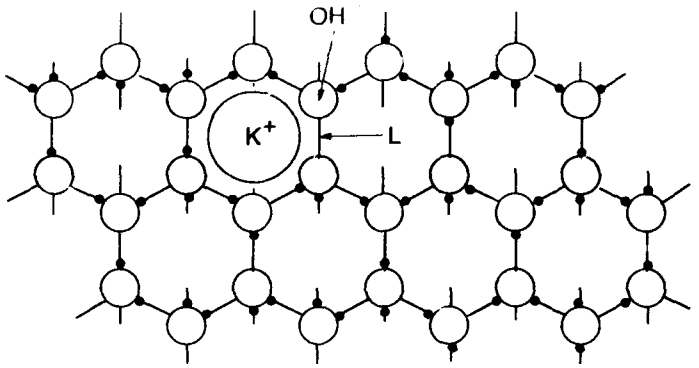

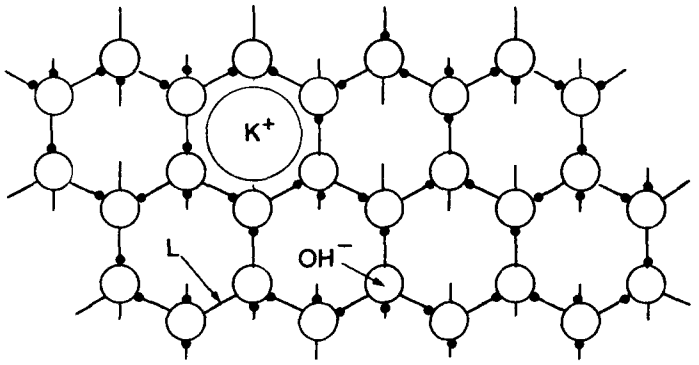

c. KOH. Top: Diagram to indicate how KOH dissolved in ice is thought to introduce defects. The K^+ ion is interstitial, and the OH^- ion substitutes for a water molecule leaving one bond without any proton—an L-defect. Bottom: The same after L-defect and OH^- ion have gone off the KOH molecule.

Figure 17 (cont'd). Incorporation of impurities into the ice lattice.

the water molecule by the HF molecule results in the appearance of an L-defect associated with the impurity molecule. The binding energy of such an L-defect with the HF molecule obviously is not large ($\leq 10^{-2}$ eV, Jaccard 1959, Camplin et al. 1978). Since the number of possible arrangements of the L-defect in an ice lattice is enormous, practically all L-defects leave their parent molecules.

Moreover, it turns out that a single proton in the HF molecule is not bound firmly and can "jump over" along a hydrogen bond to another water molecule, because of the thermoactivation process, turning the water molecule into an H_3O^+ ion. It is important to emphasize the chemistry of HF. To a physicist the natural thing would be for an extra proton to attach to HF forming an OH^- ion, but chemically HF is a weak acid in water and prefers to lose a proton.

Thus, HF doping of ice increases the L-defect and H_3O^+ ion concentrations and lowers D-defect and OH^- ion concentrations. The latter occurs because the equilibrium concentrations of D-defects and OH^- ions in pure ice are determined by a balance between the rate of their thermoactivated production and the rate of recombination: D- with L-defects and H_3O^+ with OH^- ions. HF doping increases L-defect and H_3O^+ ion concentrations, so that the rate of recombination increases, which results in decreasing D-defect and OH^- ion concentrations. Algebraically, this can be described in terms of the products of concentrations $n_1 \cdot n_2$ and $n_3 \cdot n_4$ being constant in a state of thermal equilibrium, irrespective of doping

$$n_1 \cdot n_2 = (n_i)^2 \equiv \frac{4}{9} N^2 \exp\left\{-\frac{E_{ai}}{k_B T}\right\} \qquad n_i << N \tag{118}$$

$$n_3 \cdot n_4 = (n_D)^2 \equiv N^2 \exp\left\{-\frac{E_{aB}}{k_B T}\right\}, \qquad n_D << N\ . \tag{119}$$

Another molecule that can successfully be incorporated into the ice lattice, substituting for water molecules, is ammonia, NH_3 (Fig. 17b). Since NH_3 donates three protons (instead of two as in the case of H_2O) for four hydrogen bonds, we observe two protons at one bond at the same time, i.e., the D-defect. As a consequence of the thermoactivation process, this defect can be released and take part in the conductivity process. Besides, the NH_3 molecule can accept a fourth proton, forming an OH^- ion at a neighboring water molecule. As will be shown later, activation energies for the release of D-defects and OH^- ions from the NH_3 molecule in ice are quite sizable. Therefore, although NH_3 doping of ice increases D-defect and OH^- ion concentrations (decreasing L-defect and H_3O^+ ion concentrations in accordance with eq 118–119), its influence in terms of conductivity is not as efficient as the HF doping of ice. It is also important that NH_3 doping increase the concentration of less mobile carriers (D-defects and OH^- ions), as will be shown in the *Review of Experimental Results on Ice Conductivity and Dielectric Permittivity* section.

Lastly, the third, very important kind of impurity that considerably affects the conductivity of ice is alkali hydroxides, among which the most significant is KOH. The most plausible mechanism of incorporation of KOH into the ice structure is shown in Figure 17c. The potassium atom is accommodated in interstices, while the hydroxyl group OH is built into the lattice. As can be seen from Figure 17c, this results in the appearance of L-defects and OH^- ions linked to KOH impurity. Because of thermoactivation processes, they can be released into the ice bulk, increasing L-defect and OH^- ion concentrations and suppressing D-defects and H_3O^+ ions. Because of the extremely small binding energies of L-defects and OH^- ions with KOH molecules in ice, these impurities become efficient donors of L-defects and OH^- ions even at very low temperatures (see the *Review of Experimental Results on Ice Conductivity and Dielectric Permittivity* section).

Let us briefly discuss the question concerning the statistics of charge carriers in doped ice. This problem has been treated many times in scientific literature (see Jaccard 1959, Kröger 1974, Camplin et al. 1978). Unfortunately, in all instances known so far, this consideration was based

upon the law of mass action, the specifics of ice being disregarded, which can yield only approximate results. The dependence of defect concentrations on doping impurity concentrations in ice was considered in the greatest detail by Kröger (1974). We will give below an example of such an analysis conducted for ice doped with HF. Substitution of water molecules by HF molecules generally brings into existence the following kinds of defects:

1. HF itself in lattice points. We denote their concentration as n_{HFL}. The sequence of letters HFL implies that the proton (H) and L-defect (L) are still bound with fluorine.
2. HF without the L-defect: n_{HF}.
3. HF without a proton: n_{FL}.
4. HF without the L-defect and a proton: n_F.
5. H_3O^+ ion: $n_{H3O}{}^+$.
6. OH^- ion: $n_{OH}{}^-$.
7. L-defect: n_L.
8. D-defect: n_D.

For these eight unknown variables to be found, eight equations are required. Three of those are evident

$$N_{HF} = n_{HFL} + n_{HF} + n_{FL} + n_F$$

where N_{HF} denotes total concentration of impurity molecules HF.

The next equation implies that H_3O^+ ions are formed either coupled with OH^- ions from neutral water molecules, or when a proton is released from the HF molecule

$$n_{H_3O^+} = n_{OH^-} + n_F + n_{FL} . \tag{120}$$

In the same fashion, L-defects can appear either coupled with D-defects from a pair of normal hydrogen bonds, or can be released from the HF molecule. Therefore

$$n_L = n_D + n_{HF} + n_F . \tag{121}$$

The rest of the five equations will arise from the law of mass action being applied to reversible reactions, resulting in the appearance of charge carriers. So, from the reaction

$$HF + H_2O \Leftrightarrow F^- + H_3O^+ + L$$

it follows that

$$\frac{n_{H_3O^+} \cdot n_F \cdot n_L}{n_{HFL}} = K_{OI} \propto \exp^{(-W_{OI}/k_BT)} \tag{122}$$

where K_{OI} is the dissociation constant of this reaction and W_{OI} is the activation energy. Let us write down equations for the other four reactions

$$\left(n_{H_3O^+} \cdot n_{FL}\right)/n_{HFL} = K_{IF} \propto \exp^{(-W_{IF}/k_BT)} \tag{123}$$

$$\left(n_{HF} \cdot n_L\right)/n_{HFL} = K_{OF} \propto \exp^{(-W_{OF}/k_BT)} \tag{124}$$

$$\left(n_F \cdot n_L\right)/n_{FL} = K_{I,O} \propto \exp^{(-W_{I,O}/k_BT)} \tag{125}$$

$$\left(n_F \cdot n_{H_3O^+}\right)/n_{HF} = K_{O,I} \propto \exp^{(-W_{O,I}/k_BT)}. \quad (126)$$

If the dissociation constants are known, then all concentrations can be found. And, if activation energies are known in addition, then the temperature dependence of all concentrations can be predicted. Of course, even though this is an empirical (rather than a strictly theoretical) consideration, the actual calculations are rather cumbersome. Sometimes it is better to simplify the consideration, essentially taking into account, for instance, that the dissociation energy of the L-defect released from the HF molecule is extremely small, and hence fluorine atoms cannot keep back the L-defects

$$n_F = N_{HF} + n_D . \quad (127)$$

If in addition N_{HF} concentration is much greater than the intrinsic equilibrium concentration of Bjerrum defects, then

$$n_L \cong N_{HF}. \quad (128)$$

In this particular case, finding H_3O^+ ion concentration will also be simplified, since

$$n_{HF} \cong N_{HF} - n_{H_3O^+}, \; n_F \cong n_{H_3O^+}. \quad (129)$$

Then, from eq 126

$$n_{H_3O^+} = \frac{1}{2}\left[-K_{O,I} \pm \left(K_{O,I}^2 + 4N_{HF} \cdot K_{O,I}\right)^{1/2}\right] \quad (130)$$

where we must take the + sign.

At high temperatures or low concentrations of HF

$$K_{O,I} >> N_{HF} \quad (131)$$

and

$$n_{H_3O^+} \approx N_{HF} . \quad (132)$$

At low temperatures or high concentrations of HF

$$K_{O,I} << N_{HF} \quad (133)$$

and

$$n_{H_3O^+} \approx \left[K_{O,I} \cdot N_{HF}\right]^{1/2}. \quad (134)$$

EXPERIMENTAL TECHNIQUES FOR INVESTIGATION OF CONDUCTIVITY AND DIELECTRIC PERMITTIVITY OF ICE

Measurements of the electrical properties of ice can provide useful information, not only in respect to the σ and ε of ice, but about impurities and even the age of ice as well. In addition, since the same defects (protonic charge carriers) are responsible for both electrical and mechani-

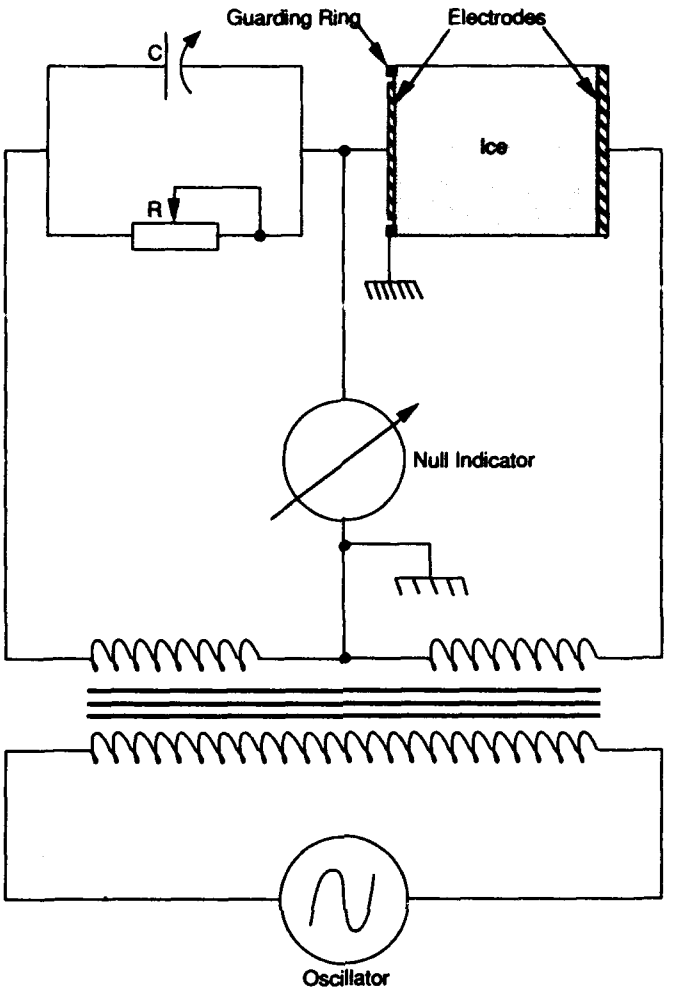

Figure 18. Schematic sketch of ac bridge circuit to measure ac impedance of ice sample, $Z = R + 1/i\omega C$.

cal properties (plasticity, anelastic relaxation time), electrical measurements in ice appear to be of use to diverse scientists working on this important material. Therefore, it is necessary to get an idea of basic experimental techniques applied in investigations of σ and ε.

Measuring circuits

The most common measuring circuit for electrical measurements in ice is the ac bridge, shown schematically in Figure 18. Its operational principle is clear from the sketch. The bridge is adjusted until the minimal readings of the null indicator are observed. The ac bridges actually used are both privately made and industry manufactured. A proper selective amplifier or even a lock-in amplifier can play the role of null detector. Such circuits are known to be used in the frequency range from 10^{-2} up to 10^{7} Hz. However, the use of ac bridges at frequencies $f \lesssim 1$ Hz encounters considerable difficulties. As a rule, this circuit is employed in the frequency range 1–10^{6} Hz. With the aid of an ac bridge, the equivalent electrical resistance $R(f)$ and capacitance $C(f)$ (considered to be in parallel) of ice is measured at a fixed frequency. Transformation of $R(f)$ and $C(f)$ into $\sigma(f)$ and $\varepsilon(f)$ is not difficult

$$\sigma(f) = \frac{L}{sR(f)}\,;\ \varepsilon(f) = \frac{L}{s\varepsilon_0}\,C(f) \tag{135}$$

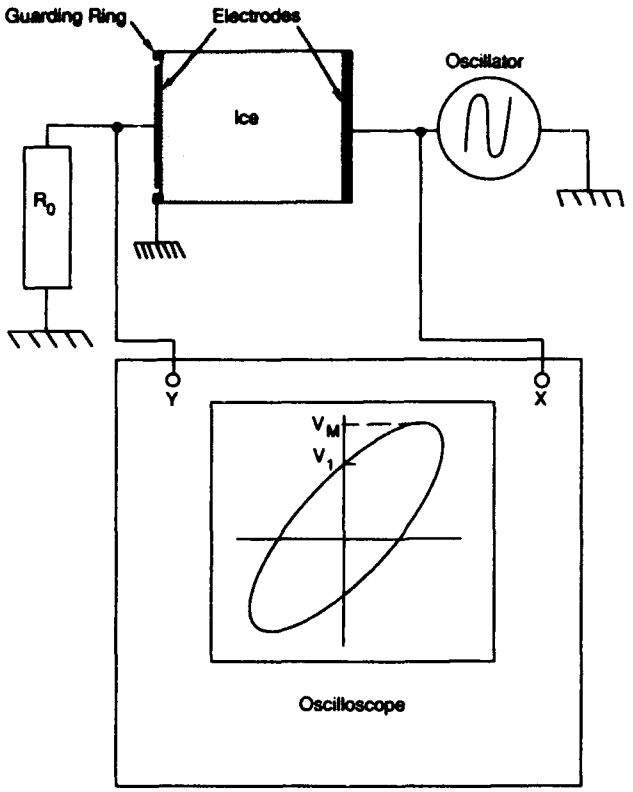

Figure 19. Schematic representation of "loop-method" for ice ac impedance measurement.

where L and s are specimen thickness and surface area.

Another extensively used circuit is represented in Figure 19. This is the so-called loop method. An XY recorder can be used as an "oscilloscope" in the low-frequency range ($f \leq 1$ Hz). The circuit has proven itself to good advantage in the frequency range of 10^{-4} to 10^{7} Hz.

It can be easily shown that

$$R(f) = R_0 V_0 / \sqrt{V_M^2 - V_1^2}; \quad C(f) = \frac{V_1}{V_0} \frac{1}{2\pi f R_0} \tag{136}$$

where V_0 is the amplitude of the oscillator voltage. From here σ and ε can be evaluated using eq 135. It is necessary for measuring resistance that R_0 be much smaller than ice impedance over all frequency ranges used in the measurements.

The third technique is based upon measurement of current passing through the sample as a function of time $I(t)$, after a rectangular voltage has been applied. So that

$$V(t) = \begin{cases} 0, & t < 0 \\ V_0 = EL, & t \geq 0 \end{cases}. \tag{137}$$

In that case, when the electrodes used ensure an efficient charge exchange with ice (a space charge built up in ice is absent near the electrodes), a dependence $I(t)$, shown in Figure 3, is observed. As can be seen from this figure, σ_∞ and σ_s are determined by the initial and final ($t >> \tau_D$) values of the current respectively. The high-frequency capacity of a specimen $C_\infty = s\varepsilon_0\varepsilon_\infty / L$ defines a short time pulse of the current (not shown on Fig. 3) with characteristic decay time, $\tau = C_\infty R_m$, where R_m is the resistance of the measuring circuit.

Static dielectric permittivity can easily be found from the relationship

$$\varepsilon_0 \varepsilon_s = \frac{L}{sV} \int_0^\infty [I(t) - I(\infty)]\, dt \,. \tag{138}$$

All three methods can be easily computerized, provided that digital storage oscilloscopes and lock-in amplifiers operated by computers are used.

Electrodes

The fabrication of proper electrodes for ice encounters great difficulties, since all metals are electronic conductors, while ice is a protonic conductor. In many cases the use of improper electrodes, causing only partial charge exchange with ice, leads to observation of "false" extra dispersions and to distortion of the results of low-frequency measurements. The following types of electrodes used with ice can be found in the literature:

1. Blocking electrodes (Gross 1975, Mounier and Sixou 1969, Zaretskii 1991).
2. Cold plasma (Auvert and Kahane 1973).
3. Palladium, or palladium black, saturated with hydrogen (Bullemer et al. 1969, Petrenko et al. 1983).
4. Ohmic electrodes with double electric layers at the ice/metal interface, (Petrenko and Chesnakov 1990a,b,c).
5. Liquid electrodes (von Hippel et al. 1973).
6. Ion exchange membranes (Kahane 1969).

Every electrode type listed above has been used in many experiments. The references given indicate either the first use of such electrodes or the most detailed description of the technique. All electrodes listed yield good reproducible results, but from our perspective, the most reliable

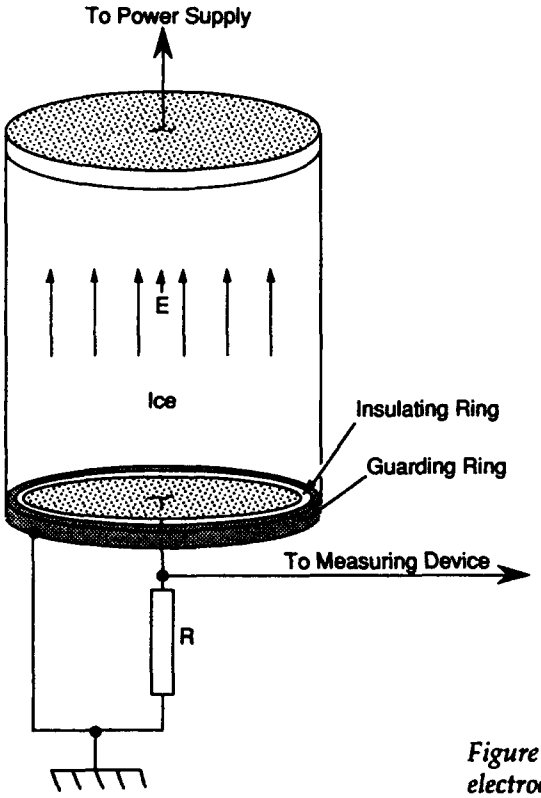

Figure 20. Cylindrical ice sample with two attached electrodes and the guard ring.

and easily built are blocking electrodes, in which the charge exchange is totally eliminated by thin dielectric films placed between ice and metal, and the Ohmic electrodes described in Petrenko and Chesnakov (1990a,b,c), in which the charge exchange is perfect, since electronic energy levels in ice and metal become equal (see the *Charge Exchange at Ice/Metal Interfaces* section). Still, it is probably a matter of taste.

Surface conductance and guard rings

As we will see later, at temperatures $T \gtrsim -25°C$, even in pure ice a considerable surface conductivity, which under certain conditions exceeds the bulk static conductivity of ice, is observed. There are several ways of checking surface conductance (use of the four-point method, for instance [Jaccard 1966]). However, the use of a guard ring, sketched in Figure 20, is the most reliable and widely used technique. The main point in using guard rings is that surface currents will not enter the measuring circuit, thus flowing down to ground. For this to occur, the electric field vector must be parallel to the surface at every point (to prevent surface currents from flowing down into the bulk and "back"). It is important, hence, that the potential of the guard ring be almost the same as at the bottom electrode. The last condition is provided when R (in Fig. 20) is very small compared to the ac impedance of the ice sample.

Influence of inhomogeneity on
the frequency dependence of ice conductivity

As a final remark on experimental techniques, let us consider the influence of the inhomogeneous distribution of charge carriers on the shape of the frequency dependence of conductivity. For homogeneous ice, complex conductivity $\tilde{\sigma}$ depends on circular frequency as (eq 67)

$$\tilde{\sigma}(\omega) = \sigma_s - \frac{i\omega\tau_D(\sigma_\infty - \sigma_s)}{1 - i\omega\tau_D}$$

where, usually, $\sigma_\infty >> \sigma_s$. Using eq 71

$$\tilde{\sigma}(\omega) \approx \frac{i\omega e_3^2}{(1 - i\omega\tau_D)\phi}. \tag{139}$$

If $\tilde{\sigma}$ depends on x $\tilde{\sigma} = \tilde{\sigma}(\omega,x)$, where x is the axis perpendicular to the electrodes, then thin layers with thickness dx will be connected in series and the "apparent" conductivity $\tilde{\sigma}_{ap}$ will be

$$\tilde{\sigma}_{ap} = L \cdot \left(\int_0^L \frac{dx}{\tilde{\sigma}(\omega, x)} \right)^{-1} = \frac{i\omega e_3^2}{\phi(1 - \omega\tau_{DM})} \tag{140}$$

where

$$\tau_{DM} = \frac{1}{L} \int_0^L \tau_D(x)\,dx\,. \tag{141}$$

Hence, we have again in eq 140 a regular Debye's dispersion, as in eq 139, but with an "average" τ_D. On the other hand, when the inhomogeneity of $\tilde{\sigma}(\omega)$ exists *along* the electrodes

$$\tilde{\sigma}_{ap} = \frac{1}{S}\int_{s}\tilde{\sigma}(\omega y, z)\,dy\,dx \qquad (142)$$

and $\tilde{\sigma}_{ap}$ is the sum of dispersions with different τ_D (and ω_D) and of different amplitudes ($\sigma_\infty - \sigma_s$). Indeed, in a real experimental situation, ice samples prepared for electrical measurements very often have an inhomogeneous distribution of charge carriers. That inhomogeneity may arise from the presence of impurity concentration gradients, dislocations and so on.

REVIEW OF EXPERIMENTAL RESULTS ON ICE CONDUCTIVITY AND DIELECTRIC PERMITTIVITY

The very first scientific research in ice conductivity of which this author is aware began more than 100 years ago (Ayrton and Perry 1877). At present, the list of papers devoted to the electrical properties of ice contains several hundred items. It is extremely difficult to conduct a comparative and critical review of such a vast amount of material. It was already a huge task in the early seventies, when Hobbs (1974) was working on his famous book. Since then the amount of information in this field has more than doubled, and here we present the material in a completely different way.

First of all, notice that all theoretical and model considerations introduced previously in this report are based upon critical analysis of the totality of experimental data. Therefore, our primary goal now is to illustrate the validity of these ideas in the context of some particular experimental research and to provide the reader with some useful numerical data on the absolute values of conductivity, activation energies, charge carrier mobility, relaxation times and dielectric permittivity, and the values of electric charges.

In pursuing this, inasmuch as the amount of material available is much more than is necessary for illustration, in the future we will be guided by the following criteria. We will consider first mainly recent works not included in Hobbs' book and, secondly, works that are remark-

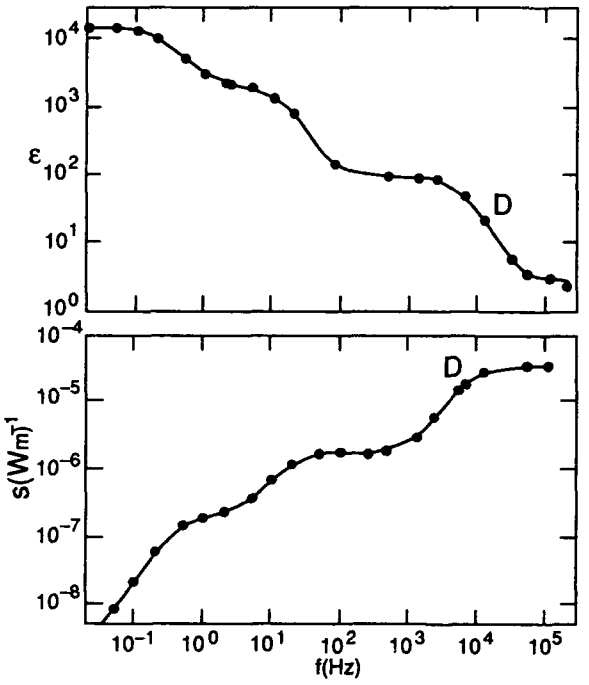

Figure 21. Frequency dependences of pure ice dielectric permittivity ε and conductivity σ; T = 270.2 K. The letter "D" indicates Debye dispersion (after Noll 1978).

able in some aspect (original techniques, precision of results, the role they played in establishing modern understanding of the subject, etc.). Of course, the choice is still rather arbitrary, and the author presents his apologies in advance.

We will begin our review by discussing the general form of dispersion curves $\sigma(\omega)$ and $\varepsilon(\omega)$. As we have seen earlier, Jaccard's theory predicts the presence of only one singularity in the spectrum (single dispersion), as shown in Figures 2 and 5. Such dispersions are observed when a limited range of frequencies close to ω_D is used. When the frequency range is widened, an extra dispersion appears. All four low-frequency dispersions (including Debye dispersion) predicted by Jaccard's model and modified for a finite-dimension specimen were detected by Maidique et al. (1970) in ice specimens being annealed for 10 months.

Three separate dispersions for $\omega \leq \omega_D$ were observed by Noll (1978) (see Fig. 21). Many other authors reported the observation of one extra dispersion at frequencies less than ω_D. As we have seen in the *Electrical Properties of Ice of Finite Size* section, these dispersions are caused by screening layers formed near the ice specimen surface that consist of various charge carriers. As mentioned already in that section, such dispersions can yield a lot of information about concentration and mobility of charge carriers (Zaretskii et al. 1987a, Zaretskii 1991). Since these dispersions appear at the "electric" boundaries of the ice specimen, where an electric potential drop occurs, then, if electrodes providing a perfect charge exchange with ice are used, these singularities disappear at frequencies $\omega < \omega_D$.

Many authors also note the presence of small additional dispersions in some ice specimens at frequencies $\omega > \omega_D$. Maidique et al. (1970), for instance, reported observing two such dispersions. The nature of these high-frequency dispersions is still unclear and under discussion. It is possible that all (or at least part) of these dispersions are determined by the existence of local inhomogeneties in ice, which we discussed in the previous section.

Measuring dispersion curves $\sigma(\omega)$ allows us to determine the values of static (σ_s) and high-frequency (σ_∞) conductivities. From measuring σ_∞ and σ_s at various temperatures, the activation energies $E_{a\infty}$ and E_{as} can be calculated. Since $\sigma \propto n \cdot \mu$, these activation energies come out to be the sum of 1) activation energies of the creation of charge carriers (E_{aB} and E_{ai} for Bjerrum defects and ions respectively) and 2) activation energies of defect motion E_{mi}. Experiments carried out on ice doped with various impurities allow us to predict charge carrier concentrations and thus to separate values of n and μ and to separate the activation energies of creation and motion of charge carriers as well. The results of such measurements are summarized in Tables 1–3. We present below the "guidance" for these experimental results.

The most well established conductivity parameters for pure monocrystalline ice are evidently high-frequency conductivity σ_∞ and its activation energy $E_{a\infty}$. Good reproducibility of these quantities, determined by the conductivity of majority charge carriers (L-defects for $T \gtrsim -50°C$), is attributable, first, to high-frequency measurements not depending upon electrode type. Second, it appears to be comparatively easy to attain a degree of purity in ice, such that σ_∞ is determined by intrinsic carriers and does not depend upon residual impurities. The same holds for τ_D and E_τ, since, according to eq 69 and 70, $\tau_D \propto \sigma_\infty$ always when $\sigma_\infty >> \sigma_s$, i.e., when the majority type of charge carrier is clearly distinguished. These four values at $T = -10°C$ are as follows

$$\left.\begin{aligned} E_{a\infty} &= (0.58 \pm 0.03)\,\text{eV};\quad E_\tau = (0.58 \pm 0.01)\,\text{eV} \\ \sigma_\infty &= (1.8 \pm 0.2)\,10^{-5}\,\Omega^{-1}\,\text{m}^{-1};\quad \tau_D \cong 5.10^{-5}\,\text{s} \end{aligned}\right\} \tag{143}$$

The Debye dispersion is reproduced very well in perfect crystals—pure, homogeneous and annealed (for relaxation of internal stresses).

Table 1. Data on high-frequency (σ_∞) and static (σ_s) conductivities of ice.

Type of ice	T (°C)	σ_∞ $(\Omega\ m)^{-1}$	σ_s $(\Omega\ m)^{-1}$	$E_{a\infty}$ *(eV)*	E_{as} *(eV)*	E_{ai} *(eV)*	E_{aB} *(eV)*	E_{m1}/E_{m2} *(eV)*	E_{m3}/E_{m4} *(eV)*	τ_D *(s)*	E_τ *(eV)*	*Reference*
4 zone refinings	−10		4×10^{-9}		0.54	1.08						Wörz and Cole (1969)
single crystals			2.5×10^{-8} (0 to −20)°C		0–0.06	1.1				5.18×10^{-5} (−10°C)	0.589	Maidique et al. (1970)
single crystals	−4 to −56		6.4×10^{-10} (−10°C)	0.53±0.01	0.70±0.07	1.4						Petrenko et al. (1983)
single crystals	−10		10^{-7}	0.37								Bullemer and Riehl (1966)
single crystals				0.624						5×10^{-5}		Camplin et al. (1978)
single crystals pure and HF-doped	−10	1.6×10^{-5}	1.1×10^{-7}	0.575	0.61	1.22	0.68	0	0.235	2×10^{-5} (0°C)	0.575	Jaccard (1959)
single crystals	0		2.5×10^{-8}							1.8×10^{-5}	0.59	von Hippel et al. (1971), Maidique et al. (1971)
single crystals	−10		$(1.1\pm0.5)10^{-8}$	0.76±0.06								Bullemer et al. (1969)
single crystals			2.3×10^{-8}		0.49	0.98						Maeno (1973)
single crystals	−10	1.8×10^{-5}		0.61						4.5×10^{-5}	0.64	Camplin and Glen (1973)
single crystals	−10									10^{-4}	0.57	Zaretskii et al. (1987a)
HCl doping	−39			0.492±0.025	0			0			0.567±0.009	Takei and Maeno (1984)
10^{-5} mol/L	−39			0.259±0.003	0.267±0.009						0.293±0.034	
HCl doping							0.79	0	0.19			Takei and Maeno (1987)
KOH doping	0 to −150	2×10^{-5}–10^{1}	up to 10^{-1}	0	0.85					2×10^{-5}	0	Zaretskii et al.
0–1 mol/L				($T \lesssim -70$°C)	($T < -70$°C)			0		0°C, pure	($T < -70$°C)	(1988)
KOH doping	−23 to −203	~2×10^{-4} (−23°C)	10^{-4} (−23°C)	0 ($T > -100$°C)	0.4 ($T > -100$°C)							Howe and Whitworth (1989)
0.032 mol/L								0				

Considerably greater scattering is observed in data from measurements of static conductivity σ_s and its activation energy E_{as}. Values of E_{as} appear to lie between 0 and 0.7 eV and σ_s (–10°C) varies in limits from 10^{-6} down to $6 \times 10^{-10}\ \Omega^{-1}\ m^{-1}$. This is explained by the difficulty in purifying ice to a level at which intrinsic ions dominate over ions supplied by impurities. That is why von Hippel (1971) and von Hippel et al. (1973) drew the conclusion that there are no intrinsic ions in ice and that all ions originate in impurities. If we refer to Table I from their work (von Hippel et al. 1971) for the value of σ_s ($2.5 \times 10^{-8}\ \Omega^{-1}\ m^{-1}$) and compare it with the minimal observed value 6.4×10^{-10}, then we might agree with them—their ions were of impurity origin. The question, however, remains open: Were the specimens in the experiments of Wörz and Cole (1969) or Petrenko et al. (1983) pure enough that their conductivity may be considered intrinsic? The following general trend is observed: The more pure the ice and the smaller σ_s, the greater is E_{as}. Therefore, the value of the activation energy of creation of an ion pair E_{ai} = 0.96 eV (Eigen and De Mayer 1956, 1957, 1958; Eigen et al. 1964), considered for a long time to be commonly acknowledged truth, should be treated as the lowest possible limit of this quantity. As the "available" upper limit we can take $E_{ai} = 2E_{as} = 1.4$ eV from the work of Petrenko et al. (1983).

Good experimental confirmation of theoretical concepts about the effect of impurities on ice conductivity (the *Protonic Charge Carriers Introduced by Doping* section) has been indicated in many papers (see, for instance, Takei and Maeno 1984, 1987; Camplin et al. 1978). The most efficient impurities for the increase of H_3O^+ ion and L-defect concentrations appear to be the acids HF and HCl. KOH doping increases OH^- ion and L-defect concentrations, so that, firstly, ice with amazingly large conductivity (up to $\sigma_s = 10\ \Omega^{-1}\ m^{-1}$ at $T \approx 0$°C) can be obtained and, secondly, considerable conductivity (σ_s) is observed at temperatures as low as –200°C (Zaretskii et al. 1988).

The determination of charge carrier mobilities in ice is an extremely difficult task, since, because of small values of μ_i and the "hop" mechanism of motion, the regular technique for measuring the Hall effect is inapplicable in this case. (The Hall effect will be discussed in the report, *Surface of Ice*, listed in the *Foreword*.) Hopes of using "saturation currents" for determining μ_i are not justified, because of reasons pointed out by Maidique et al. (1971) in their critique of Eigen's work, and also because when high voltage is applied to a system with ice/metal interfaces, various physical phenomena that make the interpretation of results more complicated are observed (see Part II).

Nonetheless, several new techniques for determining charge carrier mobilities in ice have been developed and employed during the last 25 years. These are the stationary and transient injection currents measurement technique (Eckener et al. 1973, Petrenko et al. 1983, Petrenko and Ryzhkin 1984b), the ice field effect transistor (Petrenko and Maeno 1987), and the low-frequency dispersion measurement technique (Petrenko and Ryzhkin 1984a, Zaretskii et al. 1987, Zaretskii 1991). The idea of determining μ_i and n_i from the parameters of low-frequency dispersions was presented in the *Electrical Properties of Ice of Finite Size* section. Other techniques mentioned above will be described and discussed later in Part II. The results of determining charge carrier mobilities in ice are summarized in Table 2. At first glance only the data on L-defect mobilities seem to be satisfactory. At $T = -10$°C, $\mu_4 \approx (2\text{–}5) \times 10^{-8}\ m^2/V\ s$. This mobility drops exponentially with decreasing temperature, the activation energy being 0.19–0.235 eV (see Table 1).

Still, there is no reliable information about D-defect mobility. There is only indirect evidence that $\mu_3 < \mu_4$.

Data on ion mobilities are distinguished at first glance by large scattering (from 5×10^{-7} down to 2.5×10^{-8} for H_3O^+ and from 4×10^{-7} down to 2×10^{-10} for OH^-). However, if we discard large values obtained by the now-discredited method of saturation currents and values obtained through measurements of low-frequency dispersions (which still are not accuracte enough) as well, it appears that positive ion mobility lies within the limits 2.7×10^{-8} and $1.1 \times 10^{-7}\ m^2/V\ s$

Table 2. Mobilities of charge carriers in ice.

T (°C)	μ_1 (m^2/V s)	μ_2 (m^2/V s)	μ_3 (m^2/V s)	μ_4 (m^2/V s)	*Method used*	*Reference*
-13 to -36	$(1.1\pm0.1)\times10^{-7}$				Analysis of conductivity decay	Kunst and Warman (1983)
-10	2.5×10^{-8}				σ_s and E_{as} measurements	Wörz and Cole (1969)
0 to -20	5×10^{-7}				Saturation currents	Maidique et al. (1988)
-123		$\leq4\times10^{-7}$			Doping with KOH	Zaretskii et al. (1988)
-5 to -40	10^{-9}- 10^{-7}				Proton injection	Petrenko et al. (1983)
0	2.7×10^{-8}			5×10^{-8}	Doping with HF	Camplin et al. (1978)
-10				1.8×10^{-8}	Doping with HF	Jaccard (1959)
		$\geq2\times10^{-10}$				Howe and Whitworth (1989)
-10	$(2.4\pm1.6)\times10^{-7}$				Saturation currents	Bullemer et al. (1969)
-10	3.5×10^{-8}				HF doping	Camplin and Glen (1973)
-33.1	9.2×10^{-8}	2.7×10^{-8}			Ice field transistor	Petrenko and Maeno (1987)
-145 to -178	$(9\pm1)\times10^{-8}$				Transient injection of protons	Eckener et al. (1973)
-10	$\equiv10^{-6}$			1.7×10^{-8}	Low-frequency dispersions	Zaretskii et al. (1987a)
-33	$(6.7\pm0.8)\times10^{-7}$				Low-frequency dispersions	Zaretskii (1991)
-20	6×10^{-8}				Proton injection	Petrenko and Ryzhkin (1984b)
-10		2.4×10^{-8}			Recombination injection	Petrenko and Chesnakov (1990c)

—not bad at all! The author of this review prefers the data obtained in transient injection experiments (Eckener et al. 1973), in which a minimum of assumptions was used. The same H_3O^+ ion mobility was found by Petrenko and Maeno (1987) using field effect transistors. So, it is likely that $\mu_1 \equiv 9 \times 10^{-8}$ m^2/V s. We can consider it safely established that both H_3O^+ and OH^- ions move with zero activation energy; this is in good agreement with concepts about the tunneling of protons along hydrogen bonds.

Table 3. Ratio of effective electric charge of H_3O^+ ion (e_1) and of D-defect (e_3) to proton charge (e).

e_1/e	e_3/e	*Reference*
(0.61 ± 0.02)	0.39 ± 0.01	Zaretskii et al. (1988)
0.73	0.44	Camplin et al. (1978)*
0.62 ± 0.01	0.38 ± 0.01	Hubmann (1979a)
0.626	0.374	Takei and Maeno (1987)
0.64 ± 0.03	0.36 ± 0.03	Scheiner and Nagle (1983)

* Data fitted without requiring $e_1+e_3 = e$; may cause some errors in their values in Tables 1–3.

In this section we are not going to consider in detail the surface conductivity of ice, since its nature evidently differs appreciably from Jaccard's model, which is actually a theoretical framework for this report.

It will be more convenient to discuss the problem of the surface conductivity of ice in one of our future reports, specially devoted to ice surfaces. Here we restrict ourselves to Figure 22, adopted from the work of Bullemer and Riehl (1966), which illustrates the relationship between bulk static conductance and surface conductivity.

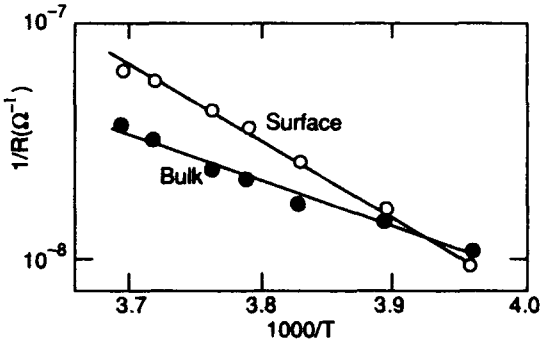

Figure 22. Temperature dependence of bulk and surface conductance of pure ice specimen (after Bullemer and Riehl 1966).

Let us now briefly consider experimental results on measurements of ice static dielectric permittivity ε_s and compare these results with the predictions of Jaccard's model.

Note first of all that theory yields quite a consistent dependence of ε as a function of ω, both in the region of principal Debye dispersion (see eq 74) and in the low-frequency dispersion region, as was described earlier. The predicted absolute value of static dielectric permittivity $\varepsilon_s \approx 10^2$ (–10°C) and its increase with temperature decrease (see eq 72) are also confirmed. As we will see in Part II, the value of ε_s is brilliantly predicted in those cases when the values of σ_i and σ_B become comparable (so called "crossover," discussed in Part II), which again follows from eq 72. Yet, the theory in its present form has some problems. For example, it does not account for the slight anisotropy of ε observed in a number of experiments. Let us refer to one of those recent works by Takei and Maeno (1987) where they found that

$$\varepsilon_s - \varepsilon_\infty = \frac{2.41 \times 10^4 K}{T - 2.2K}, \quad \vec{E} \parallel \vec{C} \tag{144}$$

$$\varepsilon_s - \varepsilon_\infty = \frac{2.3 \times 10^4 K}{T - 48.7K}, \quad \vec{E} \perp \vec{C}. \tag{145}$$

As can be seen from eq 144 and 145, instead of the predicted behavior of $(\varepsilon_s - \varepsilon_\infty)$ according to Curie's law (see eq 72)

$$(\varepsilon_s - \varepsilon_\infty) \propto \frac{1}{\phi} \propto \frac{1}{T} \tag{146}$$

the Curie-Weiss law is observed

$$(\varepsilon_s - \varepsilon_\infty) \propto \frac{1}{T - T_c} \tag{147}$$

which implies a transition to the ordered phase at $T \leq T_c$. There is a considerable discrepancy in T_c in the data of various authors who performed experiments on pure monocrystalline ice. It ranges from 0 K, according to Ruepp and Käss (1969), up to 48.7 K, according to Takei and Maeno (1987). Some errors in measuring ε_s in "pure" ice at low temperatures can arise because of increasing screening lengths and an apparent drop of ε_s (see the *Electrical Properties of Ice of Finite Size* section). Hence, critical temperatures T_c observed in pure ice can be treated as the lower limit of actual critical temperatures. In fact, Tajima et al. (1982) found the transition of KOH-doped ice into a partially ordered state to occur at $T = 72$ K.

In general, we should infer that at present Jaccard's theory (along with its further development) describes well, both quantitatively and qualitatively, the diverse electrical properties of ice. As a brilliant illustration of this, I ask the reader to admire Figure 21 once again!

PART II. ADVANCED TOPICS AND NEW PHYSICAL PHENOMENA

In this part we treat more advanced and special questions concerning the electrical properties of ice. Most of these belong to the frontiers of research in the "physics" of ice, as an object of solid state physics. The results and physical models presented here should be, for the most part, of interest to physicists and chemists doing direct research on ice, rather than the larger group of readers who intend to use information about ice properties only for some applications.

CHARGE EXCHANGE AT ICE/METAL INTERFACES

The electric charge exchange between ice and metal determines the conditions for electric current flow through ice via metallic electrodes. Such an exchange plays an essential role in the process of chemical reactions at the ice/metal interface. Common metal oxidation can serve as an example of such reactions. A future report devoted to electro–optical effects in ice finds that photochemical reactions also proceed at such interfaces, which implies electron exchange between ice and electronic conductors (metals, semiconductors).

It has been common knowledge for a long time that stable electric currents cannot pass through an ice/metal interface, even when precious metals (Pt, Au), which have a surface that is not oxidized by contact with ice, are used. Applying constant voltage to ice with two metallic electrodes results in a short current "pulse," which attenuates exponentially according to the presence of several relaxation times (see the *Electrical Properties of Ice of Finite Size* section and the previous section). That is, no regular metallic electrodes are capable of providing a stable charge exchange between ice and metal, which is necessary for a stable dc flow.

Hydrogen saturated Pd electrodes are an exception, but in this case Pd and ice exchange protons, rather than electrons (see the *Proton Injection from Pd Electrodes into Ice* section for details). Note also that there is a charge exchange between metal and a quasi-liquid surface layer, since there are surface currents present.

There are no obstacles to dc flow through water and two metallic electrodes. Insofar as electronic level structures in water and ice are rather similar (which can be inferred from optical measurements), such differences in the properties of ice/metal and water/metal interfaces are puzzling.

The key to the mystery was found at first in the work of Evtushenko et al. (1988), in which for the first time a technique was developed that ensures a stable dc flow through the ice/metal interface. The ultimate understanding was achieved thanks to work by Petrenko and Chesnakov (1990b) and Chesnakov (1990). I present below a brief account of the results of these investigations.

Since the electronic level structure of water and ice are similar, we will start with water, whose charge exchange with metal is well known (see for instance Bockris 1979, Vihj 1973). The mutual arrangement of electronic energy levels in metal electrodes and water before ($V = 0$) and after ($V > 1.23$ V) a voltage was applied is shown in Figure 23. The charge exchange being realized is between the Fermi-level of the metal E_f and the hydrogen level E_{H2} of water at the cathode (according to eq 23) and between E_f and oxygen level E_{O2} at the anode (according to eq 24). The "hydrogen" system includes H_3O^+ ions, and atoms and molecules of hydrogen. E_{H2} can be looked upon as an electron chemical potential in this system. The same is true for E_{O2} and the "oxygen" system, which comprises OH^- ions, and atoms and molecules of oxygen. In water $E_{H2} - E_{O2} = \Delta = 1.23$ eV. For efficient electron exchange between two levels to be realized, their equalization is required. In the case of water, where the potential difference being applied between anode and cathode $V \geq 1.23$ eV $= \Delta$, this equalization occurs automatically because of

the double charged layers being formed at the water/metal interface.

The double layer of the anode consists of positively charged holes in metal and (negatively charged) OH^- ions, "stuck" to the electrode surface in water. The cathode double layer is formed by electrons in metal and H_3O^+ ions "stuck" to the cathode. The action of such charged double layers on the potential is analogous to the action of flat, charged electrical capacitors—they provide an electrical potential drop, necessary for level equalization. If $V > \Delta$, the rest of the voltage drops at water bulk. Electrons, passing from water to metal and back, overcome an energy barrier having a width about that of the double charged layer. In the case of water, the width of this barrier is several angstroms and electrons penetrate it easily by tunneling. In the case of ice, the width of a similar layer, which is nothing more than a screening layer consisting of ions, is about 1 μm (μm = 10^4Å), since, first, the ionic concentration drops by several orders of magnitude and, second, the effective dielectric permittivity, acting at a range of several intermolecular distances, decreases (from ≈ 80 down to 3.2). And as we remember from an earlier section, the screening length $1/\kappa$ is proportional to $\sqrt{\varepsilon/n}$ (see eq 95, we have to use for water $\varepsilon \approx 80$ and for ice $\varepsilon = \varepsilon_\infty = 3.2$). As a result, for the potential difference being applied to ice with two metallic electrodes attached, although the double charge layers equalizing electronic energy levels do form, the width of these layers is so great that electrons cannot overcome it through the tunneling process. As a result, dc does not flow! ($\Delta = 1.23 + 0.06 = 1.29$ eV is also greater in the case of ice.) Here, we have taken into account the latent heat of ice melting (0.06 eV).

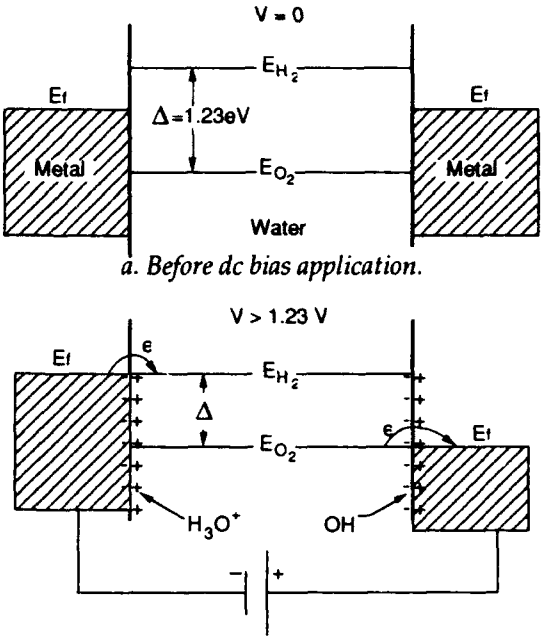

a. Before dc bias application.

b. With dc bias applied.

Figure 23. Electronic energy levels in water and two metal electrodes.

However, as was shown by Evtushenko et al. (1988), the problem of charge exchange between ice and metal can be solved, provided that at first thin and dense charged double layers are formed at the metal/water interface, and are then frozen down to $T \lesssim -10°C$. These thin ion layers at the anode and cathode provide good conditions for charge exchange between ice and metal electrodes. The layers themselves appear to be very stable and can exist for one day at $T \cong -10°C$ and for one week at $T < -20°C$. Such a long lifetime is explained by a large discharge time and constant RC of such a system, where $C \sim 10^{-4}$ F/cm^2 and $R \gtrsim 10^{-9}$

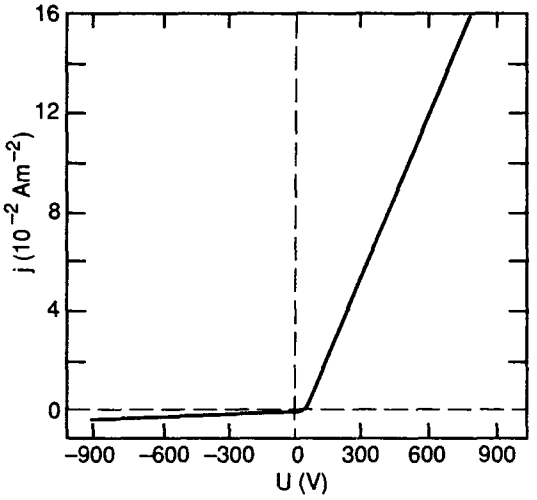

Figure 24. Current–voltage characteristic of ice specimen with two Pt electrodes. Electrically charge double layers were formed at Pt/water interfaces and then frozen down; T = –10°C (after Evtushenko et al. 1988).

$\Omega\,cm^2$, which yields $\tau \gtrsim 10^5$ s ($T \cong -10°C$). An interesting peculiarity of electrodes processed in this way is that they let current pass in only one direction; i.e., they appear to be quite good rectifiers, as indicated in Figure 24 (see also Fig. 30) The rectification ratio reaches values of 10^4 and more. Further on, we will refer to these electrodes as ohmic, because of their ability to let electric current pass essentially without voltage drop (above $\cong$ 1.5 V, necessary to compensate for "frozen" potential difference). After the preparation process is over, the electrodes (with the double layers of ions and thin layer of ice) can be removed from the bulk of ice and used with other specimens (monocrystals for instance). They have already found a use in several research works.

RELAXATION TIMES OF ELECTRIC POLARIZATION AND ELECTRIC FIELDS IN ICE

The question of electric field and polarization relaxation rates has general scope and can be found in many real applications. An electric polarization can arise owing to both various external effects (external electric fields, mechanical loadings, temperature gradients) and internal changes, such as crack growth. Once electric polarization $\vec{P}$ appears, how fast (or for what characteristic time) will it decay? Since $\vec{P}$ will be "dissolved" by means of protonic charge carrier motion, then it might seem we have already found an answer to this question in earlier sections. First of all, this is Debye relaxation time τ_D, determined by the majority charge carrier motion. In the case of ice having boundaries, slower relaxation processes, determined in terms of minority charge carrier motion, can be observed at time intervals longer than τ_D. However, we might expect that the better part of the polarization will disappear with the most rapid characteristic time τ_D. Although we hear this answer from most people doing electric measurements on ice, it is absolutely wrong!

Let us try to illustrate this fact. Consider a very large ("infinite") ice volume. and a relaxation process of electric polarization $\vec{P}$, arising in a finite domain of this ice volume. Obviously, the following equation, familiar from electrodynamics, holds

$$\operatorname{div} \vec{E} = \frac{\rho}{\varepsilon_\infty \varepsilon_0} = -\operatorname{div} \vec{P}/\varepsilon\varepsilon_0 \tag{148}$$

where ρ = space charge density.

Taking into account that curl $\vec{E} = 0$ (quasi-stationary approximation), we can conclude from eq 148

$$\vec{E} = -\frac{\vec{P}}{\varepsilon\varepsilon_0} + \vec{f}(t) \tag{149}$$

where the vector $\vec{f}$ can depend only upon time. But taking into account that there is no electric field at infinity (that is why we consider "infinite" ice) $\vec{f}(t) = 0$ and

$$\vec{E} = -\vec{P}/\varepsilon\varepsilon_0 . \tag{150}$$

We are interested in this particular case in the most rapid process, determined in terms of majority charge carriers, i.e., carriers having maximal conductivity. In the case of ice those are usually σ_4 (L-defects)

$$\dot{\vec{P}} = \sum_{j=1}^{4} e_j j_j \cong -e_3 \vec{j}_4 \tag{151}$$

$$\vec{j}_4 = \left(-e_3 \vec{E} - \phi \vec{\Omega}\right) \frac{\sigma_4}{e_3^2} \tag{152}$$

$$\vec{\Omega} = \left[\int_0^t j_4(t)\, dt \right] = \vec{j}_4 \ . \tag{153}$$

Substituting eq 150, 151 and 153 into 152, we obtain the desired kinetic equation, defining the time dependence of $\vec{E}$

$$\dot{\vec{E}} + \vec{E}/\tau = 0 \ . \tag{154}$$

From here

$$\vec{E} = \vec{E}(0) \exp\{-t/\tau\} \tag{155}$$

where τ is defined as

$$\frac{1}{\tau} = \frac{1}{\tau_M} + \frac{1}{\tau_D} \tag{156}$$

$$\frac{1}{\tau_M} = \frac{\sigma_4}{\varepsilon_\infty \varepsilon_0} \tag{157}$$

$$\frac{1}{\tau_D} = \frac{\sigma_4}{\varepsilon_0 (\varepsilon_S - \varepsilon_\infty)} . \tag{158}$$

Note that τ_D is already familiar to us as Debye relaxation time (see eq 43 and 71) for our case of one type carriers' motion. τ_M is the still more well-known Maxwell dielectric relaxation time, intrinsic to space charge "relaxation" in ordinary conductors. As can be seen from eq 156, relaxation rate $(1/\tau)$ is equal to the sum of Debye and Maxwell relaxation rates. This result has a simple interpretation. The driving force acting upon carriers is the electric field in the case of Maxwell relaxation, while Debye relaxation time τ_D is associated with the effect of the configurational vector $\vec{\Omega}$. In general, charge carriers in ice are subjected to both $\vec{E}$ and $\vec{\Omega}$, which accelerate relaxation processes.

Of course, to obtain results (eq 154–156) it is not absolutely necessary that the ice volume be "infinite." Figure 25 illustrates this. For ice specimens cut in the form of thin plates, so that $\vec{P}$ initially was normal to the plates, we can then neglect the end effects and the exact solution is again given by the equation

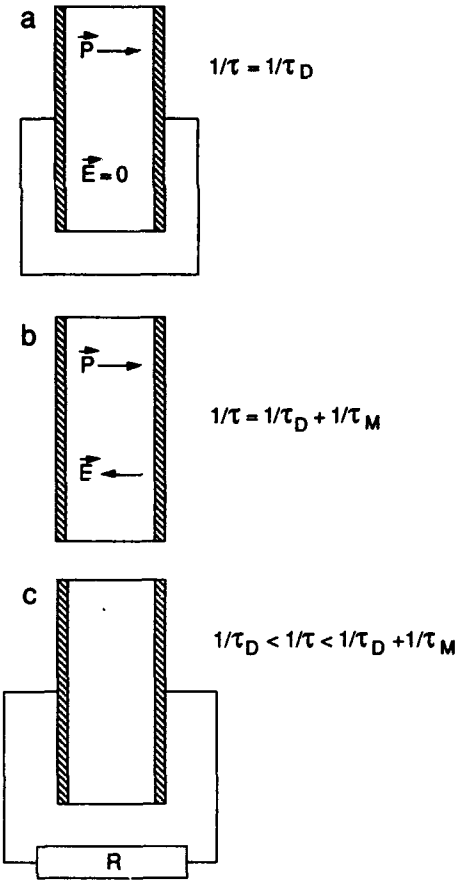

Figure 25. Characteristic time τ with which electric polarization of ice relaxes for different boundary conditions.

$$\dot{\vec{p}} + \vec{p}/\tau = 0 \tag{159}$$

where τ depends upon forces acting upon carriers, which depend on boundary conditions. Note that given R_{ice} as an ohmic ice resistance, then in the Figure 25c circuit we have for $R_{ice}/R \to 0$

$$\frac{1}{\tau} \to \frac{1}{\tau_D} + \frac{1}{\tau_M} \tag{160}$$

and for $R_{ice}/R \to \infty$

$$\frac{1}{\tau} \to \frac{1}{\tau_D}. \tag{161}$$

These remarks illustrate the importance of ice resistance and input circuit resistance ratio for correct determination of relaxation times!

RECOMBINATION INJECTION OF IONS INTO ICE

In the *Concentration of Charge Carriers* section, we considered physical laws that determine charge carrier concentration in ice in a state of thermal equilibrium and in the absence of external excitations. The next four paragraphs will be concerned with the electrical properties of ice in strong electric fields. As we shall see below, the application of an electric field can lead to a considerable increase or decrease of equilibrium proton charge carrier concentrations, depending upon electric field strength, boundary conditions and specimen thickness.

We will start with a description of so-called recombination injection. This phenomenon was originally discovered in pure water (Petrenko and Chesnakov 1990d) and later also in pure ice (Petrenko and Chesnakov 1990c). A reversible increase in ac conductivity of ice and water thin layers, through which a weak direct current was passed, was observed. An example of this effect of direct current on water conductivity is shown in Figure 26.

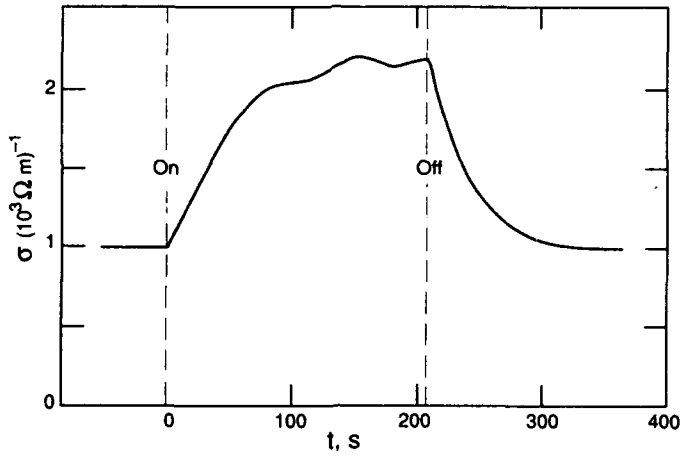

Figure 26. Dependence of ac conductivity of pure water σ on time t, when a small dc bias (3 V) was applied; ac conductivity was measured at f = 1 kHz; T = 20°C; space between two Pt electrodes was 3 mm. Dashed lines indicate moments when the bias was turned on (t = 0 s) and turned off (t ≅ 210 s) (after Petrenko and Chesnakov 1990d).

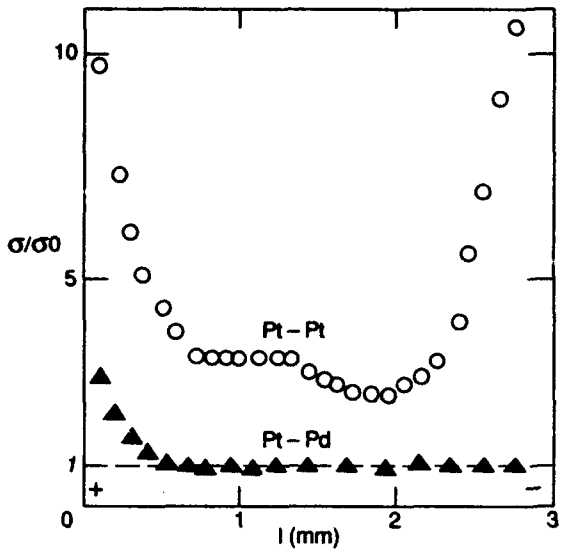

Figure 27. Alternating current conductivity of water (f = 1 KHz) normalized on equilibrium conductivity σ_0 in the space between two electrodes. The upper curve is for a couple of Pt electrodes, while the lower curve is for a Pd cathode and a Pt anode; 5-V dc bias is applied; T = 20°C (after Petrenko and Chesnakov 1990d).

The conductivity increase is completely reversible, i.e., it ceases after the dc bias is switched off and is not related to electrodes dissolving in water or ice. The effect is equally successfully observed when electrodes made from Pt, Au, C or stainless steel are used. The threshold voltage, at which an increase of σ arises, appeared to be equal to the threshold electrolysis voltage (about 1.5 V in the case of water and slightly less than 2 V in ice). It has been shown by measuring conductivity between two micro-electrodes that the conductivity increase is not uniform throughout the space between electrodes (Fig. 27). The maximal increase of σ is observed close to the anode and cathode, damping exponentially as distance from the electrodes increases. To this end, the characteristic width of excess conductivity zones coincides well with the diffusion length of ambipolar H_3O^+ and OH^- ions' diffusion

$$\lambda_d = \sqrt{2D\tau_L} \tag{162}$$

where D is the diffusion coefficient of the less mobile ion (OH^-) and τ_L is the non-equilibrium ions' lifetime. It has been found that in water $\lambda_D \approx 3.4 \times 10^{-4}$ m ($T = 20°C$), and in ice $\lambda_D \approx 4.5 \times 10^{-5}$ m ($T = -30°C$). Under the same conditions, the non-equilibrium ions' lifetime is $\tau_L = 7$ seconds in the case of water and $\tau_L = 2$ seconds in the case of ice. It turned out that an increase in σ in zones adjacent to the electrodes is caused by formation of excessive OH^- and H_3O^+ ions, concentrations of which must be approximately equal owing to constraints imposed by space charges.

The key to understanding the mechanism of excess conductivity was provided by experiments in which a Pd cathode was used. Pd absorbs atomic hydrogen, generated in the electrolysis process according to the reaction defined by eq 23, from water. In cases when the atomic hydrogen does not get into water (or ice), the zone of excessive conductivity does not form near the cathode (Fig. 27). It is assumed that the excess ions form because of energy release in the atomic hydrogen and oxygen recombination process

$$H + H \rightarrow H_2 + 4.5\ eV \tag{163}$$

$$O + O \rightarrow O_2 + 5.1\ eV\,. \tag{164}$$

The quantities 4.5 and 5.1 eV are adopted from the book of Sokolov (1976).

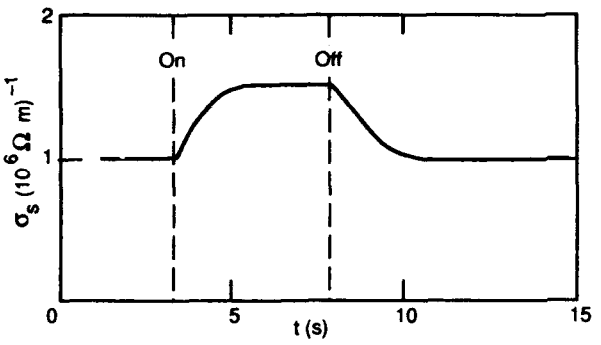

Figure 28. Variations in low-frequency conductivity of pure ice measured at 30 Hz when 10-V dc bias was turned on and off; T = –30°C; *sample thickness is 0.5 mm; ohmic electrodes were used (after Petrenko and Chesnakov 1990c).*

The energy released in each recombination, defined by eq 163 and 164, exceeds by many times the energy required for producing an ion pair (~1 eV in the case of ice [see the *Review of Experimental Results on Ice Conductivity and Dielectric Permittivity* section] and 0.59 eV in the case of water [Fletcher 1970]).

Therefore, we can assume that at least part of this "tremendous" energy is spent on producing new ion pairs. Non-equilibrium ions, originating near the anode and cathode, then diffuse into the specimen bulk, thus increasing the bulk conductivity. For this phenomenon to be observed in ice, ohmic electrodes, described in the *Charge Exchange at Ice/Metal Interfaces* section, must be used. The effect of weak electric current (~10^{-6} A/cm^2) on ice conductivity is represented in Figure 28. Conductivity was measured in this experiment at a frequency of 30 Hz << ω_D; i.e., the measured conductivity corresponds to static conductivity. The latter is determined by OH^- and H_3O^+ ion motion. The relative change of high-frequency conductivity σ_∞ is practically undetectable in this case, since $\sigma_\infty >> \sigma_s \sim \Delta\sigma_s$.

The phenomenon described here is of great interest, because it allows us to determine the lifetimes and diffusional lengths of charge carriers in water and ice by direct methods.

It is curious that for thin ice (and water) specimens having thickness L less than diffusional length λ_D, nonlinear current–voltage characteristics are observed (Fig. 29). They can be readily explained theoretically. Let us consider an ice specimen with $L << \lambda_D$, such that ionic concentration n_i can be regarded as uniform, independent of coordinates. Also let α be the number of ion pairs produced as a consequence of passing a single electron charge e through the specimen ($\alpha > 1$). Then the balance between production and recombination of ions will be defined by the equation

$$L\left(G - \beta n_i^2\right) + \alpha \frac{I}{e} = 0 \tag{165}$$

where G is the rate of thermal production of ions in ice and βn_i^2 (β = const) is the recombination rate in the bulk. For current density J, the following relationship holds

$$J = \sigma_s E \approx \left(\frac{e^2}{e_1}\right)(\sigma_1 + \sigma_2)\frac{V}{L} = \left(\frac{e^2}{e_1}\right)[\mu_1 + \mu_2]\, n_i \frac{V}{L}. \tag{166}$$

From eq 165 and 166 we readily obtain (for weak currents $\alpha \frac{I}{e} << G$)

$$J = \left(\frac{e^2}{e_1}\right)[\mu_1 + \mu_2]\sqrt{\frac{G}{\beta}} \cdot \frac{V}{L} \propto V \tag{167}$$

i.e., Ohm's law. For large currents $\left(\alpha \frac{I}{e} >> G\right)$ we have

$$J = \frac{\alpha}{\beta}\frac{e^3}{e_1^2}[\mu_1 + \mu_2]^2 \frac{V^2}{L^3} \propto V^2. \tag{168}$$

Figure 29 illustrates perfectly the transition from Ohm's law, in the case of small currents, to square current dependence from voltage as current increases.

In conclusion, let us note that the energy release near the cathode and anode, which obviously results in an increase in the number of ions, may also increase the number of Bjerrum defects in comparable quantities. However, since the concentration of the latter exceeds by several orders of magnitude the ions' concentration in pure ice, this does not alter n_B appreciably. It appears that for Bjerrum defects the phenomenon described next is much more essential.

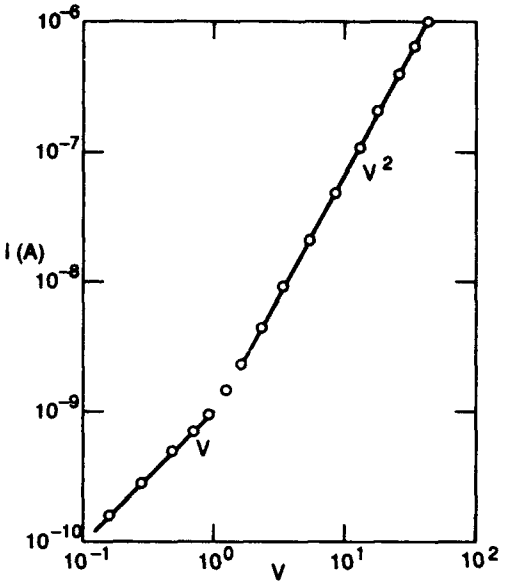

Figure 29. Current–voltage characteristic of a thin (20-μm) ice specimen with ohmic electrodes; T = –30°C; electrode area 2 cm² (after Petrenko and Chesnakov 1990c).

RECOMBINATION EXTRACTION OF CHARGE CARRIERS FROM ICE

First, a decrease in σ_∞, a static electric field being applied, was observed by Petrenko et al. (1983) (see Fig. 2 of their paper). However, at that time no importance was attached to this observation. Later, an effect of static electric fields on ice conductivity, which is opposite to that just described in the previous section, was observed and studied in the work of Petrenko and Schulson (1992a, b). It appeared that high-frequency conductivity ($\omega > \omega_D$) decreased by a factor between 2 and 10 while a relatively small direct voltage was being applied to pure ice specimens (Fig. 30). The relative decrease of σ_∞ when a direct electric field is applied becomes noticeable starting at a temperature of –10°C, and it increase rapidly at lower temperatures.

The phenomenon is practically insensitive to the type of electrodes used. So, it has, to the first approximation, the same magnitude both for ohmic electrodes as well as for common stainless steel electrodes; i.e., the effective charge exchange between ice and electrodes does not play such a significant role as it did in the case of recombination injection. This observation is well illustrated by Figure 30. As can be seen from this figure, the value of the observed decrease in σ_∞ is comparable for both dc bias polarities. At the same time, dc flows readily in the positive direction, when the electrodes operate in the ohmic mode, and

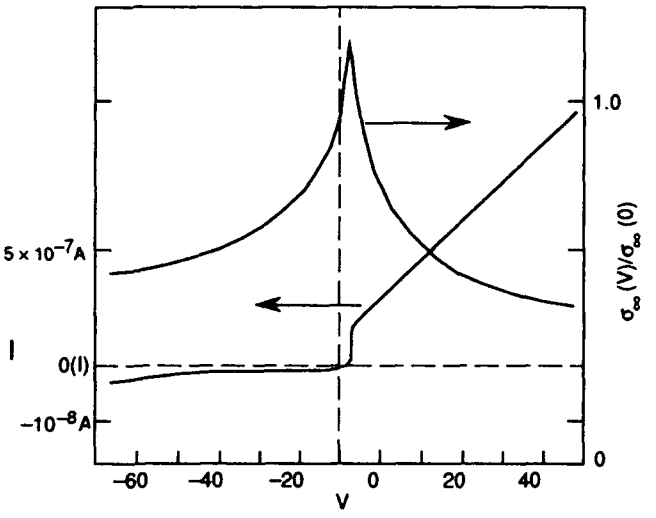

Figure 30. Dependences of normalized high-frequency conductivity σ_∞ and direct current I on voltage for thin (0.11-mm) single crystal of ice; T = –40°C; stainless steel ohmic electrodes were used; scales for positive and negative polarities of current vary in 20 times (after Petrenko and Schulson 1992a, b).

practically does not flow in the opposite direction. In terms of potential distribution, this means that in the first case the potential difference is applied to the ice bulk and in the second case it almost completely drops at two ice/metal interfaces.

The dependence of ice conductivity measured at high frequency on specimen thickness is shown in Figure 31. Ohmic electrodes have been employed in this experiment and an electric field has been applied in a "straight" direction. An increase in σ_∞ for ice thickness less than 10–20 μm is caused by the effect of recombination injection (which predicts $\sigma_\infty \sim L^{-2}$, see the previous section, eq 168), and also by the effect of roughness present at the surface of the electrodes. As for the characteristic σ_∞ increase in the specimen thickness range from 25 to 100 μm, it is easily reproducible and evidently reflects the internal distribution of majority charge carriers in a thin ice specimen. To account for the dependence $\sigma_\infty(L)$ shown in Figure 31, the authors of this study assumed that ice/metal interfaces are "drains" for Bjerrum defects; i.e., the recombination rate of L^- and D^+ defects at the interfaces is much higher than in the bulk. As a result, the charge carrier concentrations decrease profoundly in layers in which thickness is comparable to diffusion lengths. When the potential difference is applied, the recombination rate at the interfaces increases even more for two reasons. The first is the increase of defect densities n_D and n_L inside layers of space charge of thickness about the screening length ≤ 1 μm, since the rate of recombination is proportional to $(n_D n_L)$. The second is additional drift of carriers in the electric field to the interfaces. Simple numerical evaluations performed by Petrenko and Schulson may confirm the assumed mechanism. Although the exact mechanism of the direct electric field effect on σ_∞ is not absolutely clear yet, the fact of essential and reversible decrease in majority charge carrier concentrations is reliably established. This phenomenon promises interesting applications in studies of ice properties that depend upon majority carrier concentrations—the plastic flow and inelastic relaxation of ice, for instance.

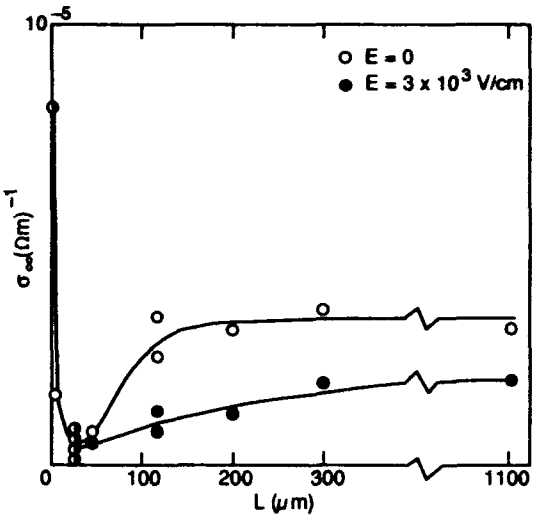

Figure 31. Dependence of σ_∞ on sample thickness L; T = –40°C; single crystalline, pure ice samples used with ohmic electrodes (after Petrenko and Schulson 1992a).

PROTON INJECTION FROM Pd ELECTRODES INTO ICE

The method of injection current measurement has been very efficiently employed for a long time in the study of electrical properties of ordinary semiconductors and dielectrics (Lampert and Mark 1970). By studying the charge carriers' injection into the bulk of the investigated material, one can determine such important parameters as charge carrier mobility, their equilibrium concentrations, the energy position of traps and the traps' concentrations.

In this method the carriers' space charge is "injected" into a material from an electrode. The charge value, and hence the number of charge carriers, is known because those quantities are determined by the laws of electrostatics. Since the concentration is already known, then the mobility can be calculated from conductivity measurements.

Let us clarify the main ideas of such experiments by following simple reasoning. Suppose a direct electric voltage V is applied to a conductor with two electrodes (Fig. 32). The electrode

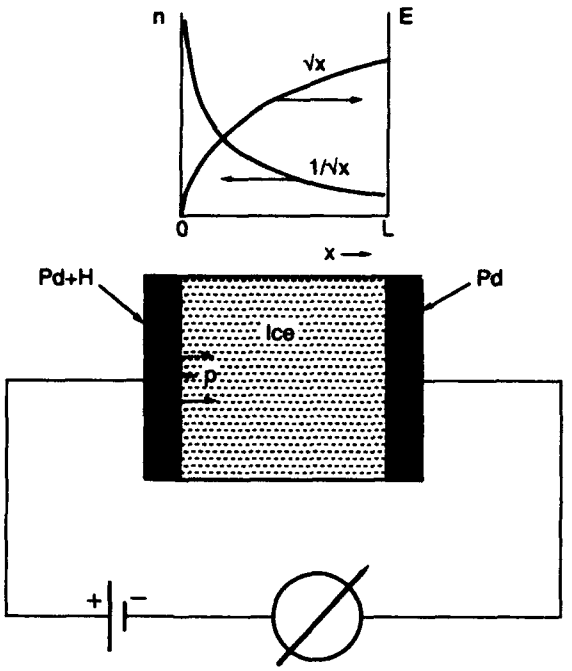

Figure 32. Injection of protons into ice from Pd electrode saturated by hydrogen. Pd cathode works as proton acceptor. Upper diagram illustrates distribution of protonic concentration n *and electric field* E *inside the specimen bulk.*

under positive potential is able to inject positive charge carriers with charge value e; i.e., this electrode is an "infinite capacity" reservoir of such carriers. Therefore, the carrier concentration in the vicinity of the electrode $n(+0) = \infty$, which implies that the electric field $E(+0) = 0$, because of "infinite" conductivity of the media at this point. The other electrode, at the point $x = L$, is the charge carrier receiver. Apparently, when a voltage V is applied, the carriers will be "pushed" into the bulk, increasing the conductivity of a specimen. In the case when concentrations of injected carriers are much greater than equilibrium concentrations, we can readily write down a closed system of equations that defines injection current density J, electric field strength E and carrier concentrations n

$$\frac{dE}{dx} = \frac{\rho}{\varepsilon\varepsilon_0} = \frac{en}{\varepsilon\varepsilon_0} \text{ (Poisson's equation)} \tag{169}$$

$$J = ej = en\mu E = \text{const} \tag{170}$$

$$\int_0^L E dx = V;\ E(+0) = 0;\ n(+0) = \infty. \tag{171}$$

The solution is given by an elegant formula

$$J = \frac{9}{8}\varepsilon\varepsilon_0\mu\frac{V^2}{L^3} \tag{172}$$

in which there appears only one unknown parameter, μ, which can be found from experimental measurement of J. Therefore, we can determine charge carrier mobility by means of injection current measurements. That is not all. The concentration of injected carriers is

$$n = \frac{3}{4}\frac{\varepsilon\ \varepsilon_0}{e\ L^2} V\sqrt{\frac{L}{x}} \tag{173}$$

and the "average" bulk concentration is

$$\langle n \rangle = \frac{1}{L} \int_0^L n(x)\,dx = \frac{3}{2} \frac{\varepsilon\ \varepsilon_0}{e\ L^2} V. \tag{174}$$

If equilibrium charge carriers with concentration n_0 are present in the investigated material, then at small voltages V (small level of injection) a linear zone will be observed on the voltage–current characteristic, i.e., Ohm's law

$$J_0 = e\,\mu\,n_0 \frac{V}{L}. \tag{175}$$

The transition from dependence (eq 175) to eq 172 will occur in the region where $J \approx J_0$. From here it follows that

$$V_{tran} \approx \left(\frac{8}{9} \frac{e\ L^2}{\varepsilon\ \varepsilon_0}\right) n_0 \tag{176}$$

i.e., having determined V_{tran} from current–voltage characteristics, we can calculate n_0. So, the injection currents technique allows us to determine charge carrier concentrations and mobilities in those materials in which the Hall effect cannot be measured—because of extremely small mobility, for instance, as in the case of ice.

At first glance the injection of protonic charge carriers into ice is extremely complicated, since there are four types of such carriers in ice and their motion is correlated through a configuration vector Ω. In fact, the mathematical description of injection currents theory in ice is complicated and space-consuming. The results of this theory are nevertheless simple and clear, which allows us to interpret them successfully in the context of the consideration just performed.

The theory of injection currents in ice was developed for the first time in the work of Petrenko et al. (1983), in which a solution was obtained for one particular case: the injected proton concentration exceeded the equilibrium ion concentration, but was still much less than the Bjerrum defect concentration. The general problem was solved later (Petrenko and Ryzhkin 1984b). Either a proton can be injected into ice from outside, which introduces an H_3O^+ ion and a D-defect simultaneously (see Fig. 8), or protonic "hole" occurs, which is equivalent to the production of another defect pair—an OH^- ion and an L-defect. The equations describing the proton and protonic "hole" injection into ice are the same. Therefore, it is enough to consider the case of proton injection as an example.

The theoretical current–voltage characteristic of injection protonic currents in ice, adopted from the paper of Petrenko and Ryzhkin (1984b), is shown in Figure 33. Zone I (Ohm's law) is observed when the average concentration of injected

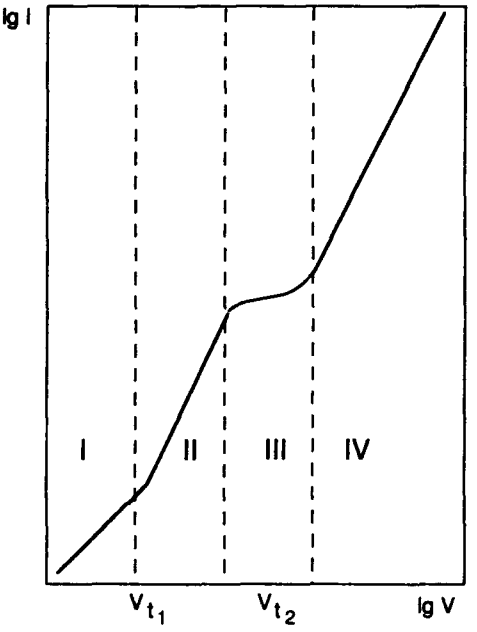

Figure 33. Theoretical current–voltage characteristic for proton injection into ice (see explanations in the text [after Petrenko and Ryzhkin 1984b]).

protons n_p is much less than equilibrium ionic concentration n_i. When n_p becomes greater than n_i, but is still less than equilibrium Bjerrum defect concentration n_B, zone II must be observed, in which $J \sim V^2$

$$J = \left(\frac{9}{8}\,\varepsilon_s\,\varepsilon_0\,\mu_1\,\frac{e\,V^2}{e_1\,L^3}\right). \tag{177}$$

As can be seen from this formula, we can determine H_3O^+ ion mobility μ_1 from measurement of J. Note also that the magnitude of injection currents in zone II is proportional to a large ($\sim 10^2$) static dielectric permittivity of ice ε_s. The magnitude of the transition voltage V_{t1} is characterized by the condition that $n_p \approx n_i$. Hence, using eq 176 and $\varepsilon = \varepsilon_s$, one can determine the equilibrium ion concentration.

When voltage magnitude and level of injection are increased, it may happen that $n_p \geq n_B$. In this case, since for injected carriers $n_i = n_B$ holds, the concept of majority and minority charge carriers ceases to exist. The constraint on carrier motion imposed by the configuration vector is also eliminated, the carrier motion becomes uncorrelated, and ε drops from $\varepsilon_s \approx 100$ to $\varepsilon_\infty \approx 3.2$. This leads to the following observation in zone IV, where the current magnitude is the square of the voltage, but the proportionality coefficient is smaller

$$J = \frac{9}{8}\,\varepsilon_\infty \varepsilon_0 \left(\frac{\mu_1\,\mu_2\,e}{e_1\,\mu_1 + e_3\,\mu_3}\right)\frac{V^2}{L^3}. \tag{178}$$

This allows us to calculate both the minimal mobility of the two (μ_1 or μ_3) from measurement of J and the equilibrium Bjerrum defect concentration from the V_{t2} value.

If measurements of current in the case of protonic "hole" injection were performed, we could determine all four mobilities $\mu_1,\ldots,\mu_4$ and all four equilibrium concentrations $n_1,\ldots n_4$. However, experimental studies in the field of injection currents are much less successful than theoretical ones. In all experimental works on injection currents in ice, hydrogen-saturated Pd or palladium black were used as proton injecting electrodes. Here, hydrogen, which could be dissolved in Pd with concentrations close to one, gives its single electron to Pd and readily migrates in the Pd lattice. Pd can be saturated with hydrogen in a water electrolysis process (when Pd is a cathode) or in a heating process under high pressure in a hydrogen atmosphere. Such protonic in-

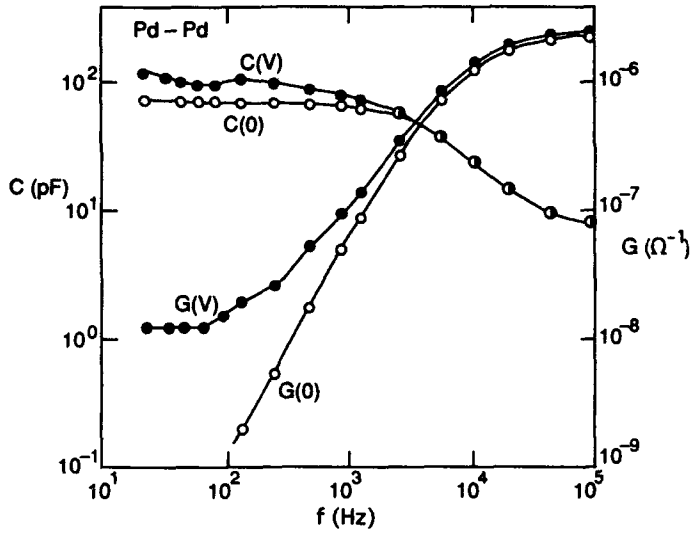

Figure 34. Dispersion curves for pure, monocrystalline ice specimen with two H-loaded Pd electrodes of area = 15 × 9 mm², thickness = 0.7 mm, temperature = −16°C. C(0) and G(0) are the specimen capacitance and conductance without dc bias; C(V) and G(V) are the same with dc bias of V = 2.0 kV (after Petrenko et al. 1983).

jection into ice was first carried out by Engelhart and Riehl (1965, 1966), who measured current–voltage characteristics of thin (~ 0.5 mm) ice specimens with Pd electrodes. In this study they were not able to obtain zones in which current was distinctly proportional to the square of the voltage, and the current–voltage characteristics were obviously complicated by the effect of proton traps present in the imperfect ice crystals used in those experiments. Nevertheless, quantitative evaluations that can be made on the basis of existing theories indicate that in those first studies, the injection of protons into the bulk was undoubtedly achieved. The same is not true for their later research (Engelhart et al. 1969), performed on ice specimens of such large thickness (10 cm) that, although the zone of square dependence was observed in current–voltage characteristics, it cannot be explained in terms of space proton injection ($J \sim L^{-3}$).

To prove that ice bulk conductivity (σ_s and σ_∞) increases as a result of proton injection, Petrenko et al. (1983) made measurements at ac along with dc measurements that eliminate any doubts concerning the effect of ice/metal interface resistance on current–voltage characteristics. The changes in $\sigma(\omega)$ and J due to proton injection into ice are shown in Figures 34 and 35. Using stationary currents of monopolar proton injection made it possible for H_3O^+ ion mobility to be determined (see Table 2).

A remarkable experimental study on the measurement of transient injection currents in ice was carried out by Eckener et al. (1973). In these experiments a short laser pulse released protons from a thin palladium black film, which was kept in contact with ice. The released protons, under the action of force from a constant electric field, were moving from anode to cathode, thus producing a current pulse, the duration of which was equal to the transit time of protons through an ice specimen

$$t = \frac{L}{\mu_1 E} = \frac{L^2}{\mu_1 V}. \tag{179}$$

The value of H_3O^+ ion mobility, which is obviously the most reliable data for today, has been obtained by this method (see Table 2).

The extensive use of the injection current technique in ice is limited by basic difficulties in preparation of electrodes that would efficiently inject protons into ice. Contamination processes at the ice/Pd interface, which are poorly controlled, deteriorate the reproducibility of results considerably.

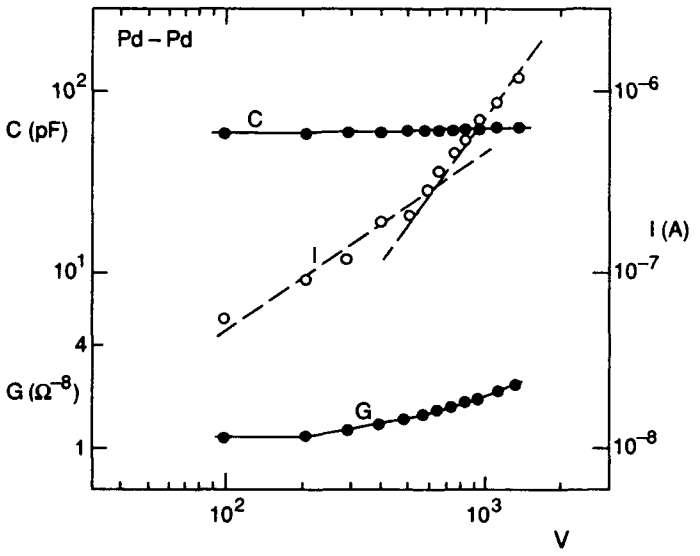

Figure 35. Direct current I, *capacitance* C *and conductance* G *at 100 Hz, as functions of bias voltage* V *for specimen with two H-loaded Pd electrodes of area = 6 × 9 mm², thickness = 0.4 mm, temperature = –20°C. Broken lines of slopes 1 and 2 have been drawn for the current characteristics (after Petrenko et al. 1983).*

FIELD EFFECT TRANSISTOR MADE OF ICE

The operation principle of the field effect transistor, if one tries to describe it in a few words, is as follows. Let us consider a conductor/dielectric interface, as shown in Figure 36. Suppose that normal to this interface, a static electric field is applied, $E(-0) = E_\perp$, which attracts charge carriers to the interface. A thin layer of excess concentration N_1 (dimension m^{-2}) will form in the conductor along the interface. Since the electric field at the infinity $E(+\infty) = 0$, then from the well-known Gauss electrostatic theorem it follows that

$$E_\perp = \frac{e_1 N_1}{\varepsilon_d \varepsilon_0} \tag{180}$$

where ε_d is the dielectric permittivity of the dielectric. Then the surface conductivity of the conductor, resulting from the applied field, is

$$\lambda_s = e_1 N_1 \mu_1 = \varepsilon_d \varepsilon_0 E_\perp \mu_1 . \tag{181}$$

Formula 181 shows how the value of charge carrier mobility μ_1 can be determined, if the applied field $E_\perp$ is known from the experimental conditions and λ_s is measured. If there are two types of charge carrier present in the conductor (for instance, H_3O^+ and OH^- ions in ice), then in order for the second type of charge carrier mobility to be determined, we should just change the polarity of $E_\perp$!

In case of ice, this apparent simplicity is complicated by the presence of two more charge carriers: D- and L-defects. However, the effect of the electric field on their concentration is negligibly small compared to the change in ion concentrations. This fact is easy to understand if we recall that the carrier concentration $n_i(x)$ depends upon the magnitude of electric potential at a given point (x), as

$$n_i = n_{i\infty} \exp\left\{-\frac{e_i \varphi(x)}{k_B T}\right\} \tag{182}$$

where $\varphi(x)$ is the electric potential and $n_{i\infty}$ is the carrier concentration at infinity, where there is no electric field and $\varphi = 0$. Since the value of the ions' electric charge $e_1 = 0.62\ e$ is much greater than $0.38\ e$, which is the Bjerrum defect charge, then the effect of the electric field is also much more profound for ions.

As long as $\sigma_{ion} < \sigma_B$ in the surface layer, the static conductivity will be determined by ions, so that

$$\lambda_s \approx \left(\frac{e}{e_1}\right)^2 \varepsilon_\infty \varepsilon_0 \mu_1 E_\perp \tag{183}$$

where the factor $(e/e_1)^2 \approx 2.6$ follows from eq 70, which describes the static conductivity of ice. When $E_\perp$ is increasing,

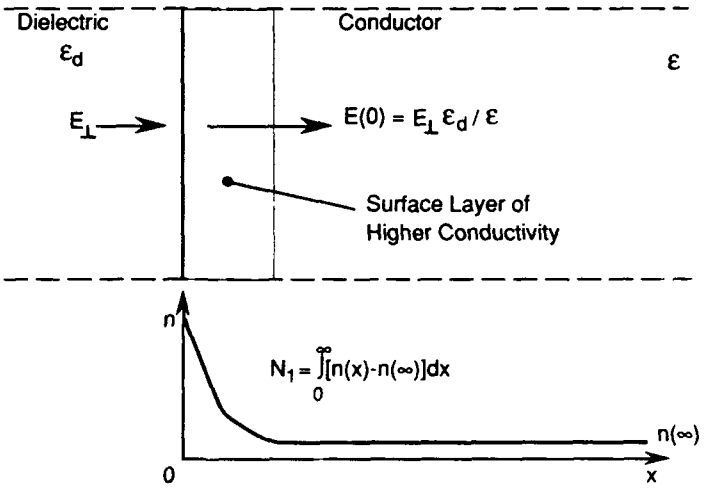

Figure 36. Dielectric/conductor interface with applied static electric field $E_\perp$. The diagram below shows schematically a distribution of charge carrier concentration n.

σ_{ion} can exceed σ_B, since the ionic concentration grows faster than Bjerrum defect concentration. Bjerrum defects cease to be majority charge carriers and their mobility and charge appear in eq 183. So, by means of measuring σ_s at different magnitudes and polarities of electric field $E_\perp$, we can determine all four mobilities.

The field effect transistor made of pure ice was experimentally realized by Petrenko and Maeno (1987). The layout of such a transistor is shown in Figure 37. A thin (about 1000 Å) dielectric layer of SiO_2 is placed onto a conducting substrate made of Si. Gold electrodes are deposited onto the SiO_2 layer by means of photolithography, and are then used for surface conductivity measurements. To increase the total length of contact and thus reduce the measured surface conductivity, the electrodes had the shape of two combs inserted toothwards into each other, as shown in the upper section of Figure 37. A bias was applied between the Si substrate and ice, and a layer was formed at the SiO_2/ice interface with an excess concentration of either H_3O^+ ions ("plus" is at ice) or OH^- ions ("plus" is at Si).

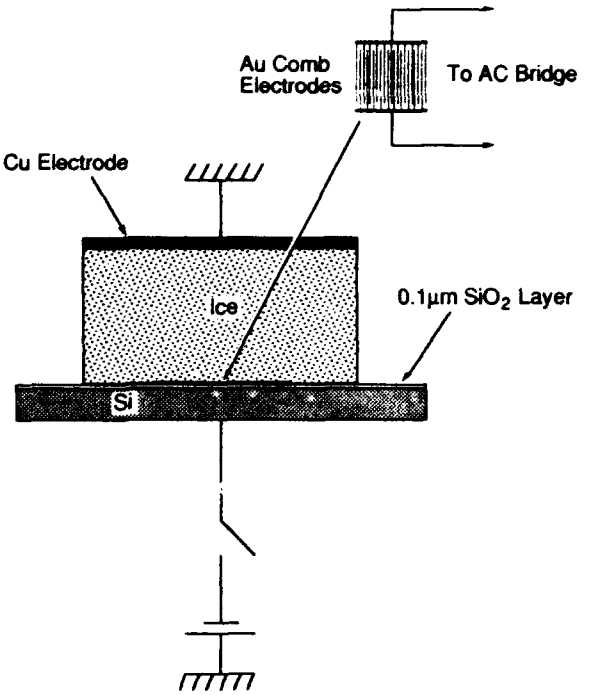

Figure 37. Field effect ice transistor (after Petrenko and Maeno 1987).

Figure 38 illustrates the alternation of the surface conductivity of ice, when rectangular voltage pulses of different polarity are applied. The values of μ_1 and μ_2 determined in this experiment can be found in Table 2.

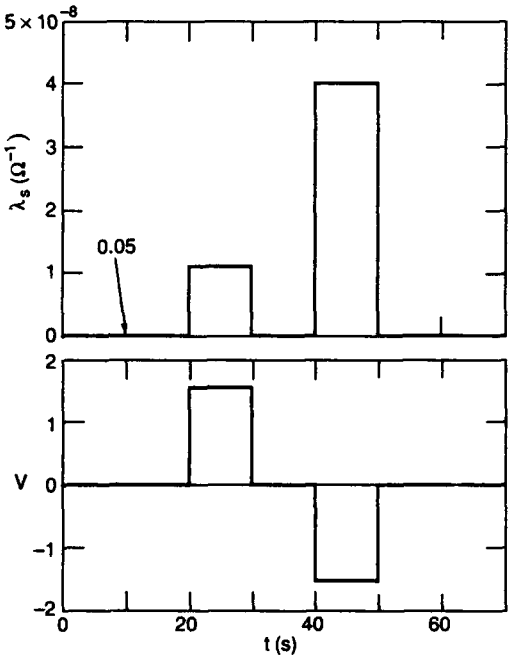

Figure 38. Time diagrams of ice surface conductivity λ_s and dc bias (V) applied to the transistor shown in Figure 37; T = −33.1 °C; surface conductivity was measured at f = 10 Hz (after Petrenko and Maeno 1987).

"CROSSOVER" IN THE DIELECTRIC PERMITTIVITY OF ICE

Until now, we have referred to static dielectric permittivity of ice ε_s as a large quantity, about 10^2. For the most part this is true. But in some instances, at particular temperatures and impurity concentrations, ε_s can decrease drastically and achieve small values, comparable with those of $\varepsilon_\infty \approx 3.2$. This phenomenon, which has become known as "crossover," can be successfully explained in the context of Jaccard's model of the electrical conductivity of ice.

If we examine attentively formula 72, which describes ε_s as a function of temperature ($\phi = 3.85\, k_B T r_{00}$) and conductivities σ_{ion}, then we will notice that if the following relationship is satisfied

$$\frac{\sigma_1 + \sigma_2}{e_1} = \frac{\sigma_3 + \sigma_4}{e_3} \tag{184}$$

the second term in formula 72 reduces to 0 making ε_s equal to ε_∞.

The physical interpretation of such a significant drop in ε_s is that if the above condition (eq 184) is satisfied, then the charge carriers moving under the action of an external electric field—the fluxes of ions and Bjerrum defects—appear to be equal (see eq 64). Therefore, the configuration vector $\Omega = 0$ all the time, i.e., the predominant orientation of hydrogen bonds is not formed. Consequently, there is no additional returning force from Ω acting upon the charge carriers. It is this force, resulting from Ω, that converts pairs of major charge carriers into "elastic dipoles." In other words, under the condition of eq 183, inasmuch as $\Omega = 0$, the correlation in charge carrier motion ceases and they will move in the same fashion as in an ordinary conductor. In this case, no further contribution to ε_s apart from ε_∞ (dielectric permittivity of media) can be expected!

In very pure ice the "crossover" phenomenon is not observed, since

$$\sigma_{ion} = (\sigma_1 + \sigma_2) << (\sigma_3 + \sigma_4) = \sigma_B . \tag{185}$$

This is related to the fact that at high temperatures (0 to –10°C), $\sigma_B \approx \sigma_\infty$ exceeds by about two or three orders of magnitude the ionic conductivity $\sigma_{ion} \approx (e_1/e)^2\, \sigma_s$. If the temperature is decreased, σ_B and σ_{ion}, since they have comparable values of activation energies—about 0.5–0.6 eV—will never become equal until they reach the lower limit of ac measurements possible in pure ice ($\approx$ 150 K).

However, the picture changes drastically if there are impurities present in ice, since their effect at σ_{ion} and σ_B is different (see the *Concentration of Charge Carriers* section).

So, for example, when H_3O^+ "impurity" ions are introduced, σ_{ion} is almost constant at high temperatures, while σ_B decreases rapidly, as temperature decreases. Temperature dependencies for σ_B and σ_{ion} in ice doped with a small amount of HF (1.3×10^{14} cm^{-3}) are shown in Figure 39. Close to the point $T_{cr} = 230$ K, σ_B and σ_{ion} become equal, and at lower temperatures they change places: $\sigma_B < \sigma_{ion}$. In other words, at the point of intersection ("crossover"), the ions turn from minority into majority charge carriers, and Bjerrum defects become the minority charge carriers. So, we have

$$\text{at } T > T_{cr}: \sigma_\infty \approx \sigma_B ;\ \sigma_s \approx \left(\frac{e}{e_1}\right)^2 \sigma_{ion} \tag{186}$$

$$\text{at } T < T_{cr}: \sigma_\infty \approx \sigma_{ion} ;\ \sigma_s \approx \left(\frac{e}{e_3}\right)^2 \sigma_B . \tag{187}$$

Figure 40 illustrates a sharp decrease of ε_s in the vicinity of T_{cr} in HF-doped ice. Hubmann (1978) observed "crossover" in NH_3-doped ice (5×10^{-5} mol/L) when the pressure was increased, since the latter increased σ_{ion} and decreased σ_B.

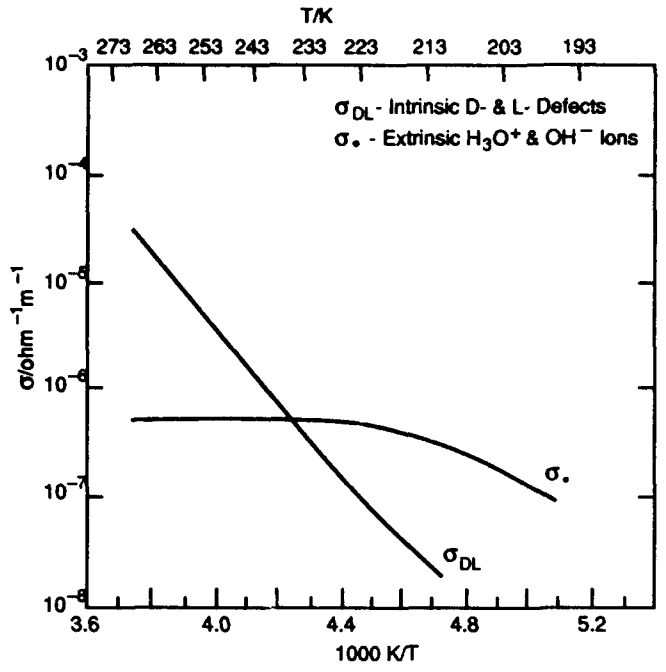

Figure 39. Temperature dependences of H_3O^+ ion conductivity $\sigma_\bullet$ and Bjerrum defects' conductivity σ_{DL} calculated from experimental results, using best-fit method. Ice doped by HF in the concentration of $(1.3 \pm 0.1) \times 10^{20}$ molecules/m^3 (after Camplin et al. 1978).

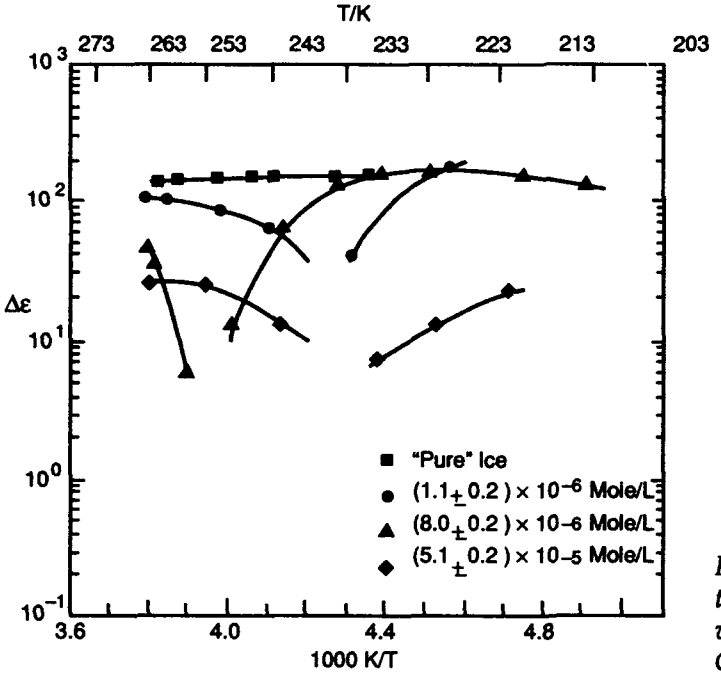

Figure 40. $\Delta\varepsilon = \varepsilon_s - \varepsilon_\infty$ as a function of temperature for ice doped with HF concentrations (after Camplin and Glen 1973.)

A remarkable example of "double crossover" can be found in an old report by Steinemann (1957)—which became a classic—who studied dielectric permittivity of HF-doped ice. At the high temperatures used by Steinemann (–3°C), it is possible to pass through the "crossover" point twice, since σ_B changes by an amount proportional to n_{HF}, and σ_{ion} by an amount proportional to $\sqrt{n_{HF}}$. Therefore, the equation

$$\sigma_B = \sigma_{ion} \rightarrow \sigma_{B0} + a_1 n_{HF} = \sigma_{i0} + a_2 (n_{HF})^{1/2}$$

can be satisfied at two different values of n_{HF} (see Fig. 41).

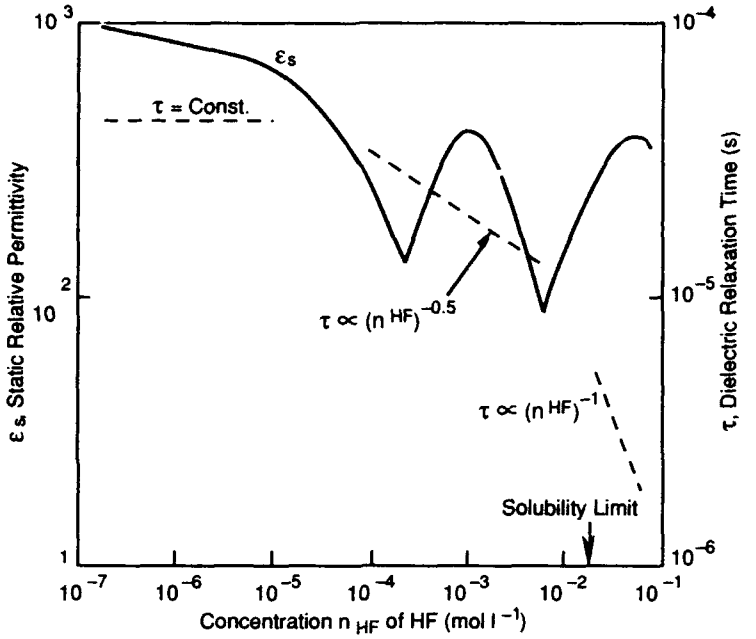

Figure 41. Static relative permittivity ε_s and dielectric relaxation time τ at –10°C as a function of the concentration n_{HF} in the solution from which the polycrystalline ice was formed (after Steinemann 1957).

THERMALLY STIMULATED DEPOLARIZATION

The method of Thermally Stimulated Depolarization (TSD) is successfully used in studies of dielectrics and materials with low conductivity. Its generally accepted advantages are top instrumental simplicity and high sensitivity. Figure 42 illustrates the basic principles of TSD measurements.

In this method the material under investigation is first cooled under conditions of an external electric field $\vec{E}$ being applied. Under the action of this field, an electrical polarization $\vec{P}$ arises in the material (ice in our case), which, after cooling to a sufficiently low temperature, appears to be "frozen," i.e., it remains after the external field is switched off. Here, the concept of "low temperature" is relative, since for alkaline halide crystals room temperature is already sufficiently low.

When the specimen is heated (usually at a constant rate $dT/dt = \gamma$) the frozen electric dipole moment relaxes. An electric current, usually measured by an electrometer and by an XY recorder, flows through the external circuit. The analysis of the $I(t)$ recording frequently allows us to determine important parameters of the conductivity processes.

Let us illustrate this with a simple example. The relaxation rate of electric polarization $\vec{P}$ can be described in terms of simple exponential time dependence

$$P = P_0 \exp\left\{-\frac{t}{\tau}\right\}. \tag{188}$$

The relaxation time τ as a rule is defined in terms of some thermoactivation process, so that

$$\tau = \tau_0 \exp\left\{\frac{E_A}{k_B T}\right\} \tag{189}$$

where E_A is an activation energy.

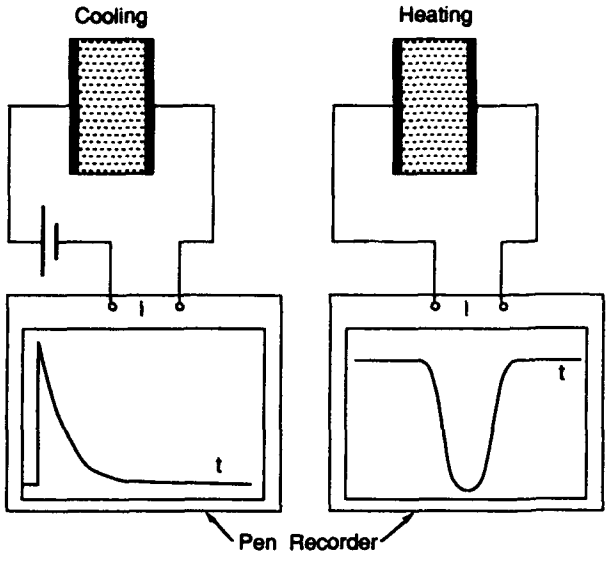

Figure 42. Schemes of polarization (cooling) and depolarization (heating) in the TSD technique.

As we have already seen in the *Relaxation Times of the Electric Polarization and Electric Fields in Ice* section, the current density $\vec{J}$ and dielectric polarization $\vec{P}$ are related through the simple relationship (eq 151)

$$J = \frac{dP}{dt}$$

and, taking into consideration eq 188, we obtain

$$J = -\frac{P}{\tau}. \tag{190}$$

Now, substituting eq 189 into 190 and considering that

$$P = -\int_{t}^{\infty} J(t)\,dt \tag{191}$$

we ultimately obtain

$$\frac{J(t)}{\left[\int_{t}^{\infty} J(t)\,dt\right]} = \frac{1}{\tau} = \frac{1}{\tau_o}\exp\left\{\frac{-E_A}{k_B T}\right\}. \tag{192}$$

From this it can be seen that if a graph of the natural logarithm of the left side of eq 192 is plotted versus $\{1/k_B T\}$, then it will be a straight line with slope E_A! That is, in this way the value of the activation energy of the charge transfer process, which leads to relaxation of P, can be determined. Furthermore, since

$$P_o = \int_{o}^{\infty} J(t)\,dt$$

then the area below the bell-shaped curve of TSD (Fig. 42) contains information about the num-

ber of "polarized and frozen" dipoles, P being the result of their reorientation. Those are the basic principles underlying the TSD method. Quite often the simple TSD analysis presented above is complicated in practice by the presence of several relaxation processes instead of one. For example, the initial "conserved" polarization P_0 might be defined in terms of reorientation of several different concentrations and activation energies of elementary dipoles.

In the heating process different dipoles will relax at different temperatures. Thus, instead of one "simple" bell-shaped TSD current pulse, we will observe several. For the analysis of such situations, several special techniques have been developed that allow us to separate one relaxation process from another. Let us look at some of those.

If it is possible to guess by the shape of the curve $J(t)$ how many peaks there are on this curve, then we can employ computer analysis, seeking to find the best fitting theoretical curve.

Another method that allows us to amplify separate "peaks" on the background of other peaks is switching on the external field E, not during the whole cooling period of the investigated specimen, but only in that temperature range in which this peak will "develop" afterwards. Then higher temperature peaks will not appear, because the temperatures are too low for their production. TSD "peaks" at lower temperatures will have enough time to relax during the cooling process, after the external field has been switched off.

A modification of this method is thawing of different dipoles systems in turn; i.e., when the temperature is increasing and after the first (the lowest temperature) peak is passed, the temperature is decreased again and this already "developed" peak does not contribute to a new thawing cycle. Then this procedure is repeated until the next peak, and so on.

For ice research the TSD method is attractive because it provides a way to study conductivity processes at temperatures so low that ac measurements become either impossible or strongly impeded. The research in TSD on pure and doped-ice monocrystals started over two and a half decades ago (see Engelhart and Riehl 1965, Gelin and Stubbs 1965). Detailed experimental studies of TSD in ice were carried out by Bishop and Glen (1969), Loria et al. (1978), Johari and Jones (1975) and Apekis and Pissis (1987). In the last report the reader can find an extensive list of papers concerned with TSD in ice. In many papers the observation of several TSD peaks has been reported, the magnitude and location of which depend upon doping impurity types and concentrations (see Zaretskii et al. 1987b, for instance). Two examples of "thermograms," adopted from this report, are shown in Figure 43. In the reports of various authors concerned with ice TSD, a considerable discrepancy can be found in activation parameter values, calculated from those "thermograms," and their various interpretations. We deliberately avoid commenting on these numerical data for the reason explained below.

In all the cited experimental reports, the analysis was performed on the basis of simple model considerations just discussed. However, such considerations are not applicable in the case of ice, because of the presence of the configuration vector $\vec{\Omega}$, which plays the role of the force field. Under typical conditions of TSD measurement, when a thin ice specimen is placed between shorted electrodes (the resistance of the measuring circuit is much less than the resistance of ice), the electric field within the ice $E \cong 0$, and the major force driving charge carriers is $\vec{\Omega}$. Therefore, it is more correct to speak about relaxation of the configuration vector $\vec{\Omega}$ rather than relaxation of polarization P. Since we have

$$\frac{d\Omega}{dt} = (j_1 - j_2) - (j_3 - j_4) = \frac{J_i}{e_1} - \frac{J_B}{e_3} \tag{193}$$

$$J_i = e_1(j_1 - j_2); \quad J_B = e_3(j_3 - j_4) \tag{194}$$

$$j_i = -\eta_i \phi \Omega \sigma_i ; \quad E = 0 ; \quad \text{grad } n_i = 0 \tag{195}$$

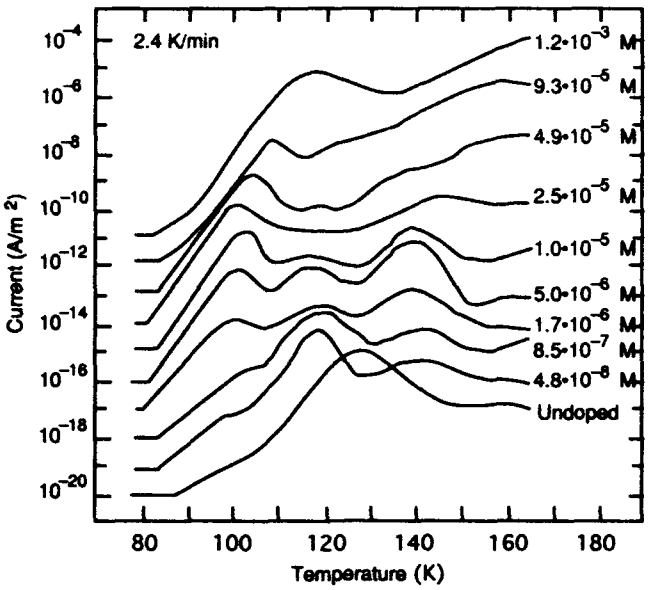

a. Ice doped with HCL in different concentrations.

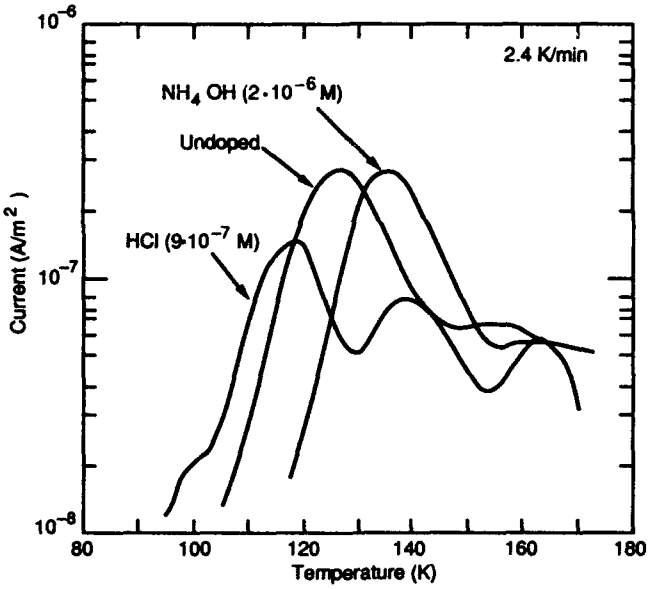

b. Pure ice and ice doped with HCl and NH_4 OH.

Figure 43. TSD currents of ice specimens (after Zaretskii et al. 1987b).

then instead of eq 190 we obtain for current density

$$J = J_{ion} + J_B = \phi \Omega \left(\frac{\sigma_B}{e_3} - \frac{\sigma_{ion}}{e_1} \right). \tag{196}$$

But this is an absolutely amazing result! Equation 196 predicts that in the relaxation process during heating, the TSD current will alter the direction at the "crossover" point, i.e., where $\sigma_B/e_3 = \sigma_{ion}/e_1$. That is, relaxation currents, initially flowing in the direction opposite to the

applied external field, after that point, change direction and flow with it! This peculiarity was theoretically pointed out for the first time by Zaretskii et al. (1987b), and experimentally the direction change of TSD currents in ice was reported by Johari and Jones (1975). Later, this phenomenon was studied in detail by Aziev et al. (1987). In the report of Zaretskii et al. (1987b), it was also demonstrated that a similar current inversion can be observed within another regime of so-called Thermally Stimulated Currents (TSC). Within this regime a specimen is heated in a strong, constant electric field and currents flowing through it are measured. In fact, such current inversion had already been observed in the work of Dengel et al. (1964), in which the alternations of current direction occurred at $T = 112$ K and $T = 144$ K. At that time such unusual behavior of TSC was interpreted in terms of the transition of ice into a ferroelectric state! Now, however, in the wake of numerous structural studies, we know that there is no ferroelectrical transition in ice in this temperature range. It is easy to show, considering relaxation of $\vec{\Omega}$ rather than relaxation of $\vec{P}$, that

$$\frac{d\vec{\Omega}}{dt} = -\frac{\vec{\Omega}}{\tau_D} \tag{197}$$

and instead of eq 192 employed for determining of E_A in the TSD method, an essentially more complicated equation arises

$$\frac{J(t)\cdot\beta(t)}{\int_t^\infty J(t')\,\beta(t')\,dt'} = \frac{1}{\tau_o}\exp\left\{\frac{E_A}{K_B T}\right\} \tag{198}$$

where

$$\beta = \frac{\left(\frac{\sigma_{ion}}{e_1^2} + \frac{\sigma_B}{e_1^2}\right)}{\left(\frac{\sigma_B}{e_3} - \frac{\sigma_{ion}}{e_1}\right)}. \tag{199}$$

The extensive, accumulated experimental data should be processed using formula 198 rather than 192. However, this rather time-consuming procedure has never been used. Still, if there is confidence (from independent experiments) that the "crossover" does not occur within the investigated temperature region, then we can also use (with low accuracy) the more simple relationship (eq 192).

CONCLUSION

At this point we finish the consideration of the electrical properties of ice. Some particular aspects that are usually considered along with the electrical properties of ice will be transferred to future reports to avoid undue complexity and length of this account. Special questions discussed herein are, as a rule, on a frontier between various fields of physics. Thus, we will consider in detail the surface conductivity of ice in the report, *Surface of Ice*. There the results of measurements of the Hall-effect will also be discussed, since some fairly reliable data are obviously related to surface conductivity only. Thermoelectric effects will be considered in the report, *Thermal Properties*, along with diffusion processes in ice.

In the report concerned with electromechanical effects, we will also consider the effect of

pressure on electrical properties, pseudo piezoelectric properties and electromagnetic emission from cracks in ice. All these phenomena are interrelated. In the report, *Electro-optical Effects in Ice*, both intrinsic and impurity-caused photoconductivity of ice will be described as well as photoelectrical phenomena at ice/electron conductor interfaces.

As a unifying framework in the description and discussion of the electrical properties of ice, the author employed Jaccard's theory. This seems to have helped preserve a single, coherent framework in presenting the material. Such intensive use of this theory, in spite of its evident merits, does not imply that Jaccard's theory has no drawbacks and is able to cover all "white spots" on the ice physics map. Nor is it a unique theory. Jaccard's theory is empirical or half-empirical, i.e., it was not derived from "first principles." This theory is based upon, firstly, the concept of two fundamentally different types of charge carriers (ions and Bjerrum-defects) and, secondly, concepts about changes occurring in ice structure as a result of motion of these defects.

As far as the first aspect is concerned, then, our ideas about the real microscopic structure of ice defects may change strongly—and already are changing. The author refers the reader to a report from the present series called *The Structure of Ordinary Ice I_h—Part II. Real Structure of Ice, Defects*, in which a description is given of alternative models of protonic structure defects: a soliton model, a lattice reconstruction model and a model of radicals.

As far as the second whole set of concepts on which Jaccard's model rests is concerned, I believe it will remain whole, and this make the model extremely viable. In fact, for the validity of the model, it is important that the hydrogen bonds along which the defects move would reorient in the manner perceived by Jaccard. This will be retained in all other models (the soliton model, for instance). Thus the whole mathematical description suggested by Jaccard will remain!

The model appears to be able to account not only for ac and dc conductivity and dielectric permittivity, but for numerous physical phenomena that appeared after the reports of Jaccard (1959, 1964).

This theory, of course, owing to its empirical and schematic nature, cannot give answers to all questions, such as why the mobilities of ions and Bjerrum defects are what they are. The answer to this and other questions must be obtained in the context of theory still in development, based upon the quantum theory of solids.

LITERATURE CITED

Apekis, L. and P. Pissis (1987) Study of the multiplicity of dielectric relaxation times in ice at low temperatures. *Journal de Physique C1*, **48**: 125–133.

Auvert, G. and A. Kahane (1973) Discussion. In *Physics and Chemistry of Ice* (E. Whalley, S.J. Jones and L.W. Gold, Ed.). Ottawa: Royal Society of Canada, p. 270–271.

Ayrton, M.E. and Perry (1877) *Proceedings of Physics Society (London)*, **2**: 178.

Aziev, E.A., A.V. Zaretskii, V.F. Petrenko and M.P. Tonkonogov (1987) Negative currents of thermally stimulated depolarization in NH_4OH doped ice. Chernogolovka: Institute of Solid State Physics of Academy of Science of USSR.

Bishop, P.G. and J.W. Glen (1969) Electrical polarization effects in pure and doped ice at low temperature. In *Physics of Ice* (N. Riehl, B. Bullemer and H. Engelhardt, Ed.). New York: Plenum Press, p. 492–501.

Bockris, J. O'M. (1979) *Quantum Electrochemistry*. New York: Plenum Press.

Bullemer, B. and N. Riehl (1966) Bulk and surface conductivity of ice. *Solid State Com.*, **4**: 447–448.

Bullemer, B., H. Engelhardt and N. Riehl (1969) Protonic conduction of ice. *Physics of Ice* (N. Riehl, B. Bullemer and H. Engelhardt, Ed.). New York: Plenum Press, p. 416–442.

Camplin, G.C. and J.W. Glen (1973) The dielectric properties of HF-doped single crystals of ice. In *Physics and Chemistry of Ice* (E. Whalley, S.J. Jones and L.W. Gold, Ed.). Ottawa: Royal Society of Canada, p. 256–261.

Camplin, G.C., J.W. Glen and J.G. Paren (1978) Theoretical models for interpreting the dielectric behavior of HF-doped ice. *Journal of Glaciology*, **21**(N85): 123–141.

Chesnakov, V.A. (1990) Experimental study of physical process on ice-electron conductor interfaces. Ph.D. Thesis, Institute of Solid State Physics of Academy of Science of USSR, Chernogolovka.

Chesnakov, V.A., V.F. Petrenko, I.A. Ryzhkin and A.V. Zaretskii (1987) Photoelectrical phenomena at ice-semiconductor interfaces. *Journal de Physique, C1*, **48**: 99–103.

Cole, K.S. and Cole, R.H. (1941) Dispersion and absorption in dielectrics. *Journal of Chemistry and Physics*, **9**: 341–351.

Decroly, J.C., H.V. Granicher and C. Jaccard (1957) Caractère de la conductivité électrique de la glace. *Helvetica Physica Acta*, **30**: 465–467.

Dengel, O., U. Eckener, M. Plitz and N. Riehl (1964) Ferroelectric behaviour of ice. *Physics Letters*, **9**: 291–292.

Eckener, U., D. Helmreich and H. Engelhardt (1973) Transit time measurements of protons in ice. In *Physics and Chemistry of Ice* (E. Whalley, S.J. Jones and L.W. Gold, Ed.). Ottawa: Royal Society of Canada, p. 242–245.

Eigen, M. and L. De Mayer (1956) Ein stationäres Feldverfahren zur Untersuchung von Dissoziationsprozessen in Feüssigkeiten und Festkörpern. *Z. Elektrochem.*, **60**: 1037–1048.

Eigen, M. and L. De Mayer (1957) Berichtigungzu der Mitteilung. *Z. Electrochem.*, **61**: 856.

Eigen, M. and L. De Mayer (1958) Self-dissociation and protonic charge transport in water and ice. *Proceedings of the Royal Society*, **A247**: 505–533.

Eigen, M., L. De Mayer and H. Spatz (1964) "Über das Kinetische Verhalten von Protonen and Deuteronen in Eiskristallen. *Z. Electrochem.*, **68**: 19–29.

Engelhardt, H. (1973) Protonic conductivity of ice. In *Physics and Chemistry of Ice* (E. Whalley, S.J. Jones and L.W. Gold, Ed.). Ottawa: Royal Society of Canada, p. 226–235.

Engelhardt, H. and N. Riehl (1965) Space-charge limited proton currents in ice. *Physics Letters*, **14**: 20–21.

Engelhardt, H. and N. Riehl (1966) Zur Protonischen Leitfähigkeit von Eis-Eihkristallen bei tiefen Temperatures und hohen Feldstärken. *Physik der Kondensierten Materie*, **5**: 73–82.

Engelhardt, H., B. Bullemer and N. Riehl (1969) Protonic conduction of ice. Part II: Low temperature region. In *Physics of Ice* (N. Riehl, B. Bullemer and H. Engelhardt, Ed.). New York: Plenum Press.

Evtushenko, A.A., M.B. Martirosyan and V.F. Petrenko (1988) Experimental study of electrical properties of ice grown in constant electric field. *Soviet Physics—Solid State*, **30**: 2133–2138.

Fletcher, N.H. (1970) *The Chemical Physics of Ice*. Cambridge University Press.

Gelin, H. and R. Stubbs (1965) Ice electrets. *Journal of Chemical Physics*, **12**: 967–971.

Glen, J.W. (1974) The physics of ice. USA Cold Regions Research and Engineering Laboratory, Monograph II-C2a.

Glen, J.W. (1975) Mechanics of ice. USA Cold Regions Research and Engineering Laboratory, Monograph II-C2b.

Gross, G.W. (1975) Dielectric relaxation spectrum and conductivity of ice crystals doped with ionic impurities. Annual Report. *Conference on Electric Insulation and Dielectric Phenomena, 1976.* Washington, D.C.: National Academy of Sciences, p. 347–358.

Haltenorth, H. and J. Klinger (1969) Diffusion of hydrogen fluoride in ice. In *Physics of Ice* (N. Riehl, B. Bullemer and H. Engelhardt, Ed.). New York: Plenum Press, p. 579.

Hobbs, P.V. (1974) *Ice Physics*. Oxford, United Kingdom: Clarendon Press.

Howe, R. and R.W. Whitworth (1989) The electrical conductivity of KOH-doped ice from 70 to 250 K. *Journal of Physics and Chemistry of Solids*, **50**: 963–965.
Hubmann, M. (1978) Effects of pressure on the dielectric properties of ice Ih single crystals doped with NH_3 and HF. *Journal of Glaciology*, **21** (85): 161–172.
Hubmann, M. (1979a) Polarization processes in the ice lattice, Part I. *Z. Physik B*, **32**: 127–139.
Hubmann, M. (1979b) Polarization processes in the ice lattice, Part II. *Z. Physik B*, **32**: 141–146.
Jaccard, C. (1959) Étude théorique et expérimentale des propriétés électriques de la glace. *Helvetica Physica Acta*, **32**: 89–128.
Jaccard, C. (1964) Thermodynamics of irreversible processes applied to ice. *Physik der Kondensierten Materie*, **3**: 99–118
Jaccard, C. (1966) Four-point method for measuring the volume and surface conductivities of a thin sample. *Zeitschrift Angewandte Mathematik und Physik*, **17**: 657–663.
Johari, G.P. and S.J. Jones (1975) Study of low temperature transitions in ice Ih by thermally stimulated depolarization measurements. *Journal of Chemistry and Physics*, **62**: 4213–4223.
Johari, G.P. and E. Whalley (1981) The dielectric properties of ice in the range 272–133 K. *Journal of Chemical Physics*, **75**: 1333–1340.
Kahane, A. (1969) Experimental and theoretical studies of the DC conductivity of ice. In *Physics of Ice* (N. Riehl, B. Bullemer and H. Engelhardt, Ed.). New York: Plenum Press, p. 443–449.
Kröger, F.A. (1974) *The Chemistry of Imperfect Crystals*. Chapter 18. In *Ice*, 2nd ed., vol. 2. Amsterdam: North Holland Publishing Co., p. 783–799.
Kunst, M. and J. Warman (1983) Nanosecond time-resolved conductivity studies of pulse-ionized ice. Part 2. The mobility and trapping of protons. *Journal of Chemistry and Physics*, **87**: 4093–4095.
Lampert, M.A. and P. Mark (1970) *Current Injection in Solids*. New York, London: Academic Press.
Long, D. (1968) *Energy Bands in Semiconductors*. Interscience.
Loria, A., E. Mazzega, U. del Pennino and G. Andreotti (1978) Measurements of electrical properties of ice Ih single crystals by admittance and thermally stimulated depolarization techniques. *Journal of Glaciology*, **21**(85): 219–230.
Maeno, N. (1973) Measurement of surface and volume conductivities of single ice crystals. In *Physics and Chemistry of Ice* (E. Whalley, S.J. Jones and L.W. Gold, Ed.). Ottawa: Royal Society of Canada, p. 140–143.
Maeno, N. (1981) *The Science of Ice*. Hokkaido University Press (in Japanese).
Maidique, M.A., A. von Hippel and W.B. Westphal (1970) Transfer of protons through *pure* ice in single crystals, Part III. *The Dielectric Relaxation Spectra of Water, Ice, and Aqueous Solutions and Their Interpretation*. Laboratory for Insulation Research, Massachusetts Institute of Technology, Technical Report 8.
Maidique, M.A., A. von Hippel and W.B. Westphal (1971) Transfer of protons through *pure* ice Ih single crystals. III. Extrinsic versus intrinsic polarization; surface versus volume conduction. *Journal of Chemistry and Physics*, **54**: 150–160.
Malmberg, C.G. and A.A. Maryott (1956) Dielectric constant of water from 0° to 100°. *Journal of Research of the National Bureau of Standards*, **56**: 1–8.
Mounier, S. and P. Sixou (1969) A contribution to the study of conductivity and dipolar relaxation in doped ice crystals. In *Physics of Ice:* (N. Riehl, B. Bullemer, H. Engelhardt, Ed.). New York: Plenum Press, p. 562–570.
Nagle, J. (1974) Dielectric constant of ice. *Journal of Chemistry and Physics*, **61**: 883–888.
Nagle, J. (1979) Theory of the dielectric constant of ice. *Chemical Physics*, **43**: 317–328.
Noll, G. (1978) The influence of the rate of deformation on the electrical properties of ice monocrystals. *Journal of Glaciology*, **21**(85): 277–289.

Nye, J.F. (1985) *Physical Properties of Crystals.* Oxford, United Kingdom: Clarendon Press.
Ossipyan, Y.A. and V.F. Petrenko (1988) The physics of ice. *Europhysics News,* **19**(5): 61–64.
Pauling, L. (1935) The structure and entropy of ice and of other crystals with some randomness of atomic arrangement. *Journal of the American Chemical Society,* **57**: 2680–2684.
Petrenko, V.F. and V.A. Chesnakov (1990a) On a nature of charge carriers in ice. *Soviet Physics—Solid State,* **32**: 2368–2373.
Petrenko, V.F. and V.A. Chesnakov (1990b) Investigations of physical properties of ice-electronic conductor interfaces. *Soviet Physics—Solid State,* **32**: 2655–2660.
Petrenko, V.F. and V.A. Chesnakov (1990c) Recombination injection of charge carriers in ice. *Soviet Physics—Solid State,* **32**: 2947–2952.
Petrenko, V.F. and V.A. Chesnakov (1990d) Recombination injection of H_3O^+ and OH^- charge carriers in electrolysis of water. *Dokl. Akad. Nauk (Soviet Physics—Doklady),* **314**: 359–361.
Petrenko, V.F. and N. Maeno (1987) Ice field transistor. *Journal de Physique, C1,* **48**: 115–119.
Petrenko, V.F. and I.A. Ryzhkin (1984a) Dielectric properties of ice in the presence of space charge. *Physica Status Solidi(b),* **121**: 421–427.
Petrenko, V.F. and I.A. Ryzhkin (1984b) Space charge limited currents. *Soviet Physics—JETP,* **87**: 558–569.
Petrenko, V.F. and E.M. Schulson (1992a) The effect of static electric fields on protonic conductivity of ice single crystals. In *Physics and Chemistry of Ice* (N. Maeno and T. Hondoh, Ed.). Hokkaido University Press, p. 149–155.
Petrenko, V.F. and E.M. Schulson (1992b) The effect of static electric fields on protonic conductivity of ice single crystal. *Philosophical Magazine B,* **66**: 341–353.
Petrenko, V.F., R.W. Whitworth and J.W. Glen (1983) Effect of proton injection on electrical properties of ice. *Philosophical Magazine B,* **47**(3): 259–78.
Ruepp, R. and M. Käss (1969) Dielectric relaxation of the bulk and surface conductivity of ice single crystals. In *Physics of Ice* (N. Riehl, B. Bullemer and H. Engelhardt, Ed.). New York: Plenum Press, p. 555–561.
Ryzhkin, I.A. (1985) Superionic transition in ice. *Solid State Com.,* **56**: 57–60.
Ryzhkin , I.A. (1992) New stages of ice properties understanding. In *Physics and Chemistry of Ice* (N. Maeno and T. Hondoh, Ed.). Hokkaido University Press, p. 141–148.
Scheiner, S. and J. Nagle (1983) Ab initio molecular orbital estimates of charge partitioning between Bjerrum and ionic defects in ice. *Journal of Physics and Chemistry,* **87**: 4267–4272.
Sokolov, B.A. (1976) *Radical Recombination Luminescence of Semiconductors.* Moscow: Nauka.
Steinemann, A. (1957) Dielektrische Eigenschaften von Eiskristallen. *Helvetica Physica Acta,* **30**: 581–610.
Tajima, Y., T. Matsuo and H. Suga (1982) Phase transition in KOH-doped hexagonal ice. *Nature,* **299**: 810.
Takei, I. and N. Maeno (1984) Dielectric properties of single crystals of HCL-doped ice. *Journal of Chemistry and Physics,* **81**: 6186–6190.
Takei, I. and N. Maeno (1987) Electric characteristics of point defects in HCl-doped ice. *Journal de Physique, C1,* **48**(3): 121–126.
Turner, G.J. and C.D. Stow (1986) DC conductivity of the ice surface. *Solid State Com.,* **58**: 403–405.
Vihj, A. K. (1973) Electrochemistry of metals and semiconductors; the application of solid state science to electrochemical phenomena. New York: M. Dekker.
von Hippel, A. (1971) Transfer of protons through pure ice Ih single crystals. II. Molecular models for polarization and conduction. *Journal of Chemistry and Physics,* **54**: 145–149.
von Hippel, A., D.B. Knoll and W.B. Westphal (1971) Transfer of protons through pure ice Ih single crystals. I. Polarization spectra of ice Ih. *Journal of Chemistry and Physics,* **54**: 134–144.

von Hippel, A., A.H. Runck and W.B. Westphal (1973) Ice chemistry: Is ice Ih a proton semiconductor? *Physics and Chemistry of Ice* (E. Whalley, S.J. Jones and L.W. Gold, Ed.). Ottawa: Royal Society of Canada, p. 236–241.

Wörz, O. and R.H. Cole (1969) Dielectric properties of ice Ih. *Journal of Chemistry and Physics*, **51**: 1546–1551.

Zaretskii, A.V. (1991) Experimental determination of the H_3O^+ ions mobility in ice from 160 to 240 K. *Summaries of International Symposium on the Physics and Chemistry of Ice, Sapporo, Japan, September 1–6, 1991*, p. 204.

Zaretskii, A.V., V.F. Petrenko and V.A. Chesnakov (1988) The protonic conductivity of heavily KOH-doped ice. *Physica Status Solidi(a)*, **109**: 373–381.

Zaretskii, A.V., V.F. Petrenko, I.A. Ryzhkin and A.V. Trukhanov (1987a) Theoretical and experimental study of ice in the presence of a space charge. *Journal de Physique, C1*, **48**: 93–98.

Zaretskii, A.V., V.F. Petrenko, A.V. Trukhanov, E.A. Aziev and M.P. Tonkonogov (1987b) Theoretical and experimental study of pure and doped ice Ih by the method of thermally stimulated depolarization. *Journal de Physique, C1*, **48**: 87–91.

REPORT DOCUMENTATION PAGE

Form Approved
OMB No. 0704-0188

1. AGENCY USE ONLY (Leave blank)	2. REPORT DATE	3. REPORT TYPE AND DATES COVERED
	August 1993	

4. TITLE AND SUBTITLE

Electrical Properties of Ice

5. FUNDING NUMBERS

Contract DAAL 03-91-G-0164

6. AUTHORS

Victor F. Petrenko

7. PERFORMING ORGANIZATION NAME(S) AND ADDRESS(ES)

U.S. Army Cold Regions Research and Engineering Laboratory
72 Lyme Road
Hanover, New Hampshire 03755-1290

Thayer School of Engineering
Dartmouth College
Hanover, NH 03755

8. PERFORMING ORGANIZATION REPORT NUMBER

Special Report 93-20

9. SPONSORING/MONITORING AGENCY NAME(S) AND ADDRESS(ES)

U.S. Army Research Office
Research Triangle Park
Durham, NC 27709

10. SPONSORING/MONITORING AGENCY REPORT NUMBER

11. SUPPLEMENTARY NOTES

12a. DISTRIBUTION/AVAILABILITY STATEMENT

Approved for public release; distribution is unlimited.

Available from NTIS, Springfield, Virginia 22161

12b. DISTRIBUTION CODE

13. ABSTRACT (*Maximum 200 words*)

This report examines the electrical properties of ice in the frequency range of 0–10^7 Hz, attempting to be suitable both as a simple and clear textbook for students and non-specialists and as a comprehensive review of recent developments and discoveries in the field. Corresponding to this double goal, the report consists of two parts. The first one is written in textbook style and contains most general theoretical and experimental results essential for understanding of unique electrical properties of ice. The theoretical interpretation of ice conductivity and ice dielectric permittivity is based on ice being a protonic semiconductor. Jaccard's elegant model is used to mathematically describe the electrical properties, and is expanded on cases of ice samples having finite size, boundaries and interfaces, and an inhomogeneous electric field. The statistics of charge carriers in pure and doped ice is discussed in detail, as are experimental techniques for measurements of conductivity and dielectric permittivity. The first part contains a comprehensive review of experimental results on ice conductivity, ice dielectric permittivity, mobility and electric charges of protonic charge carriers and activation energies of their generation and motion. The second part includes more complicated physical phenomena—proton injection, dielectric crossover, ice field effect transistor, thermostimulated currents, theory of ice/metal interface, field extraction of charge carriers and a recombination injection.

14. SUBJECT TERMS

Dielectric properties
Electrical properties
Ice
Ice physics
Ice point defects
Protonic conductor

15. NUMBER OF PAGES
80

16. PRICE CODE

17. SECURITY CLASSIFICATION OF REPORT	18. SECURITY CLASSIFICATION OF THIS PAGE	19. SECURITY CLASSIFICATION OF ABSTRACT	20. LIMITATION OF ABSTRACT
UNCLASSIFIED	UNCLASSIFIED	UNCLASSIFIED	UL